DETECTION OF RPW INFESTED DAMAGED DATE-PALM TREES USING DIELECTRIC MEASUREMENTS

BY

FORHAD HOSSAIN

A Thesis Presented to the
DEANSHIP OF GRADUATE STUDIES

KING FAHD UNIVERSITY OF PETROLEUM & MINERALS

DHAHRAN, SAUDI ARABIA

In Partial Fulfillment of the
Requirements for the Degree of

MASTER OF SCIENCE

In

ELECTRICAL ENGINEERING

May, 2018

KING FAHD UNIVERSITY OF PETROLEUM & MINERALS

DHAHRAN- 31261, SAUDI ARABIA

DEANSHIP OF GRADUATE STUDIES

This thesis, written by **FORHAD HOSSAIN** under the direction his thesis advisor and approved by his thesis committee, has been presented and accepted by the Dean of Graduate Studies, in partial fulfillment of the requirements for the degree of **MASTER OF SCIENCE IN ELECTRICAL ENGINEERING.**

Dr. Sheikh Sharif Iqbal
(Advisor)

Dr. Ali Ahmad Al-Shaikhi
Department Chairman

Dr. Essam Eldin Mohammad Hassan
(Member)

Dr. Salam A. Zummo
Dean of Graduate Studies

Dr. Hussein Attia
(Member)

Date

DEANSHIP OF GRADUATE STUDIES

Dedicated to

My Parents

&

My Grandma

Their Prayers and Perseverance which led to this accomplishment

ACKNOWLEDGMENTS

In the name of Allah, the Most Gracious and the Most Merciful

All praises and glory be to Allah (SWT) for blessing me with opportunities flourish and showering upon me his mercy and guidance all through the life. I pray that He continues the same the rest of my life. And may his peace and blessings of Allah be upon Prophet Muhammad, a guidance, and inspiration to our lives. My sincere thanks to the government of Saudi Arabia to provide me with a generous scholarship and giving me the chance to be a part of King Fahd University of Petroleum & Minerals.

This thesis cannot be done without the help and guidance of my professors, colleagues and friends. Thank you all for your help and support. Special thanks for my thesis advisor *Dr. Sheikh Sharif Iqbal* for introducing me to the microwave field with his precious suggestions, encouragement, patience and his unlimited support. I am also very grateful to my thesis committee members, Dr. Essam Hassan and Dr. Hussein Attia for their care, cooperation and constructive advice.

Special thanks to Irfan Ahmad and Amjad Saleem Awan for sharing their experience in fabrication, measurements and experimental process. I also want to thank my colleagues and friends for their encouragements and various help that they provided throughout my graduate studies at KFUPM.

TABLE OF CONTENTS

LIST OF TABLES

LIST OF FIGURES

ABSTRACT

Full Name : [FORHAD HOSSAIN]

Thesis Title : [Detection of RPW infested Damaged Date-palm Trees using Dielectric Measurements]

Major Field : [Electrical Engineering]

Date of Degree : [April 2018]

In Saudi Arabia, the date palm trees are widely cultivated for 300 types of date fruits. There are almost 25 million palm trees that produce around 1.1 million tons of date [1]. But in recent years, this Middle Eastern heritage is threatened by the infestation of a virulent pest known as red palm weevils (RPW's). So, early detection of RPW infestation is essential to avoid serious economic consequences and safety hazards. Popular methods of detecting infested date trees include; visual inspection, thermal imaging, chemical and acoustic detection. Visual and chemical methods are prone to human errors and can only detect advanced stage of infestation. Thermal and acoustic methods use a scientific process for early detection of the infestation but are influenced by the thermal and acoustic noises present in the environment.

In this work, the change in the dielectric properties of the tree due to RPW infestation will be studied. Due to the difference in the dielectric constants of the date tree (healthy/damaged) and the red palm weevil (larva/pupa/adult), two techniques are proposed to monitor the infestation. First technique involves microwave sensor for detecting initial stage of infestation. A microstrip patch which initially operating at 4GHz is designed and then optimized for wood superstrate which act as a dielectric resonator antenna. The resonance frequency is analyzed for the wood superstrate with healthy, partially damaged and complete damaged conditions. The designed obtained a resonance frequency shift of approximately 36% experimentally between the healthy and complete damaged date tree sample. A two port microstrip ring resonator also designed and optimized coupling gap for wood superstrate. Distinct resonance frequencies obtained for healthy and damaged wood superstrate.

The second technique use low-frequency signal to experimentally monitor the tree capacitance to determine medium to advance stage of infestation. For this technique, we have designed and analyzed semi-cylindrical capacitive sensor to measure the changes in the dielectric constant of palm trees because of RPW infestation. Three different electrode configurations of this capacitor sensor have been designed and evaluated their sensitivity for tree capacitance measurement. To validate the work, comparison is made between the simulation results and experimental work. We proved that experimental results are in close agreement with the simulation results.

ملخص الرسالة

الاسم الكامل: فرهاد حسين

عنوان الرسالة: الكشف عن RPW الموبوءة بأشجار النخيل التالفة باستخدام مقاييس العزل الكهربائي

التخصص: الهندسة الكهربائية

تاريخ الدرجة العلمية: شعبان، 1439

في المملكة العربية السعودية ، تزرع أشجار النخيل على نطاق واسع من أجل 300 نوع من ثمار التمر. هناك
ما يقرب من 25 مليون نخلة تنتج حوالي 1.1 مليون طن من التاريخ [1]. لكن في السنوات الأخيرة ، هذا التراث الشرق أوسطي مهدد من جراء الإصابة بآفة خبيثة تعرف باسم سوسة النخيل الحمراء (RPW's). لذا ، فإن الكشف المبكر عن الإصابة RPW ضروري لتجنب العواقب الاقتصادية الخطيرة والمخاطر على السلامة. الطرق الشعبية للكشف عن أشجار التاريخ الموبوءة تشمل ؛ الفحص البصري والتصوير الحراري والكشف الكيميائي والصوتي. الطرق البصرية والكيميائية عرضة للأخطاء البشرية ويمكن فقط الكشف عن مرحلة متقدمة من الإصابة. تستخدم الطرق الحرارية والصوتية عملية علمية للكشف المبكر عن الإصابة ولكن تتأثر بالضوضاء الحرارية والصوتية الموجودة في البيئة.

في هذا العمل ، سيتم دراسة التغيير في الخصائص العازلة للشجرة بسبب الإصابة RPW. بسبب الاختلاف في الثوابت العازلة لشجرة التاريخ (صحية / تالفة) وسوسة النخيل الحمراء (يرقة / خادرة / بالغ) ، يتم اقتراح تقنيتين لمراقبة الإصابة. التقنية الأولى تتضمن جهاز استشعار للكشف عن الموجات الصغرية للكشف عن المرحلة الأولية من الإصابة. تم تصميم رقعة microstrip التي تعمل في البداية على GHz4 ومن ثم يتم تحسينها للخشب الذي يعمل بمثابة هوائي مرنان عازلة. يتم تحليل تردد الرنين للخزف الخشبي مع ظروف تالفة صحية ومدمرة جزئياً وكاملة. وحصل التصميم على تذبذب في تردد الرنين يبلغ حوالي 36٪ تجريبًا بين عينة شجرة التمر السليمة والتالفة. مرنان عصابة microstrip اثنين من الميناء أيضا مصممة وفجوة اقتران الأمثل للخشب سوبيركات. الترددات الرنينية المميزة التي تم الحصول عليها لخشب صحية ومعطوبة.
تستخدم التقنية الثانية إشارة منخفضة التردد لمراقبة سعة الشجرة تجريبيا لتحديد متوسط إلى مرحلة متقدمة من الإصابة. لهذه التقنية ، قمنا بتصميم وتحليل مستشعر سعوي شبه أسطواني لقياس التغيرات في ثابت العزل من أشجار النخيل بسبب الإصابة RPW. تم تصميم ثلاثة تكوينات مختلفة للقطب الكهربائي لجهاز استشعار المكثف هذا وقيّمت حساسيتها لقياس سعة السعة. للتحقق من صحة العمل ، تم المقارنة بين نتائج المحاكاة والعمل التجريبي. لقد أثبتنا أن النتائج التجريبية متفقة بشكل وثيق مع نتائج المحاكاة.

CHAPTER 1

1 INTRODUCTION

Date fruit is a heritage and an important dietary component in most of the Arab countries. Egypt, Saudi Arabia, and Iran are the top three global producers of dates. It is reported that there are around 100 million date palm trees in the Middle East and North Africa that produces around 7 million tons of date fruit[1], [2]. In Saudi Arabia, dates are very popular for its taste and nutritional values and can be considered the main agricultural treasure. Local farms cover 157,000 hectares of national land that grows over 300 types of dates.

But in recent years, the date industry is suffering from an increasing attack of a virulent pest, known as red palm weevil (RPW). RPW with a scientific name of Rhynchophorus Ferruginous is the most disruptive and widespread insect of palm species. This deadly pest was first reported in South Asia and later found in the palm tree farms in other continents. In Saudi Arabia, the first incident of infection by RPW was reported in Al-Qatif region of the Eastern Province. Due to the warm agro-climatic condition of this region, the date farms offered this pest an ideal habitat for dwelling and breeding by large numbers. Early detection of RPW infestation is critical for saving the palm tree. This can also stop the spreading of the pest in neighboring trees of the plantation. In Saudi Arabia, visual inspection technique is popular in detecting RPW infestation. But for date palm trees, the early infestation in the lower part of the trunk often remains hidden amid leaf bases or stem

fibers. Another approach commonly used is chemical detection, where fermenting odor emitting from the wounds in infested palm can be picked up by well-trained sniffing dogs. Although this technique is 70% accurate, detection comes in a later stage of RPW infestation. In recent years, acoustic and thermal imaging techniques are becoming popular in detecting early-stage infestation of the RPW. But they require experienced manpower, as changes in thermal and acoustic measurements related to early stage of infestation are strongly affected by the noise present in nature.

This research can be divided into two sections, but both have the same common goal of identifying the changes in the dielectric properties of RPW infested date-palm trees. The first having the aim of designing and corroborating potentially portable microwave resonator able to measure changes in dielectric constant in the S-band (2-4 GHz) from the changes of its resonance frequency. The second goal of this research is to design a semi-cylindrical capacitive sensor to monitor the changes in effective capacitance and characterization of the date tree due to a different stage of infestation.

1.1 DATE PALM TREES

Date palm tree the scientific name Phoenix Dactylifera belongs to a plantation family called Palmae class is the tallest among the Phoenix species[3]. This tree can have a height of 30-50m with a diameter of 30-40cm. It has distinguished shape, consists of mainly the trunk, leaves and fronds. The general outlook of a date tree shown in Figure1.1. Date trees are easy to recognize from their leaves, which are distributed around the axis very accurately according to the system of phyllotaxy of the genus. On an average, a date has a lifespan of about 50 years. A date tree takes around 200 days from pollination to fruit development

and the amount of fruit is highly variable, 20–100 kg per adult tree depending on the environment as well as cultivation process. The date fruits are shown in Figure1.2

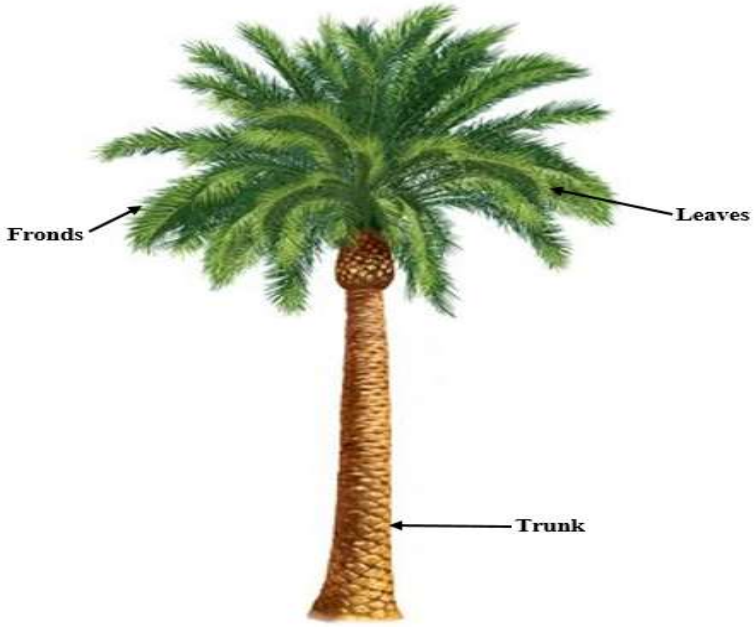

Figure 1.1: Date palm tree.

Figure 1.2: Fruits of a Date palm tree.

1.2 RED PALM WEEVIL (RPW)

In recent years, the palm tree family, especially the multimillion-dollar date-palm industries are debilitated by a virulent pest called Red Palm Weevil (RPW) with a scientific name of Rhynchophorus Ferruginous. The life cycle of RPW is shown in Figure 1.3.

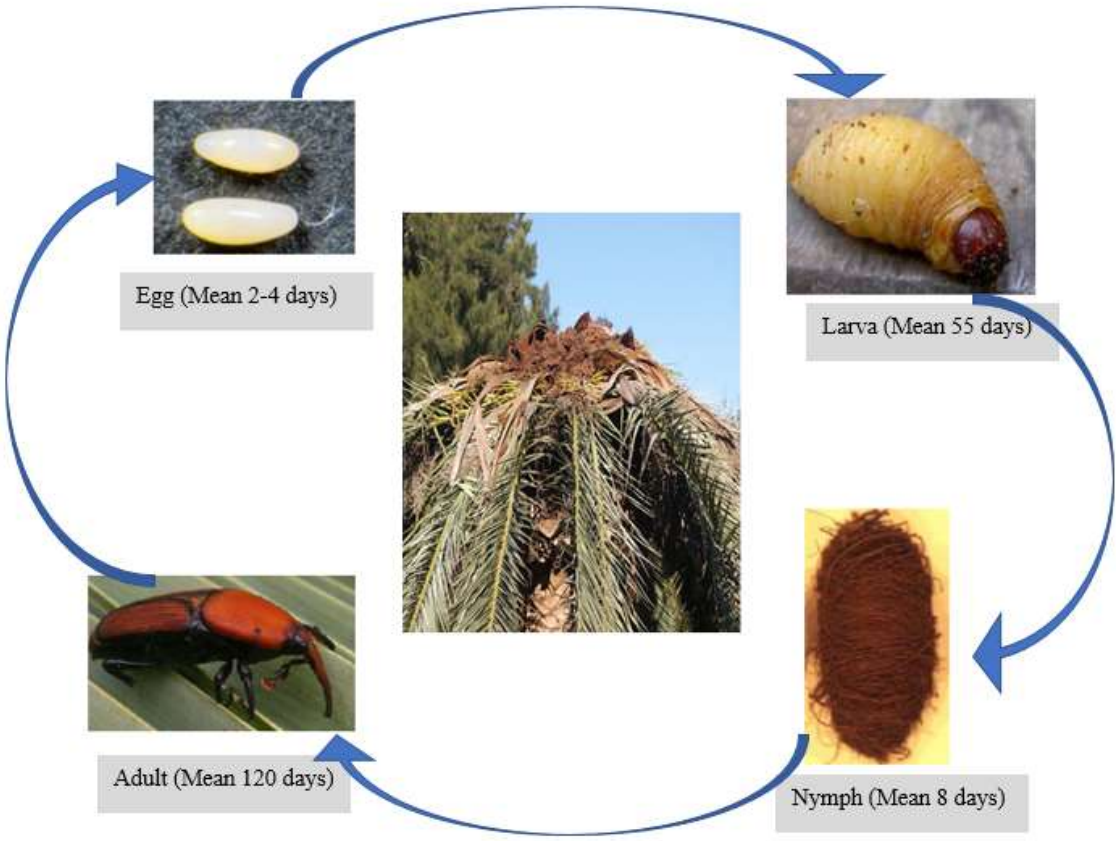

Figure 1.3: Life cycle of the date-palm tree pest: Red Palm Weevil (RPW).

Red Palm Weevils normally grow up to 4-5 cm in length and have a life cycle of approximately 3 months. The adult female RPW lay 200 to 300 eggs in damaged palm surfaces. These wounds often result from RPW's search for food or due to recently cut palms. The 2-3 mm long eggs take around 3 days to hatch into a white larva. For about 2

months, the larva feeds on the soft-fibers and terminal bud, which can produce tunnel through the internal tissue of the tree trunk. Finally, the larva forms a cocoon around it using palm fibers and leaves the tree to infect neighboring plants. This RPW lifecycle causes irreparable damage to the palm tree and often resulting in the collapse of the tree [1]. This is the deadliest pests for several types of palm trees and can completely destroy the plant within months.

1.3 RPW INCIDENCE

The incidence of RPW in coconut palm trees was first reported in India. The first incident of RPW infestation in the middle east was detected in Al-Quatif region of Saudi Arabia. Within years, the RPW infestation was detected in neighboring countries. The RPW infestation chart for the Mediterranean basin is shown in Figure 1.4[4]. Since 1984, owners of date-palm farms in Saudi Arabia are consistently requesting for state of the art solution to early detect and treat/eradicate RPW infested trees.

1.4 OBJECTIVES

(1) Conduct through literature survey to know the existing methods to detect and eradicate RPWs from date-palm trees.

(2) Study the theory of Radiofrequency sensor and capacitive sensing for the measurement of material dielectric constant.

(3) Develop high-frequency simulation (HFSS) model for analyzing of the dielectric properties related to the initial stage of RPW infestation. Design a microwave monitoring setup to experimentally corroborate the optimized simulated result.

(4) Use a semi-cylindrical plate capacitance measurement setup that uses low frequency to monitor the changes in tree capacitances for damaged tree due to RPW infestation.

(5) Compare the low and microwave frequency detection techniques and comments on their ability to detect different stages (initial or advance) of RPW infestation.

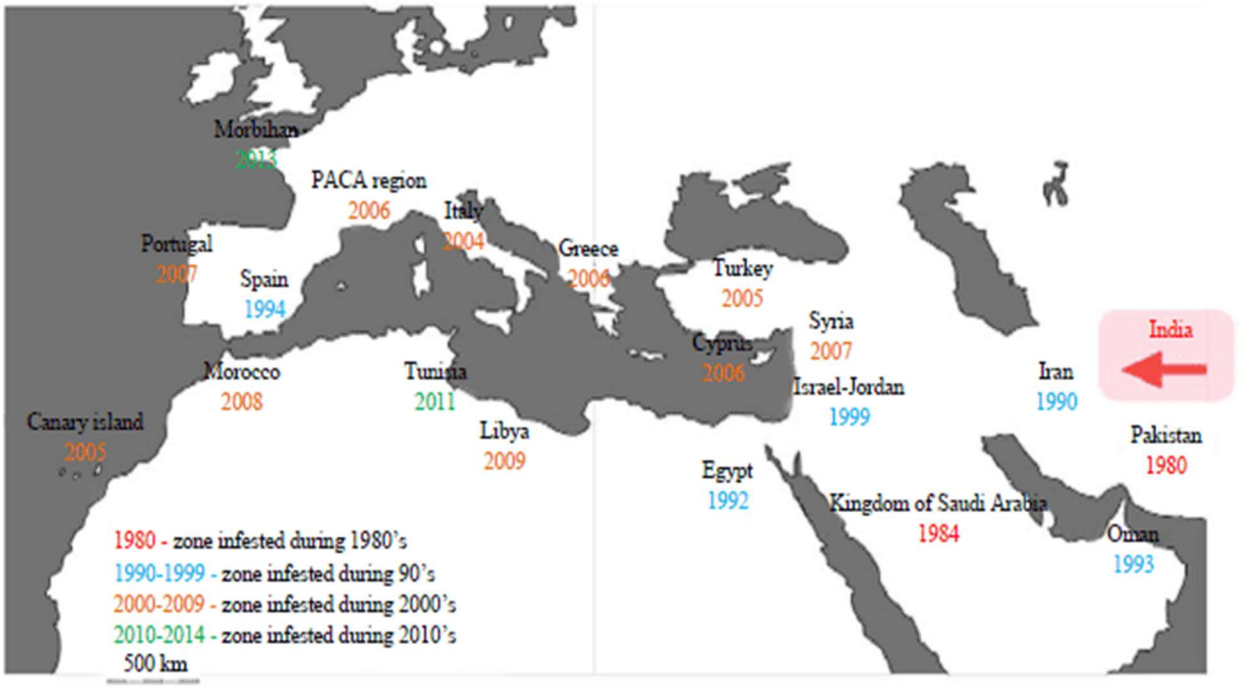

Figure 1.4: The RPW infestation throughout the Mediterranean basin [3].

1.5 THESIS ORGANIZATION

The dissertation has been divided into six chapters. Chapter 2 describes the existing RPW infestation management methods and illustrate comprehensive literature review on dielectric measurement techniques. In chapter 3, the design of a simple microwave resonator to detect the infected palm trees has been presented. This chapter discusses the numerical design of the resonator, optimization using professional simulator software (HFSS), the fabrication process of a prototype and the experimentally observed results. In chapter 4, the design of a semi-cylindrical capacitor sensor to detect the infected palm tree, fabrication and experimental processes and the comparison between the experimental and simulation results have been presented. Finally, chapter 5 draws the conclusion of this research work and propose some useful recommendation as future work.

CHAPTER 2

2 LITERATURE REVIEW

2.1 RPW INFESTATION MANAGEMENT METHODS

In the past, several methods and approaches are introduced for RPW management [5]. The block diagram of Figure 2.1 summarizes these methods for detecting and treating RPW infestation. Based on this figure, a thorough literature survey is presented here to determine the best-suited approach for RPW management in Saudi Arabian.

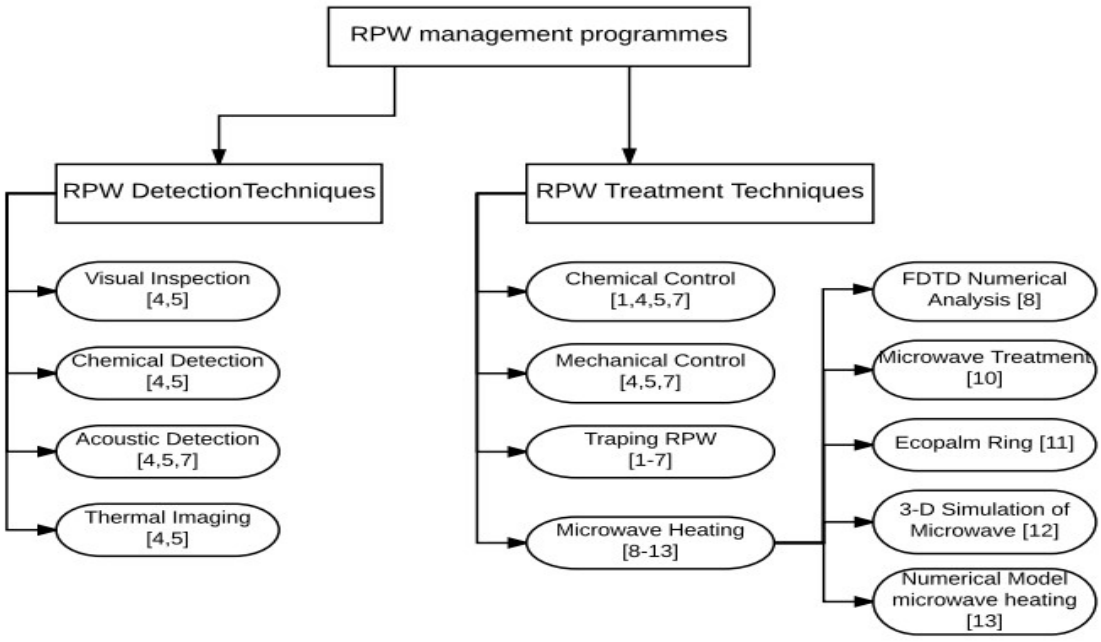

Figure 2.1: Summary of existing RPW management programs.

2.1.1 VISUAL INSPECTION

Early detection of RPW infestation is often difficult, as infected palm do not show symptoms until the infestation are at its final stage. Abraham et al [4] reported several symptoms related to the RPW infested date palm as; i) presence of tunnels on the trunk, ii) presence of chewed up tissue around the opening of tunnels, iii) sugary and creamy color viscous liquid, which eventually become brownish oozes out from the tree trunk, iv) presence of upper dead offshoots, v) leaf stokes are worn, vi) drying of outer leaves and fruit bunches as well as breaking of the stem/crown. Note that most of these symptoms only appear during the last stage of infestation and may cause the sudden collapse of the date-palm. Although most of the symptoms can be detected through visual inspection, this technique can be time-consuming, laborious and often expensive for large farms.

2.1.2 CHEMICAL DETECTION

The chemical signature produced by the RPW infested date-palm trees can play an important role for easier detection. In this technique, dogs can be used to sniff the odor/scent oozing out of the thick brownish liquid and the resulted fermenting process [6]. Trained Golden Retriever dogs are often used in this technique for their ability to detect an object from odors [6]. But the costs involved in acquiring and maintaining a trained dog makes this detection technique suitable for very large plantations. Researchers also tried electronic gas sensors to detect odors emitted from infested trees [2]. However, these sensors are not feasible because the measured results are heavily influenced by the presence of natural odors in the environment.

Figure 2.2: Pressure machine to push chemical inside a tree trunk [7].

2.1.3 ACOUSTIC DETECTION

Acoustic technique for early detection of the infestation is based on the distinct sounds made by the RPW's. A sample of this type of detection is shown in figure 2.3. At an advanced stage, a vast number of larvae gather together to feed the palm tissues. This process makes sounds that can even be heard by a human observer. But at an early stage of infestation, this sound level due to PRW infestation remains very subtle/low and separating them from environmental noises becomes very difficult. Bioacoustics features based on frequency domain analysis are used to detect sounds made by 2-week old larvae in a controlled setting [6]. Since attaching a sensitive microphone to the palm tree is difficult, laser vibrometer was introduced as a non-contact acoustic sensor. This method often requires trained personnel to set up and analyze the measured results. Another drawback of this technique is the time of the measurements. If during the acoustic measurements, the larvae remain motionless this technique fails to detect an infestation.

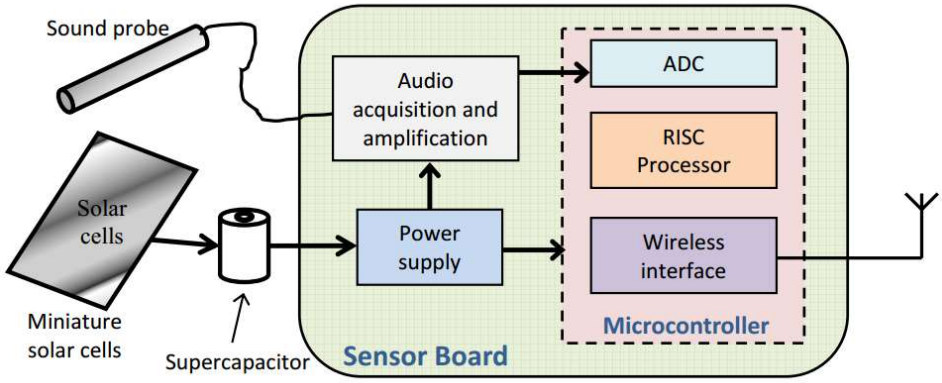

Figure 2.3: A generic model for Bioacoustics Sensor Design[6].

2.1.4 THERMAL IMAGING

Infrared cameras are recently used to detect the change in tree temperature due to RPW infestation [6]. The main reason for temperature increase is the intensive fermentation within the tree trunk, which often extends beyond 45^0C. Mohammed al Falki [7] also used this type of technique by employing a real-time temperature sensor to detect the infested palm trees.

2.2 RPW MANAGEMENT TECHNIQUES

Since early stage detection of the infested tree is mostly unsuccessful, the preventive strategies are, therefore, very important. Integrated management approach is suggested by many experts, that includes the use of pesticides (chemical compound), pest trapping mechanisms, biological control, sanitation, quarantine measures etc. In chemical treatment method, the most common practice is the application of pesticides as preventative and curative measures to reduce the spread of infestation. The female weevils are pretty much

attracted by wounds on the palm for oviposition, therefore, spraying insecticides on the wounded area is an effective way to prevent RPW. Stem injection using pressure machine shown in Figure 2.2 is now popular in gulf region to control RPW infestation [8]. However, this approach should be carried out by the skilled person to control the pressure and avoid palm tissue damages.

The use of Pheromone trap is very popular to protect palm trees from all kinds of insect. In this method, insects respond to the attractive plumes before getting trapped. But to satisfy the installation requirements, implementing this trapping technique requires direct supervision of an expert operator. Note that an improperly located trap can easily lead to an infestation in an un-infested region of the date palm plantation [2].

Figure 2.4: Setting of Pheromone Trap [2].

Basic mechanical uprooting methods are widely used to protect healthy tree form a severely infested palm. In this process, severely damaged or dead palms are often cut into small pieces before spraying them with an approved insecticide to kill existing PRWs. Then the tree parts are covered with entomological nets, and safely transferred to a dumping area. Burning the treated parts of the tree is also recommended to avoid the spread of the infestation. In the search for the more efficient and eco-friendly method for RPW management, researchers are now turning to the microwave heating technique. In this method, microwave radiation is used to induce thermal energy in the pest, heating it to a lethal temperature till they die. Although this idea is widely used in industrial production facilities, it is recently applied to eradicating RPW infestation in date plants. The drawback of this method is the collateral damage of the palm tissue caused by the microwave radiation unless they are carefully radiated and timed [9]. R. Massa et al used microwave heating for killing RPW at different stages of their lifecycle [7]. In their experiment, they first measured the permittivity and conductivity at 2.45GHz using the open-ended coaxial technique shown in Figure 2.5.

To obtain preliminary data on the lethal temperature and time needed to kill RPW, they have supplied hot air to raise the ambient temperature. Finally, they heated the artificially infested tree with microwave. Their result showed that adult RPW are more sensitive compared to larvae. The death of adults RPW required 4 min at 80^0C compared to 20 min at 50^0C for a larva. They also demonstrated that this technique effectively killed pests residing in the outer region of the trunk, compared to that of the center. C. Yamen Khatib et al introduced Eco palm ring machine for disinfestation of palm trees[10].

Figure 2.5: Permittivity measurements with the open-ended coaxial cable technique[11]**.**

This circular ring-shaped microwave device has a height of 80cm, the internal diameter is 90cm and has two modular sectors with magnetrons to cover palm trunk around its circumference. During the treatment process, the Eco palm Ring machine was positioned around infested trunk before radiating it with microwave energy. The tree-temperature was maintained at 60°C for 30 min on the external layer of the infested trunks to kill the pest. The major disadvantages of this method are the high-power requirement of the machine and its bulky size, which required a crane for transportation. To eliminate these drawbacks, Rita Massa et al., I.A. Ali et al proposed FDTD method to simulate temperature distribution inside the trunk. This considerably improved the efficiency of microwave set up in terms power requirements and size as shown in Figure 2.6 [12][13]. Further investigation is

needed to make sure that this treatment process satisfies the allowed specific absorption rate (SAR) in reaching the RPW lethal temperature.

Figure 2.6: Experimental set-up to estimate the thermal parameters; (a) the palm is radiated by a waveguide; (b) the temperature inside the palm is measured using an optical fiber thermometer[13].

2.3 DIELECTRIC MEASUREMENT METHODS

Several dielectric measurement techniques have been developed over last few decades to determine the relative permittivity of materials. This is because, different materials such as gas, liquid, powder, paste, solid etc. have different physical states. Again, in case of solids, they are available in different geometrical shapes. Due to the variations in the values of ε' and ε'', suitable frequency range different materials need different techniques for complex permittivity measurements.

Dielectric constant measurement methods can be divided into two categories:

(I) Time domain methods

(II) Frequency domain methods

The frequency domain methods have been in use over half a century. The latest addition is time domain methods, can provide fast measurement to evaluate the dielectric response of a material over a wide frequency range. Again, these two techniques can be categorized in different ways; for example, single vs. broadband methods, resonant vs. non-resonant methods, and reflection vs. transmission methods, destructive vs. non-destructive methods. Each of this technique is accompanied by pros and cons, for instance, although single frequency methods ensure high accuracy permittivity measurements, however, its time-consuming methods. In contrast, broadband methods provide quicker permittivity measurements over a wide frequency range; however, they are less accurate

2.3.1 TRANSMISSION/REFLECTION LINE METHOD

This is one of the popular broadband dielectric measurement methods, where a dielectric material is positioned inside a transmission line or waveguide to guide an electromagnetic wave through the sample [14]. In the figure below, the material under test (MUT) is placed at the end of the waveguide and terminated by a short circuit or some other known impedance [15]. The permittivity of the material is then calculated from the measured S-parameters of the line. However, this method is not useful above 10 GHz frequency because of high parasitic loss.

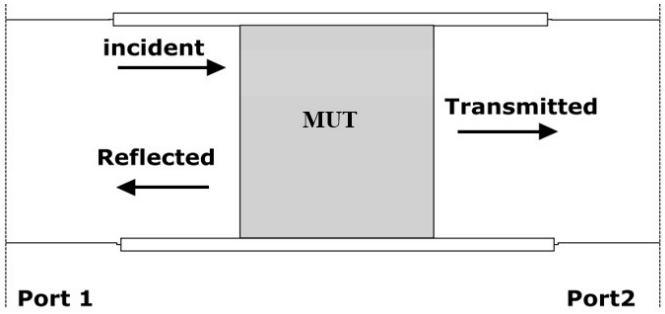

Figure 2.7: Transmission line method.

2.3.2 FREE SPACE METHOD

This method is based on broadband optical measurement suitable for homogenous materials, where dielectric constants remain unaffected by external fields [16], [17]. This method allows measurements on MUT under many environmental or physical conditions, such as high temperatures, wide frequency bands [18], [19]. This technique is shown in Figure 2.8, where a large and flat sample is placed between a pair of transmitting and receiving antennas and the S-parameter responses are analyzed using a network analyzer.

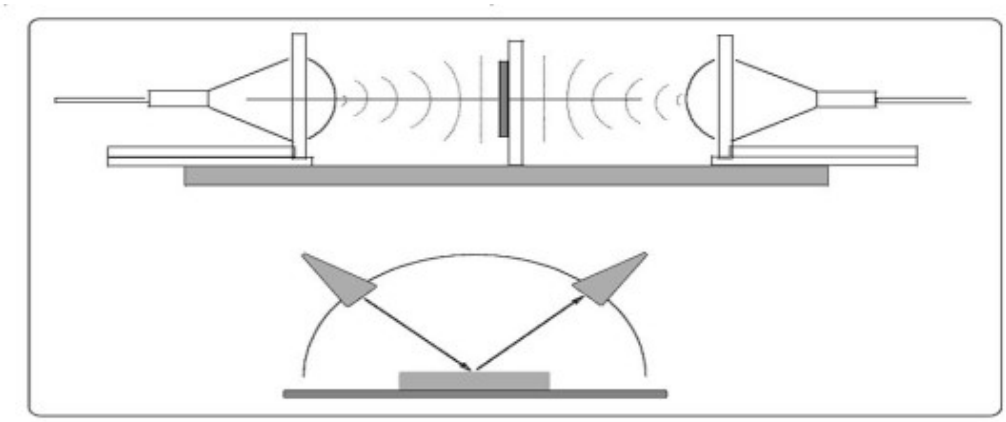

Figure 2.8: Free space methods.

2.3.3 CAVITY PERTURBATION TECHNIQUES

Cavity perturbation technique was proposed by Bethe and Schwinger [20]. In perturbation method, a dielectric sample is placed within a cavity and excited with the EM wave to observe the changes in resonance frequency and quality factor. The change of resonance frequency is mainly due to changes in the real and imaginary part of complex permittivity.

2.3.4 RESONANT TECHNIQUE

The resonant method is a widely used technique to determine the permittivity and loss tangent of low loss material. The resonant technique provides most accurate permittivity value by shielding a sample dielectric, placed inside the cavity resonator. In literature, several types of cavity resonator have been proposed, such as Fabry-Perot resonators [16], Reentrant cavities [21] and split cylindrical resonators[22].

2.3.5 OPEN-ENDED CO-AXIAL PROBE METHOD

This is a non-dispersive method, shown in figure 2.9, where the dielectric properties are estimated from the phase and amplitude change of the reflected signal [23]. In this method, the sample must be in contact with the probe and care should be taken to avoid air gaps for solid specimens. However, this method is prone to error at a low frequency and at very high frequencies and is suitable for a frequency range of 915MHz to 2.45GHz [24].

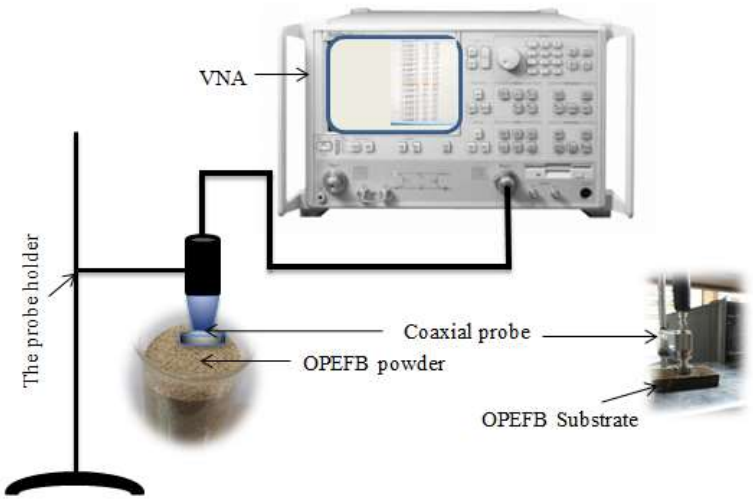

Figure 2.9: Complex permittivity measurement using open-ended coaxial cables [26].

2.3.6 MISCELLANEOUS METHODS

There are several new techniques proposed in the literature for dielectric measurement. One such new technique is to measure input impedance of an antenna over a wide band of frequencies for a known transmission medium (like air) and then to measure the impedance of the unknown dielectric sample. The measured impedances are then used to compute the permittivity of the dielectric material. This method is best suited for a frequency range of 50 MHz to 10 GHz [25].

In the literature, microstrip ring resonator has been proposed for dielectric constant measurement [26]. The theory behind this technique is that the effective permittivity will change if the dielectric substrate boundary is modified by placing a superstrate on top of the resonator. By measuring the shift in resonance frequency, permittivity change can be approximated.

Shimin et al [27] add another new dimension to the dielectric constant measurement techniques by using low-cost microstrip patch antenna to measure the dielectric constant of unknown substrates. This less expensive technique offers portability, which attracted many other researchers to improve and apply this method in other applications. A comprehensive literature review of using microstrip resonator for the dielectric constant measurement have been presented in the following section. Based on this method, the best-suited approach is adapted to detect the changes in dielectric properties of date palm trees due to RPW infestation.

2.4 DIELECTRICS RESONATOR BASED MICROWAVE SENSOR

In many applications, microstrip antennas need shielding cover or superstrate, placed over the radiating patch to provide protection from environmental hazards. Depending on dielectric properties of this protective superstrate layer, this required re-optimizing the impedance mismatch to improve the resonant response of the antenna (gain, efficiency etc). This concept of dielectric loading on microstrip structures dates back to1980 when I. J. Bahl & S. Stuchly [28] proposed a complex variational method to describe the microstrip line covered with a lossy dielectric sheet. They found that enclosing the microstrip structure with a thick sheet of the high dielectric constant material severely affects the resonant behavior. The consequence of dielectric cover is more obvious for small values of ***w/h*** ratio, where '***w***' is the width of the microstrip line and '***h***' is the height of the dielectric substrate. This is because of the increased interaction of fringing fields and the covering material for smaller values of w/h. Their studies observed the variation of characteristic impedance, effective dielectric constant, and conductor/dielectric losses with changing w/h ratios for different dielectric loaded microstrip structures.

In 1982, I. J. Bahl et al designed a dielectrically loaded microstrip antenna to demonstrate the changes in resonance behavior due to changing properties of loading material. The basic structure of a dielectric loaded rectangular microstrip antenna is shown in Figure 2.10.

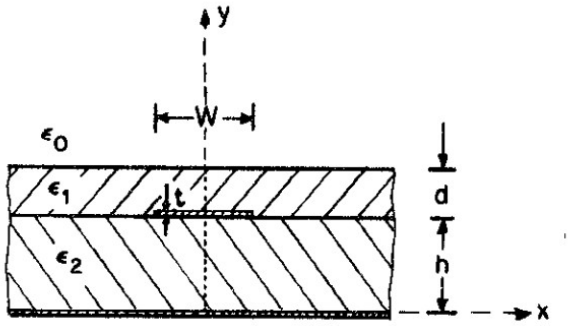

Figure 2.10: Side cross-section view of the dielectric loaded rectangular patch antenna.

Due to the dielectric cover the effective dielectric constant changes, therefore, the resonance frequency of the microstrip antenna changes. The fractional change in resonance frequency is calculated as follows

$$\frac{\triangle f_r}{f_r} = \frac{1}{2} \frac{\frac{\Delta \varepsilon_e}{\varepsilon_{e0}}}{1 + \frac{1}{2} \frac{\Delta \varepsilon_e}{\varepsilon_{e0}}} \tag{2.1}$$

Here,

ε_e = Effective dielectric constant with a dielectric layer

ε_{e0} = Effective dielectric constant without a layer

$\Delta \varepsilon_e$ = Change in dielectric constant due to the dielectric layer

$\triangle f_r$ = Fractional change in resonant frequency

f_r = Resonant frequency

The fractional change of resonance frequency obtained for optimum design at 10 GHz is 5.8%, 7.8%, and 16% for the different dielectric cover of polystyrene, ice and beryllium

oxide, respectively. They also found that, for the different dielectric layer with thickness more than 2 cm, the effect of dielectric loading on resonance frequency becomes smaller. However, with the increase of dielectric thickness, the return loss first increases and then decreases with the increase of dielectric thickness, as tabulated in Table 2.1.

Table 2:1: Experimental data of microstrip antenna parameter with dielectric superstrate [31].

Dielectric Cover	ε_{r1}	*d (cm)*	f_r *(GHz)*	*Return Loss(-dB)*	*Bandwidth (%)*
Air	1.0	=	4.104	32	2.17
Duroid	2.32	0.08	4.008	35	2.18
		0.159	3.934	26	2.22
		0.318	3.895	22	2.31
Plexiglass	2.6	0.112	3.952	33	2.18
		0.159	3.912	25	2.18
		0.318	3.874	22	2.20
Mylar	3.0	0.0064	4.070	37	2.18
		0.0128	4.058	39	2.18
		0.0384	4.010	40	2.20
Epsilam-10	10.2	0.0635	3.640	36	2.0
Custom High-k	10	0.154	3.482	24	1.75
		0.132	3.26	18	1.90

N.G. Alexopoulous [29] used Greens function and Somerfield method to propose that dielectrically loaded microstrip antenna offers increased gain, radiation resistance, and efficiency. They observed that by choosing the proper thickness of the cover, resonance

condition may be created to enhance the gain and radiation response over a substantial bandwidth. If the thickness of the dielectric cover is about half of operating wavelength, 100% efficiency may be achieved with a significant improvement in gain and radiation resistance. If the thickness of the dielectric cover is about half of operating wavelength, 100% efficiency may be achieved. In 1986 D. Shimin [27] first, analyze a rectangular microstrip patch antenna to measure the dielectric constant of a thin piece of substrates. Using a rectangular microstrip antenna, he has measured the dielectric constant of the substrate by monitoring the resonance behavior of the antenna.

In 1987 H. Y. Yang and N. G. Alexopoulos [30] also analyzed multiple dielectrics loaded printed circuit antennas using transmission line model. They considered a Hertzian electric dipole, which is entrenched in the substrate with multi-dielectrics. The proposed method achieved high gain (= 20 dB), which can be further increased by increasing the number of dielectric layers. However, this increase in gain is also associated with reduced bandwidth and bulkier antenna size. In the following year, A. Bhattacharya [31] reported that the impedance mismatch due to dielectric loading can be improved by shifting the feed point location. All other antenna parameters changed due to the loading of dielectric superstrate/cover. However, -10 dB return loss bandwidth did not change significantly with the dielectric thickness. In 1987 R. Q. Lee and A. J. Zaman et al [32], studied two-layer electromagnetic coupled microstrip antenna loaded with a dielectric layer of various thicknesses (0-0.16cm). It was found that in high gain region resonant input impedance increases and the 3-dB beamwidth decreases with the dielectric thickness, while resonant frequency and bandwidth decreases (17.1 GHz to 7.6 GHz). Besides, impedance matching becomes poor with dielectric thickness. Multiport network model [MNM] has been

extended to analyze a rectangular dielectric covered microstrip antenna. The substrate thickness is chosen to be much smaller than the wavelength (λ), so the fields underneath the patch have no variations in the Z-direction. The conductance 'G_r' and 'G_s' of a radiating edge are related to voltage distribution as follows:

$$G_{r,s} = \frac{2\,\mathrm{P}_{r,s}}{\frac{1}{b}\int_s V^2(\mathrm{s})\,\mathrm{ds}} \tag{2.2}$$

Where the integration is along the patch edge of length 'b', 'r' is radiation conductance and 's' is surface conductance and V(s) is the voltage distribution along the edge and 'Pr' is the radiated power. A modified Wolf model (MWM) was proposed in the year 1993 [33], to calculate the resonant frequency of dielectric-loaded microstrip antenna as well as multilayer resonating structures and results obtained are found to be very close to experimental data than that of full-wave analysis and almost in all cases, they are within 0.5% of published results for the fundamental mode and within 1.7% for other higher modes. It is basically cavity model, where the dynamic permittivity is calculated using the variational method. The MWM has also been applied on triangular and hexagonal patches and found useful tool for microwave Computer Aided Design (CAD) on patch antenna. The resonant frequency is calculated as follows:

$$f_r = f_{mn} = \frac{V_0}{2\sqrt{\varepsilon_{dyn}}}\left[\frac{m}{W_{eff} + L_{eff}}\right] \tag{2.3}$$

where all the parameters are defined in [33]. However, for rectangular microstrip antenna, complex resonant frequency varies more significantly, when the dielectric permittivity is greater than that of the substrate. The writer also published other papers [34], [35][36] on

the same subject area for the accurate dielectric constant measurement with different microstrip configuration shown in Figure 2.11.

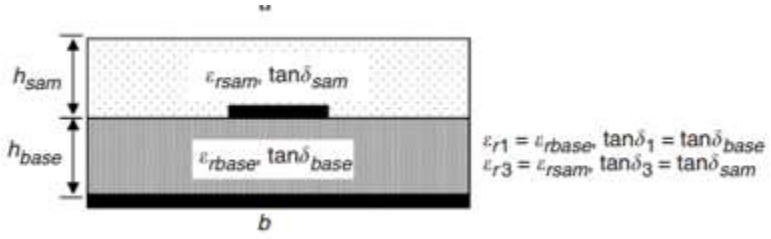

Figure 2.11: Microstrip resonator structure with dielectric cover [37].

Raj Kumar et al and Yang li et al [37]–[39] proposed a modified formula to calculate the resonant frequency of multilayered dielectric loaded microstrip antenna, given by;

$$f_r = \frac{c}{2(\mathrm{L}+2\Delta\,\mathrm{L})(\sqrt{\varepsilon_{eff}(\mathrm{f})})} \tag{2.4}$$

where, $$\varepsilon_{eff}(f) = \varepsilon_r' - \frac{\varepsilon_r' - \varepsilon_{eff}(0)}{1+P(f)} \tag{2.5}$$

$\varepsilon_{eff}(0)$ = effective dielectric constant

ε_r'= equivalent relative permittivity of single layer patch antenna

P(f) = frequency dependent factor

Their results indicate that, with increasing the dielectric thickness from 0.5 to 12.72mm, the resonance frequency decreases from 2.759 to 2.67 GHz and maximum change in 'f_r' is around 4% if the external dielectric thickness is chosen between 1 to 5 mm. However with increasing size of air gap, the resonant frequency is observed to increase.

Effects of dielectric cover on a rectangular MSA operating in TM_{10} mode have also been analyzed using Genetic Algorithm (GA)[40]. The Genetic Algorithm program for this purpose is developed using C++ language. Two addition parameters: 'ε_r' and 'h' of the dielectric is also taken as input in the optimization. The obtained results revealed that the variation of antenna properties (ε_r, h) resulted in changing resonance frequency and gain of the structure. The shift in resonant frequency of a rectangular microstrip antenna covered with a dielectric layer has also been analyzed by S. Chakraborty et al, using a neural network model [41]. The model proposed is faster and accurate than conventional methods, and results are found to be in good agreement with that of electromagnetic simulation based on the method of moments. H.A.Hammas [42], used the method of moments (MOM) to analyze the effects of dielectric loading on an aperture coupled antenna, and calculated antenna parameters, such as, radiation efficiency, half-power-beam-width (HPBW) and directivity. He has demonstrated that increasing dielectric thickness reduced the gain of the antenna.

Boybay et. al [43] proposed complementary split ring resonator for the dielectric characterization of planar materials. The sensor based on the rectangular CSRR structure etched at the ground plane to realize a stopband filter shown in Figure 2.12. The sensor measured the shift in minimum reflection coefficient and the minimum transmission coefficient as a function of the permittivity of the sample material. Their experimental results found the shift of the minimum transmission frequency from 1.3 to 0.8 GHz as the sample permittivity change from 1 to 10.

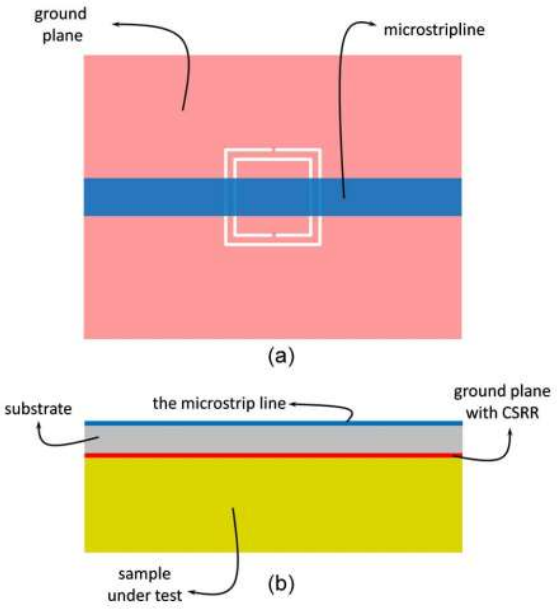

Figure 2.12: The CSRR sensor structure (a) top view (b) Cross section of side view; the sample is placed under the ground plane of the microstrip line.

Chin-Lung Yang et. al [44] analyzed single-compound triple complementary split-ring resonator (SC-TCSRR) for the determination of material complex permittivity and thickness from the resonance frequency, as shown in Figure 2.13. The advantage of this technique is that it facilitates dielectric measurement even if an air gap exists between the sample and the sensor. Such as, for a 0.2-mm air gap the observed measurement errors are 4.32% and 5.05% for the substrate thickness and permittivity, respectively. This technique are used for sensing phase functions in liquid mixture and biological tissue [45]–[56].

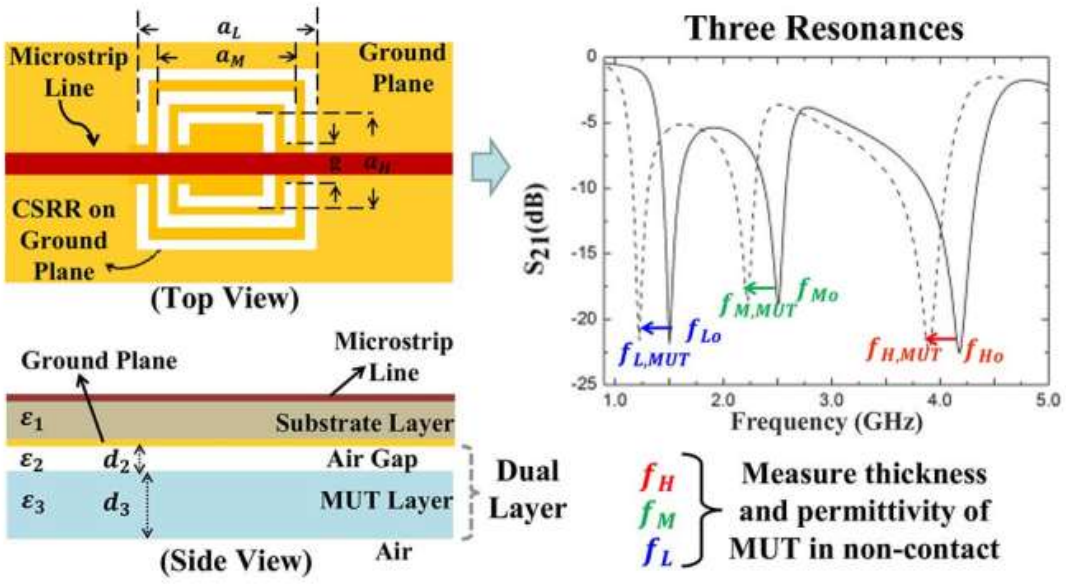

Figure 2.13: The triple resonance frequency SC-TCSRR sensor used for detecting the permittivity and thickness of a MUT layer under noncontact conditions.

2.5 SEMI-CYLINDRICAL CAPACITIVE SENSOR

Often microwave sensing is relatively costly and requires heavy equipment, like high power microwave generator, Network Analyzer etc. But a low-frequency sensing method utilizing a capacitive sensor can offer several benefits; less expensive, portable, and linear relationship between the dielectric constant and measured capacitance. Parallel plate capacitor has been used for a long time for the dielectric constant measurement of planar samples. The magnitude of the capacitance depends on the electrode surface area, the distance between the electrodes and dielectric constant of the material between the plates. However, this parallel plate is not suitable for cylindrical palm tree samples. To solve this problem a semi-cylindrical capacitor is used in this project. Cheng-Ta Chiang et. al [57] used a similar semi-cylindrical capacitor, shown in Figure 3.10, to monitor phase fractions

of the multi-phase fluid mixture. They establish a numerical method to calculate the capacitance of the semi-cylindrical structure. A. Jaworek et. al [58] proposed an RF resonance sensor in the form of two semi-cylindrical electrodes for gas/liquid volume measurements. In reference [59], [60], a similar semi-cylindrical capacitive sensor has been proposed for the measuring the water cut within a petroleum transporting pipeline. The design and application of a semi-cylindrical capacitive sensors to measure the moisture contents of soil are also presented in referent [59]. Table 2.2 lists different types of the semi-cylindrical capacitance sensors based on their application.

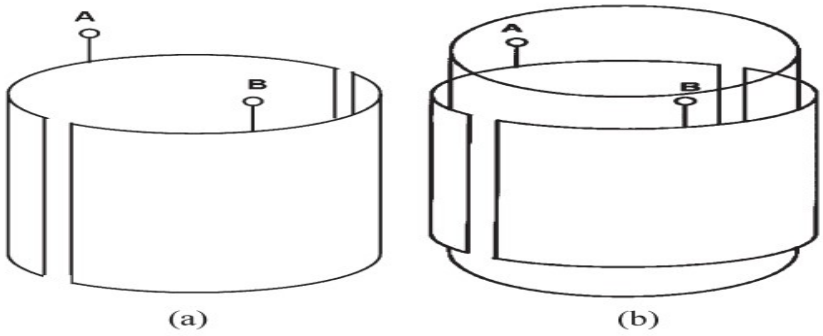

Figure 2.14: Geometry of the semi cylindrical capacitive sensor with and without dielectric fluid [57].

Table 2:2: Summary of Semi-cylindrical capacitive sensor references.

Sensor Type	Reference Number	Applications
Semi-Cylindrical Capacitive sensor	[57]	Fluid flow rate measurement
	[58]	Gas/liquid volume measurements
	[59]	Soil Moisture Measurement
	[60]	Liquid level measurement
	[61]	Measurement of Water Content in Crude Oil

CHAPTER 3

3 MICROWAVE RESONANCE BASED DETECTION OF RPW INFECTED PALM TREE

In this chapter, microwave resonance based detection is used to identify the red palm weevil (RPW) infestation of date palm trees. Typically, the material characteristics of the tree trunk (density, moisture content, bug infestation) affects its dielectric properties, which in turn interacts differently with propagating microwave signal. This principle is exploited here by optimally integrating the tree trunk as a superstrate of a microstrip patch antenna, thus creating a microwave resonator. With known dielectric properties of the healthy and damaged tree-trunk samples, monitoring the resonance behavior of this resonator should allow us to indentify the tree-trunk as healthy, partially-damaged or damaged. Commercial High Frequency Structure Simulator (HFSS) software is used to optimize the resonator and observe the resonant behavior of the structure. The prototype of the resonator is fabricated using LPKF circuit board plotter and tested using network analyzer and flatbed antenna radiation pattern measurement system. Before going into the design and experimental process in the following section I am going to review the background of the dielectric resonator and microstrip patch antenna.

3.1 MICROSTRIP ANTENNA

The history of microstrip antenna goes back to early 1950. The microstrip antenna is also known as a printed antenna. It is a simple geometry consists of a dielectric substrate with a conducting ground plane in bottom side and a conducting patch radiator on the top side.

This radiating patch can take various shapes like rectangular, circular, regular polygon, annular ring etc. A simple geometry of rectangular microtip antenna shown in figure 3.1.

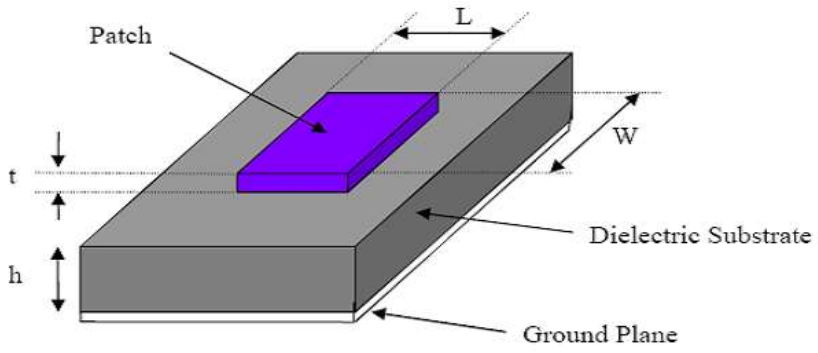

Figure 3.1: Basic structure of a rectangular microstrip antenna.

The microstrip antenna offers many advantages like low profile, easy to design, fabricate and integrate etc. But the inherent narrow-band properties of this class of antenna often limits its use in certain applications [60].

3.2 METHODS OF ANALYSIS OF MICROSTRIP ANTENNA

There are various methods for analyzing and designing microstrip antennas. Popular methods for designing rectangular microstrip antennas include [60], [61]:

1. Transmission Line Model
2. Cavity Model
3. Full Wave Model

Transmission line model provides a very lucid conceptual picture of the simplest implementation of a rectangular microstrip antenna. In transmission line model, the microstrip antenna consists of a microstrip transmission line with a pair of slots at either

end. Microstrip can be seen as a non-homogeneous line of two dielectrics: substrate and air, where most of the electric fields lines reside in the dielectric substrate and parts of field lines in the air. Therefore, the transmission line cannot support pure TEM mode and patch edges undergo fringing as shown in Figure 3.2.

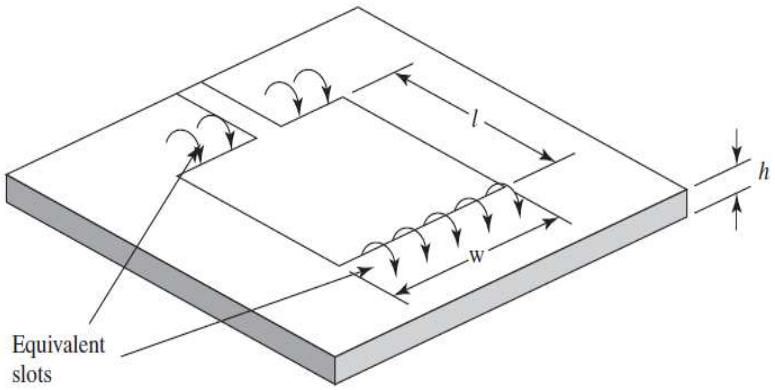

Figure 3.2: Transmission line model with fringing effect [6].

An effective dielectric constant need to obtain for accounting the fringing fields and wave propagation in the line. The effective dielectric constant can be calculated as follows [60]:

$$\epsilon_{reff} = \frac{\epsilon_r+1}{2} + \frac{\epsilon_r-1}{2}\left[1 + 12\frac{h}{e}\right]^{-1/2} \tag{3.1}$$

In cavity model, the region between the patch and the ground plane is treated as a cavity. The fringing fields around the periphery are taken care of by extending the patch length outward slot that the effective dimension becomes is larger than the physical dimension by ΔL. In the literature, equations used to calcualte ΔL is given by [60]:

$$\frac{\Delta L}{h} = 0.412\frac{(\epsilon_{reff} + 0.3)(\frac{W}{h} + 0.264)}{(\epsilon_{reff} - 0.258)(\frac{W}{h} + 0.8)} \tag{3.2}$$

Thus, the resonance frequency of the patch antenna fundamental mode TM_{01} can be calculated as follows [60]:

$$f_c = \frac{v_o}{2(L + 2\Delta L)\sqrt{\varepsilon_{reff}}} \tag{3.3}$$

where v_0 is the speed of light at free space. The patch width 'W' and physical length 'L' with good impedance matching and radiation characteristic can be calculated from [60];

$$W = \frac{v_o}{2f_r}\sqrt{\frac{2}{\varepsilon_r + 1}} \tag{3.4}$$

$$L = \frac{v_0}{2f_r\sqrt{\varepsilon_{reff}}} - 2\Delta L \tag{3.5}$$

Above equations are widely used in designing microstrip resonators excited by patch antennas.

3.3 ANALYSIS OF SUPERSTRATE BASED RESONATOR

The basic structure of microstrip patch resonator is shown in Figure 3.3. It consists of dielectric substrate of permittivity ε_1 and height h_1, which has the ground plane on one side and copper patch on the other side. The dimension of the radiating patch is identified by length L and width W, where W≥L. Above the patch there could be any numbers of dielectric layers of complex permittivity. In our design, the dielectric layer consisted of either healthy, partially-damaged or damaged tree-trunk samples. Since, practically the tree trunk is considerably larger compared to the patch antenna, the calculation of resonant frequency will consider infinitely wide superstrate in horizontal xy-plane. In our design the

patch is excited by coaxial probe and the distance of the feed location from the patch edge is 'y_0', along the patch length.

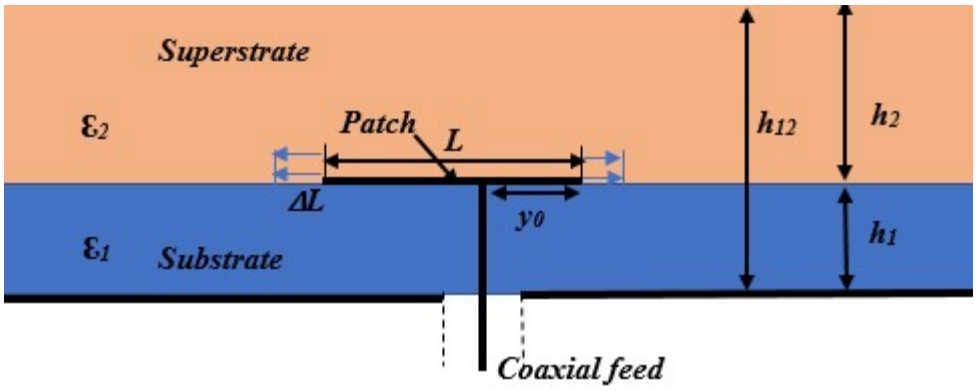

Figure 3.3: Side cross-sectional view of the coax feed patch resonator with superstrate.

The microstrip patch being a finite rectangular conductive sheet separated from an infinite ground plane by a finite dielectric layer produce standing electromagnetic wave in the substrate region between the patch and the ground plane. The inverse of the natural wavelength of the standing wave is proportional to the resonant frequency of the patch. But the resonant frequency also influenced by the parameters of the superstrate layer. In the absence of a superstrate layer, the resonance frequency for this rectangular resonator structure can be written as [60]:

$$f_0 = \frac{c}{2(\mathrm{L}+2\Delta L)\sqrt{\varepsilon_{eff\,0}}} \tag{3.6}$$

where, c is the speed of light in free space, L is the physical length of the patch, $\Delta L = \frac{h}{\sqrt{\varepsilon_{eff\,0}}}$ is length extension due the resultant of the fringing fields and $\varepsilon_{eff\,0}$ is an effective dielectric

constant. The effective permittivity of the patch can be calculated from the resonant frequency as [60];

$$\varepsilon_{eff0} = \left(\frac{c}{2(\mathrm{L}+2\Delta L) f_0} \right)^2 \tag{3.7}$$

Now to include the effect of the superstrate layer, the following equation is used to estimate the effective permittivity due to substrate and superstrate material;

$$\varepsilon_{eff1} = \varepsilon_{eff0} \left(\frac{f_0}{f_1} \right)^2 \tag{3.8}$$

Various numerical techniques can be used to solve the microstrip structures with superstrate. They include variational method, Methods of moment, conformal mapping approach [62]–[64]. Since conformal mapping require lowest computation time it is selected in this study to solve the structure. To account the fringing field effects for a given microstrip line using conformal mapping, the effective width of microstrip can be calculated as;

$$w_{eff} = w + \frac{2h_1}{\pi} \ln \left[17.08 \left(\frac{w}{2h_1} + 0.92 \right) \right] \tag{3.9}$$

The filling factor q_1 for a substrate layer can be written as;

$$q_1 = 1 - \frac{1}{2} \frac{\ln \left(\frac{\pi}{h_1} w_{eff} - 1 \right)}{\frac{w_{eff}}{h_1}} \tag{3.10}$$

The filling factor for superstrate layer can be obtained as;

$$q_2 = 1 - q_1 - \frac{1}{2}\frac{h_1 - v_e}{w_{eff}}.\ln\left[\pi\frac{w_{eff}}{h_1}\frac{\cos\left(\frac{v_e}{2}\frac{\pi}{h_1}\right)}{\pi\left(\frac{h_2}{h_1}-\frac{1}{2}\right)+\left(\frac{v_e}{2}\frac{\pi}{h_1}\right)}+\cos\left(\frac{v_e}{2}\frac{\pi}{h_1}\right)\right] \tag{3.11}$$

whereas, the quantity factor (v_e) is written as;

$$v_e = 2\frac{h_1}{\pi}\arctan\left[\frac{\pi}{\frac{\pi}{2}\frac{w_{eff}}{h_1}-2\left(\frac{h_1}{h_2}-1\right)}\right] \tag{3.12}$$

where, '**w**' is a physical width of patch and 'h_1', 'h_2' are the thicknesses of substrate and superstrate, respectively. Effective dielectric constant of the dielectric loaded structure,

written as;

$$\varepsilon_{eff1} = \varepsilon_{r1}q_1 + \varepsilon_{r2}\frac{(1-q_1)^2}{\varepsilon_{r2}(1-q1-q2)+q_2} \tag{3.13}$$

Once the superstrate loaded effective permittivity is found, then dielectric constant of superstrate material can be found by;

$$\varepsilon_{r2} = \frac{q_2}{q_1+q_2-1+\frac{(1-q_1)^2}{\varepsilon_{eff1}-\varepsilon_{r1}q_1}} \tag{3.14}$$

3.4 DESIGN OF THE RESONATOR AND SIMULATION RESULTS

Since the designed S-band (2-4 GHz) microstrip resonator consisted of microstrip patch antenna and tree-trunk as a superstrate, the design detail of the patch exciter is discussed here. Following the model discussed in previous section the physical microstrip patch antenna sensor is designed using professional electromagnetic simulator Ansys HFSS. Our final design is guided by two criteria. First, from theoretical discussion, air has the lowest dielectric constant and if considered as a superstrate should produce a resonance as the highest end of the S-band (i.e. at 4GHz). Second, the patch dimension should be large enough to adequately excite the tree-trunks to generate reasonable reflection response. Satisfying these criteria, we have designed the patch antenna to operate at 4GHz using a RT/Duroid5880 substrate with ε_r=2.2, loss tangent (tanδ) =0.0009 and h=1.6mm. The designed coaxially excited 4GHz antenna is optimized using HFSS simulator and the optimized version is shown in Figure 3.4. To reduce the diffraction and scattering effect from the edge of the ground plane as well as to minimize surface wave the ground plane and the substrate was chosen to be at least three times the rectangular patch.

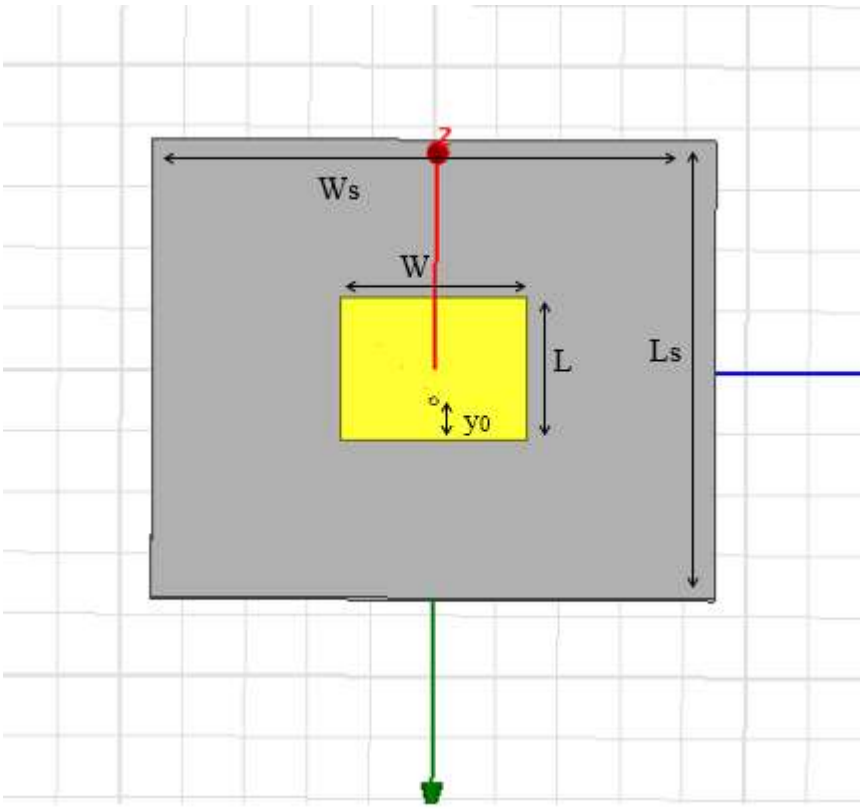

Figure 3.4: HFSS microstrip resonator configuration.

The design specifications for the patch antenna are given in Table 3.1. The simulated reflection coefficient of the patch with air superstrate is shown in Figure 3.5. Note that the natural resonance frequency observed is at 4.0GHz. The radiation pattern of the designed prototype is plotted in Figure 3.6.

Table 3:1: Patch sensor parameters for optimized S11

Parameter	Dimension	Units
Patch length, L	23.30	mm
Patch width, W	29.65	mm
Substrate/Ground length, Ls	75	mm
Substrate width/Ground, Ws	90	mm
Substrate height, h	1.6	mm
Substrate Permittivity, Ɛr	2.2	
Feed pin radius	0.6	mm

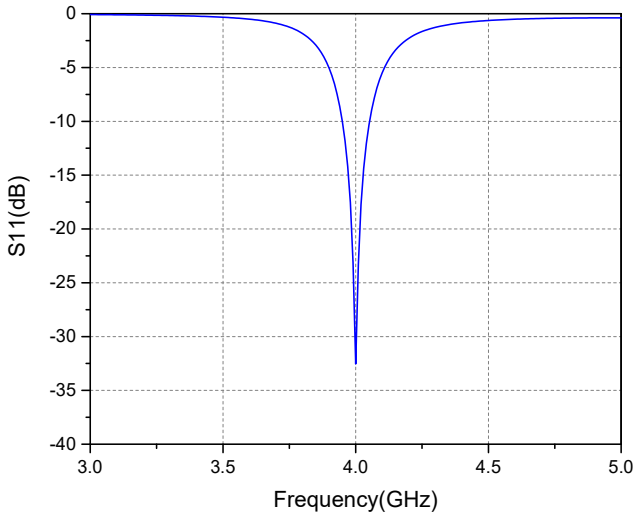

Figure 3.5: Microstrip patch resonance in air superstrate.

3.5 SIMULATION RESULTS FOR DIFFERENT SUPERSTRATES

To observe the effects of different superstrate on patch resonance, the proposed design shown in Figure 3.7 has been analyzed using a superstrate (dielectric cover) of thickness 1.6 mm with different dielectric constants of 2.2, 4.5 and 9.8. The observed resonance

responses are shown in Figure 3.8 and the corresponding data are also tabulated in Table 3.2.

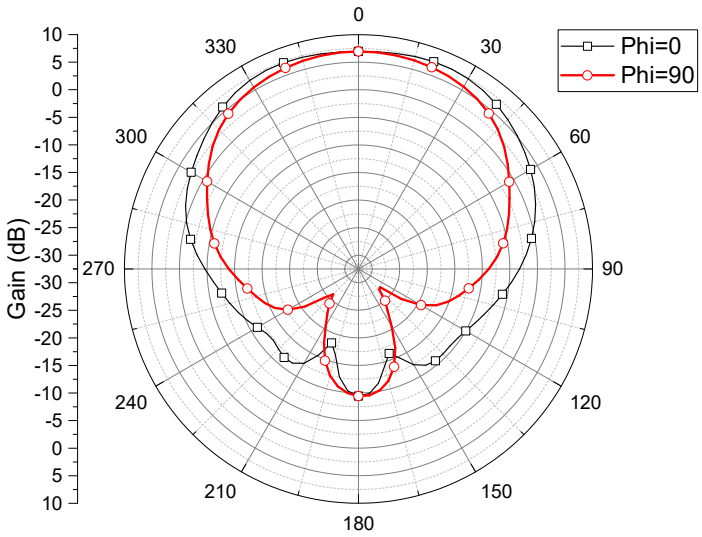

Figure 3.6: Radiation pattern of the microstrip patch at 4GHz

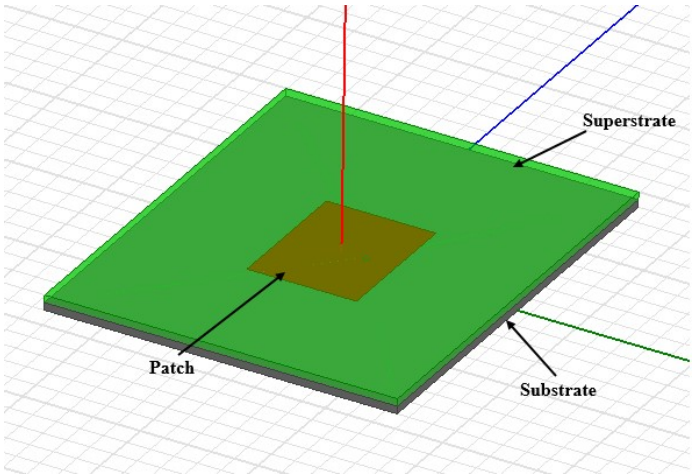

Figure 3.7: Microstrip patch antenna with a superstrate or dielectric cover.

Table 3:2: Microstrip resonator characteristics with dielectric loadings.

Dielectric materials	Dielectric constant, ε_r	Resonance frequency, f_r(GHz)	Shift in f_r (%)	Return loss (dB)	Phase at minimum, f_r (Degree)
Air	1	4	0	-33.72	0
Duroid	2.2	3.86	3.5	-24.21	11.64
TMM4	4.5	3.65	8.75	-21.48	24.92
TMM10i	9.8	3.33	17.5	-15.93	43.21

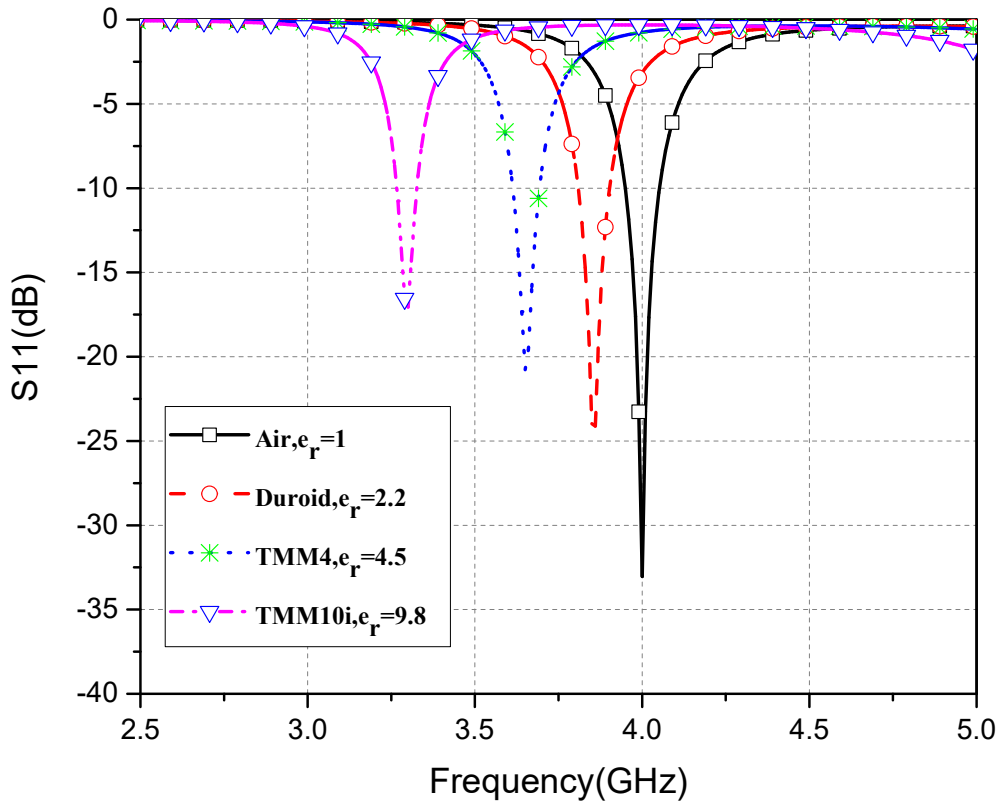

Figure 3.8: Reflection response of the resonator with different Ɛr of the dielectric superstrate.

From the simulated results it can be concluded that resonant frequency is highly sensitive to the superstrate dielectric constant (ε_r) as it shifted by 20% (max) from the original design frequency. The reduction in the magnitude of the S11 values are due to increased impedance mismatch with changing superstrate dielectric constants. Figure 3.9 plots the reflection phase response of the resonator for changing dielectric constants of the superstrate. Note that for the TMM10i superstrate, the phase jump to about 43^0.

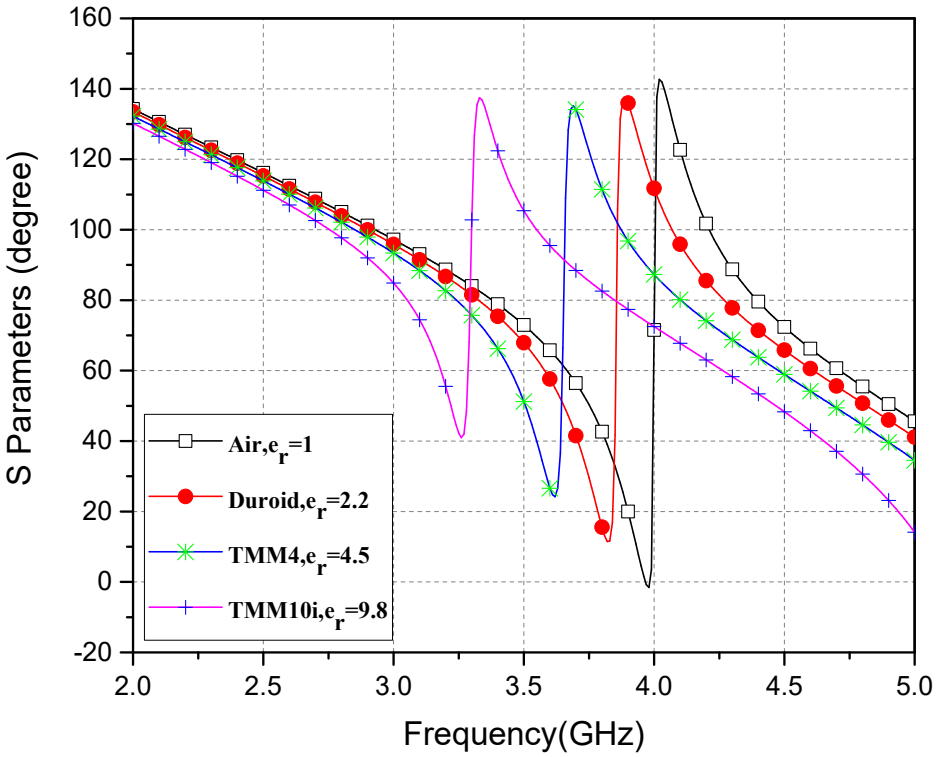

Figure 3.9: Phase of the reflection coefficient with changing ε_r of the superstrate.

3.6 DATE PALM TRUNK AS DIELECTRIC SUPERSTRATE

In this section, we will model date palm tree sample as a dielectric superstrate and study how it's affecting the resonance behavior of the microstrip resonator. Since the designed low power resonator can only scan portion of the tree at a time, we have prepared tree samples with a width of $1/6^{th}$ of the tree diameter. For simulation, we use the dielectric constant of healthy date tree sample ε_r= 34.9. The resonator structure with tree superstrate is shown in Figure 3.10 and simulation results for the thickness of 10mm, 30mm and 50mm are shown in Figure 3.11.

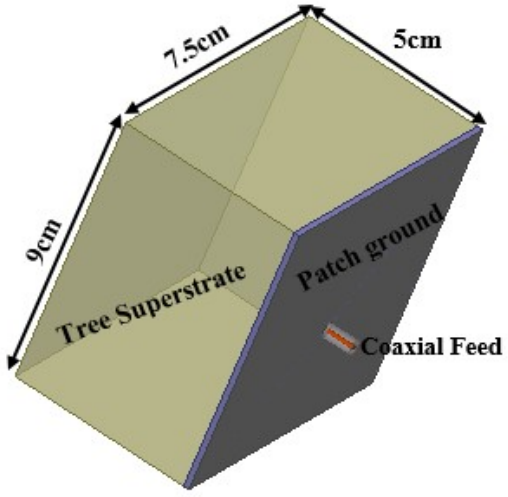

Figure 3.10: Patch resonator with wood superstrate.

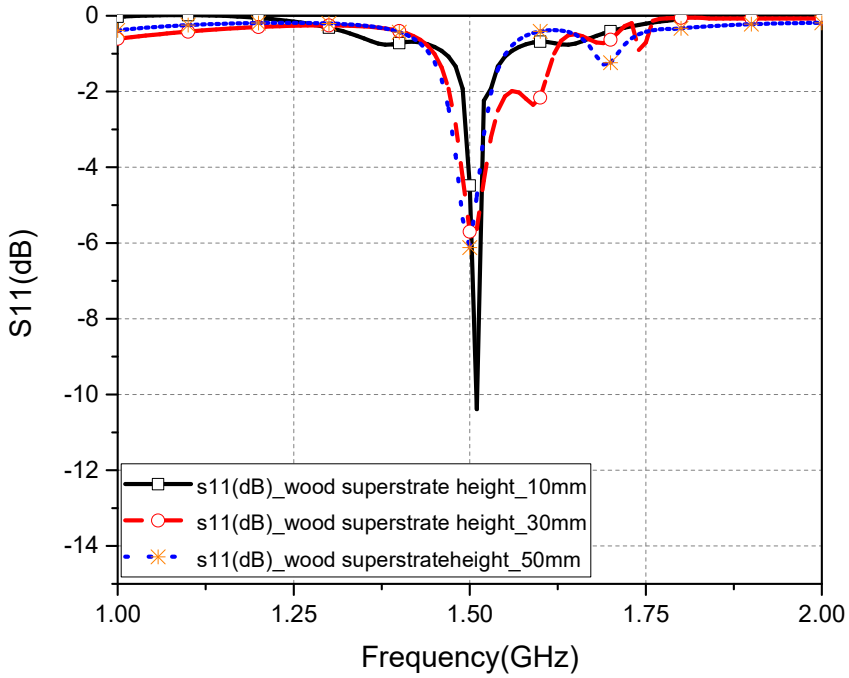

Figure 3.11: Patch resonator sensitivity with superstrate thickness

Figure 3.12 shows the effect on return loss, S_{11} of the microstrip resonator for changing the thickness of wood superstrate. Note that by increasing thickness of wood superstrate resonance frequency does not change. However, the return loss becomes poor with increasing superstrate thickness. It is also noted that increasing superstrate thickness over 50mm impedance matching fail abruptly and become uncontrollable, therefore, the design system would be useful to scan up to 50mm of wood thickness.

3.7 OPTIMIZATION AIR SPACING BETWEEN PATCH AND WOOD SUPERSTRATE

In this section, we will study the effect of the air gap between patch and wood superstrate on the resonance frequency of the microstrip resonator. The simulation is performed for the similar structure shown in Figure 3.10 with wood superstrate thickness of 50mm but in this case, the superstrate spaced away from the patch with variable distance. Figure 3.12 shows the effect on return loss, S_{11} of the microstrip resonator for changing air gap spacing between patch and wood superstrate, optimum S_{11} obtained at 0.8mm.

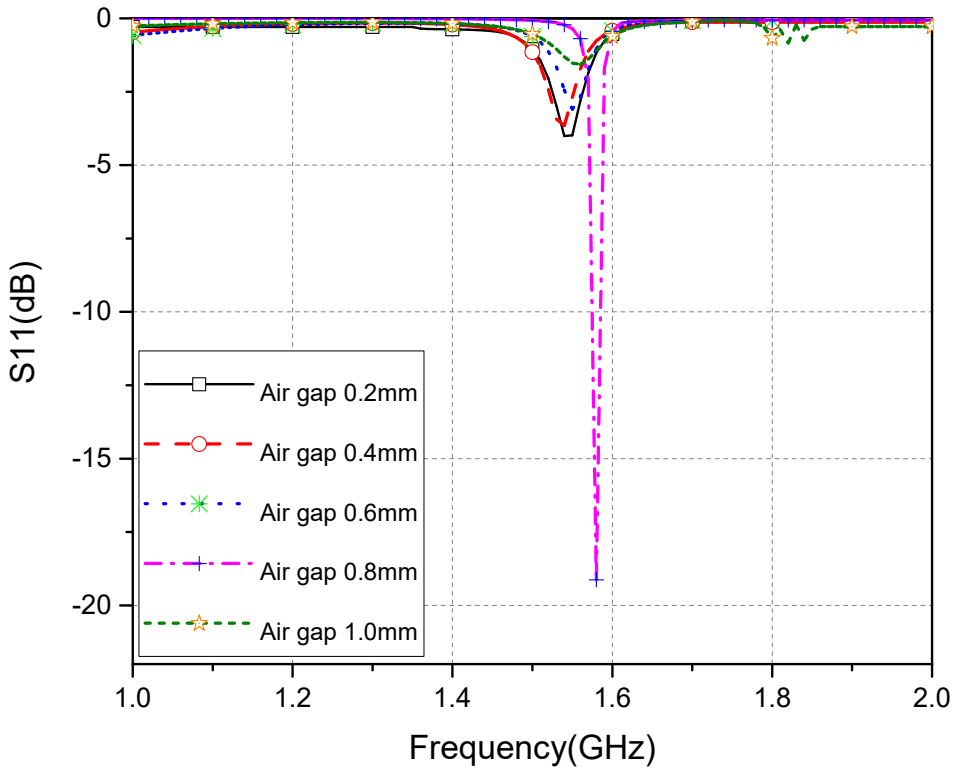

Figure 3.12: Reflection coefficient for spacing between patch and wood superstrate.

3.8 MODEL OF INFESTED PALM TREE AND RPW WEEVIL

To model the infested tree sample, if we look closely, we can see date tree is composite of fiber and pours for water transfer from root to the crown as well as air holes, which need to consider in our design. Practically, the outer surface of the palm tree is intact that is the dielectric properties same as healthy palm tissue and inside the tree trunk is infested due to the presence of weevil. These weevils chew the trunk tissue and secrete watery substance; therefore, the dielectric properties will be different inside the tree trunk from the outside surface. Our system is designed for local scanning at a time and not for hole tree. We model the tree sample as a 3D structure with dimension (75mm x90mm x50mm) and dielectric properties are of healthy tissue 34.9. Where model of damage tissue/weevil as a cylinder radius 3mm and height 50mm and clustered randomly inside the tree sample with dielectric constant 50.25. Figure 3.13 and 3.14 shows the model of infested tree sample and simulation results for the various volume fraction of infestation.

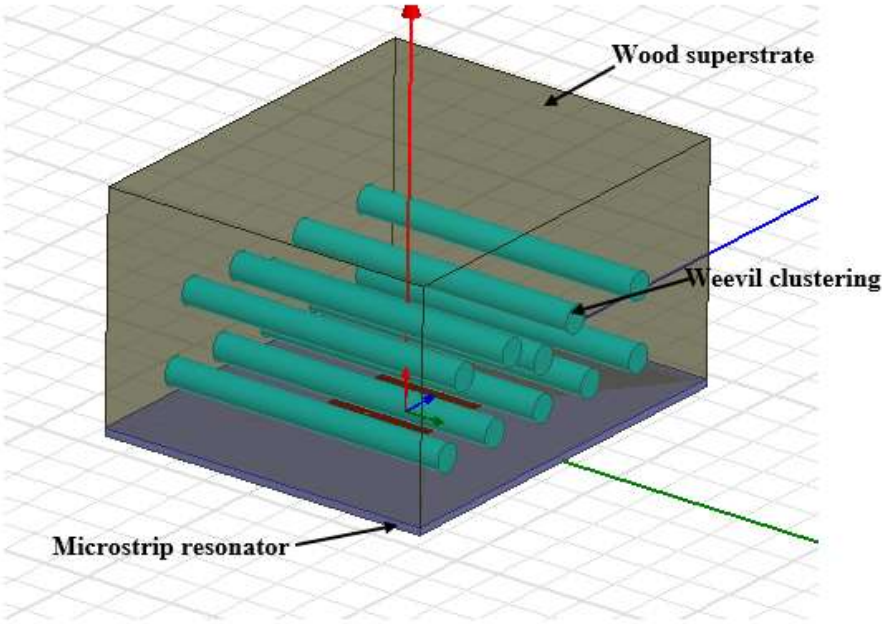

Figure 3.13: HFSS model for infested tree sample.

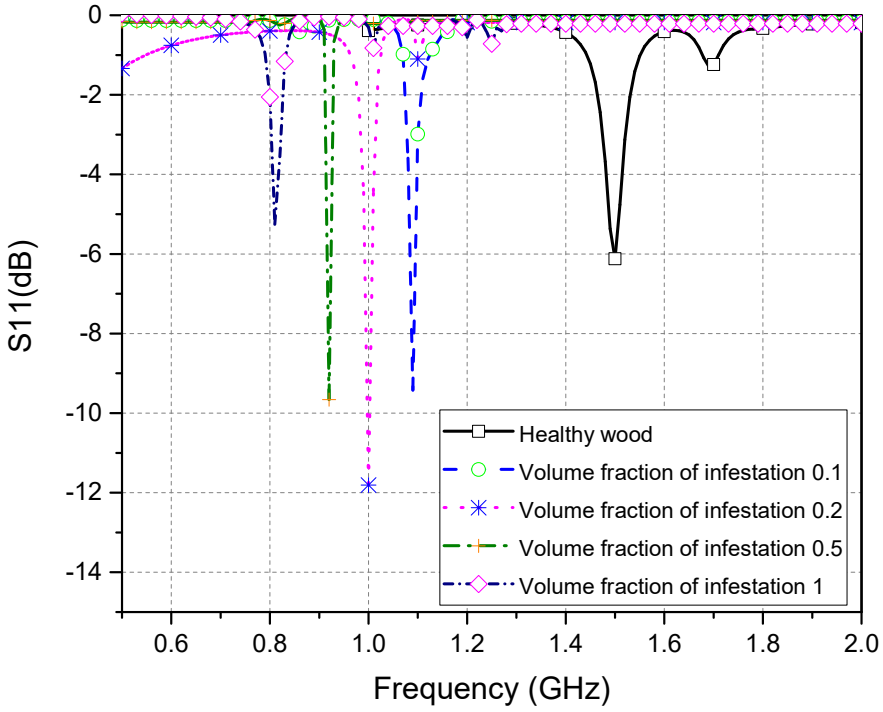

Figure 3.14: Shift of resonance frequency for changed volume fraction of infestation

3.9 EXPERIMENTAL RESULTS

This section demonstrates process involved in fabricating the prototype and experimental verification. The facilities available in the electrical engineering department in KFUPM are used to fabricate the prototype. Vector network analyzer and flatbed antenna radiation pattern measurement system are used to experimentally observe the scattering and radiation response of the resonator.

3.9.1 FABRICATION PROCESS

The optimized microstrip resonator is fabricated using LPKF ProtoMat S62 milling machine. This machine is capable of fabricating single and double-sided printed circuit boards precision with system resolution as fine as 0.01 mils (0.25 μm). Figure 3.15 shows the LPKF machine located in the EM lab of KFUPM. The fabrication process starts by exporting the CAD file from HFSS and importing it to LPKF's CircuitPro software. In this software, different layers are assigned in addition to insulating to the circuit components. Then the file is exported to BoardMaster software, where according to the the milling and drilling dimensions, locations and tools the printed circuit is plotted. The whole for coaxial feeding is also accurately implemented by this machine. The fabricated microstrip antenna is shown in figure 3.16.

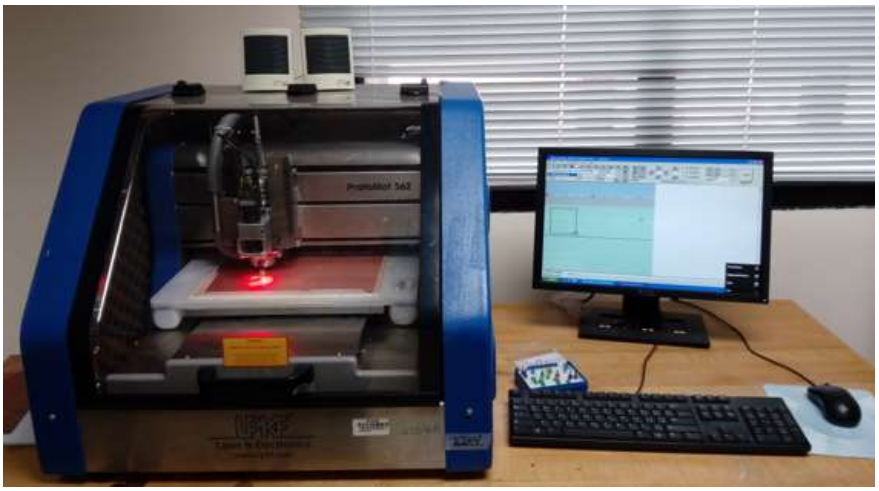

Figure 3.15: Fabrication setup: LPKF Protomat S62.

Figure 3.16: Front and back picture of the fabricated microstrip resonator.

3.10 MEASUREMENT SETUP

3.10.1 MEASUREMENT OF S-PARAMETER (S11)

Keysight Agilent E5071C network analyzer, available in Microwave Lab of KFUPM, is used to measure the reflection coefficient of the microwave sensor. The vector network analyzer, shown in Figure 3.17, can operate up to a frequency range of 20 GHz. This is an

important measurement device for any microwave engineer and extensively used to measure the reflection and transmission characteristics of active and passive circuits. Note that calibration of the network analyzer is essential before any measurement to eliminate the effects of the probes and connectors. The collected data table from the network analyzer is imported to Origin-Lab software to generate the required plots.

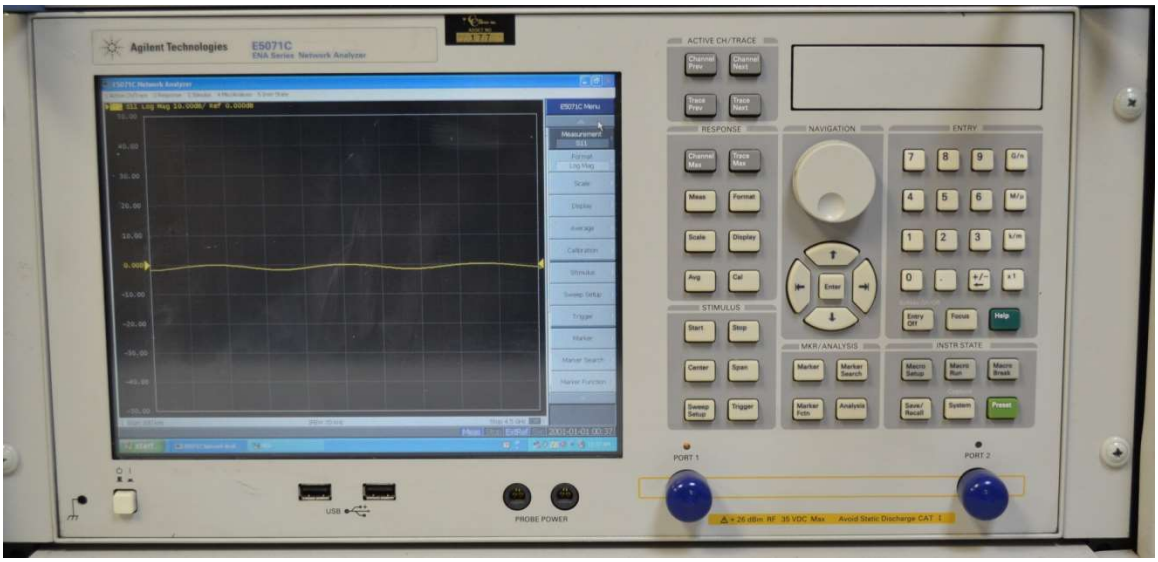

Figure 3.17: S-parameter measurements of the antenna using 20 GHz Vector network analyzer.

At first, the reflection coefficient measurements are made without the presence of tree-trunk superstrate. Figure 3.18 shows the measured reflection coefficient of the patch antenna without air superstrate. Figure 3.19 superimposed the measured and simulated reflection response of the antenna for comparison purposes. The experimental result at f_r=4.22 GHz is slightly shifted from the simulated f_r=4.0 GHz mostly due to fabrication errors.

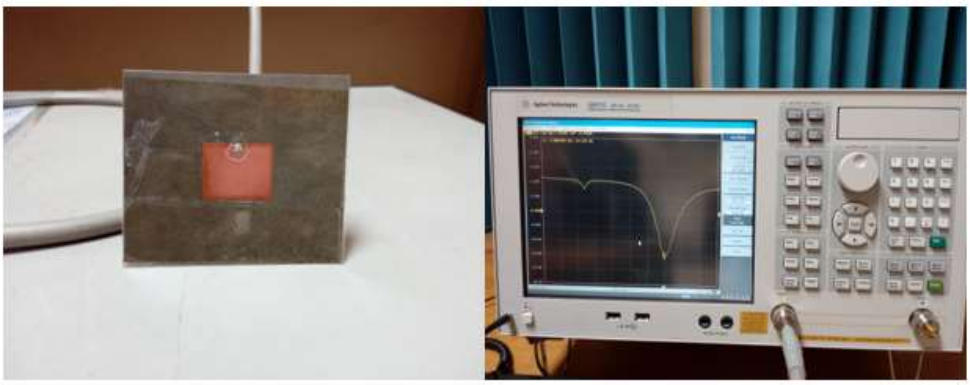

Figure 3.18: Reflection response (S11) measurement set up.

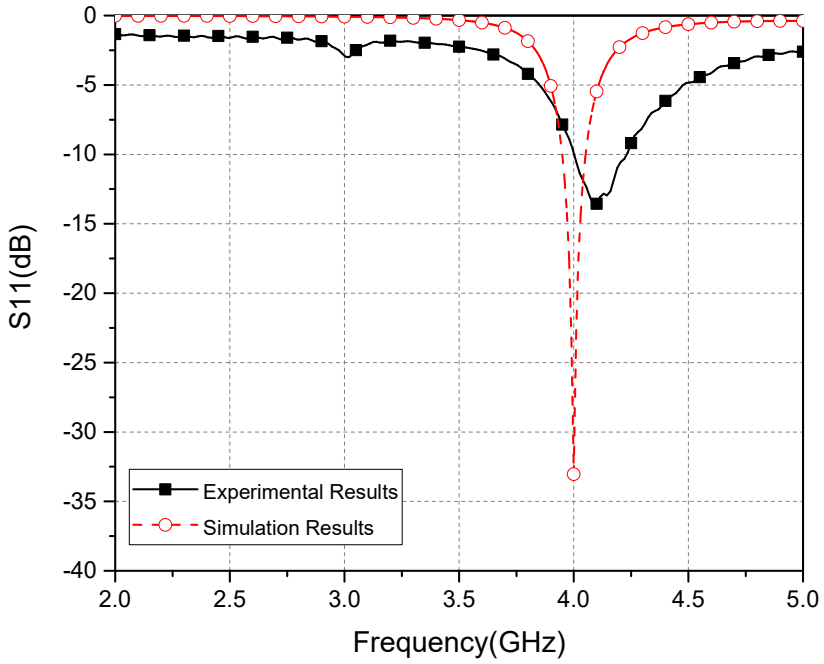

Figure 3.19: Reflection response of fabricated antenna without superstrate.

3.11 RADIATION PATTERN MEASUREMENTS

RFxpert flatbed antenna radiation patterns measurement device is used to monitor the radiation pattern of the antenna. This device is connected to a PC with special software to visualize both far-field and near-field real-time measurements. The working principle of this device can be described as follows, the flatbed consists of planar antenna with 384 elements which measure the near field response. The far field radiation patterns then calculated and displaced in the monitor through interface software. One of the advantage of this device is it does not require anechoic chamber and no need of rotatable antenna radiation pattern measurement setup.

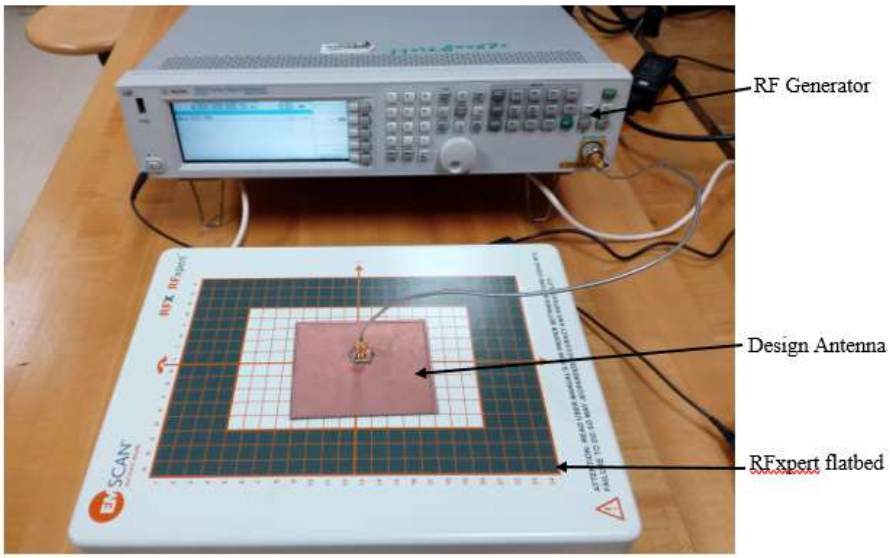

Figure 3.20: The Radiation pattern measurement setup in KFUPM lab.

Figure 3.20 shows the RFxpert measurement setup, which consists of an RF source and RFxpert scanner. Figure 3.21 and Figure 3.22 shows the simulated and measured elevation and Azimuthal plane radiation patterns of the antenna, respectively.

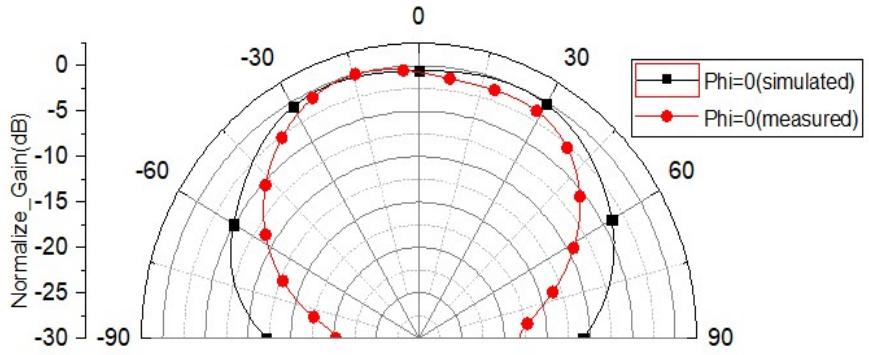

Figure 3.21: Radiation pattern of fabricated antenna at Phi=0 plane.

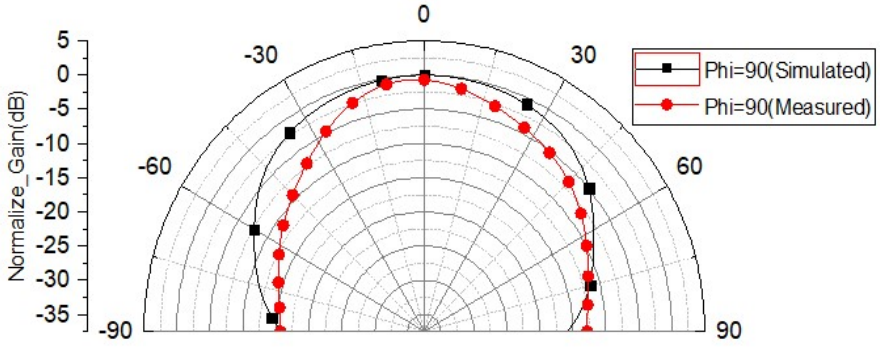

Figure 3.22: Radiation pattern of the fabricated antenna at Phi=90 plane.

3.12 COLLECTION OF THE DATE TREE TRUNK SAMPLES

To investigate the effect of the date palm tree-trunk as a superstrate, four samples are prepared with a dimension of 11cm x 9cm x 8cm, which is little larger than the simulated superstrate dimension. Figure 3.23 shows the picture of the tree-trunk samples. Note that as discussed in chapter two, the RPW infested damaged tree-trunk is highly moisturized due to chemical secretion by larva and fermentation due to bacteria, as shown in sample 1

of the figure. Although not visible, this sample has holes produced by weevil infestation. The 2nd sample I this figure represents a normally damaged dead date tree-trunk, which is totally dried and demonstrate a dielectric behavior of ordinary wood. The 3rd samples in the figure represent healthy tree-trunk with uniform fibers and have water contents, which is transported by the try trunk from the ground to top part of the tree. The 4th sample is a partially damaged tree-trunk where weevil infestation is produced small holes and limited fermentation.

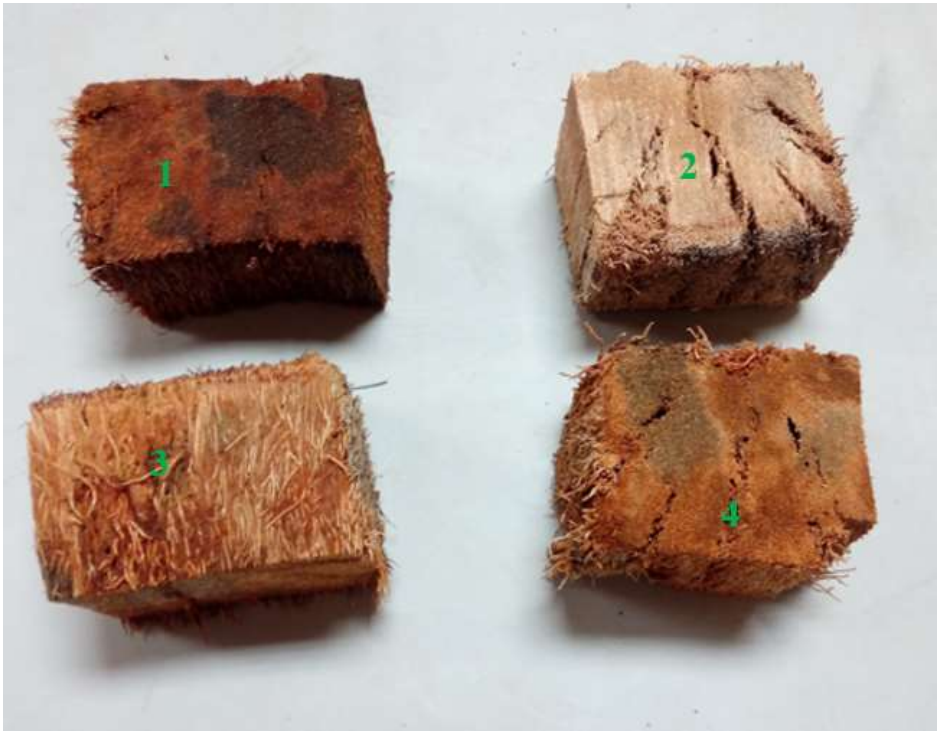

Figure 3.23: Date tree samples: (1) Highly moisturized damage tree-trunk; (2) Dry wood equivalent to normal damage tree ;(3) healthy tree-trunk; (4) Partially damaged tree-trunk sample.

The setup for the experimental procedure is shown in Figure 3.24. A test fixture comprised of microstrip patch sensor with tree trunk superstrate and connected to a VNA with SMA

cable. To avoid reflection of the antenna signal from surrounding objects, microwave absorbers are optimally placed in the experimental setup. The recorded reflection coefficients for all samples are plotted in the following figures.

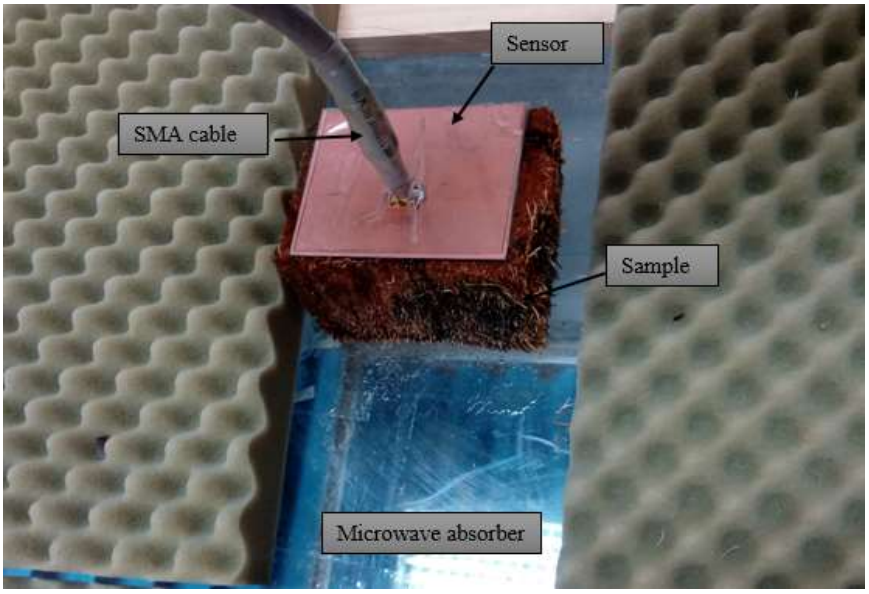

Figure 3.24: Experimental setup SMA cable, patch antenna sensor, wood sample, and microwave absorbing material.

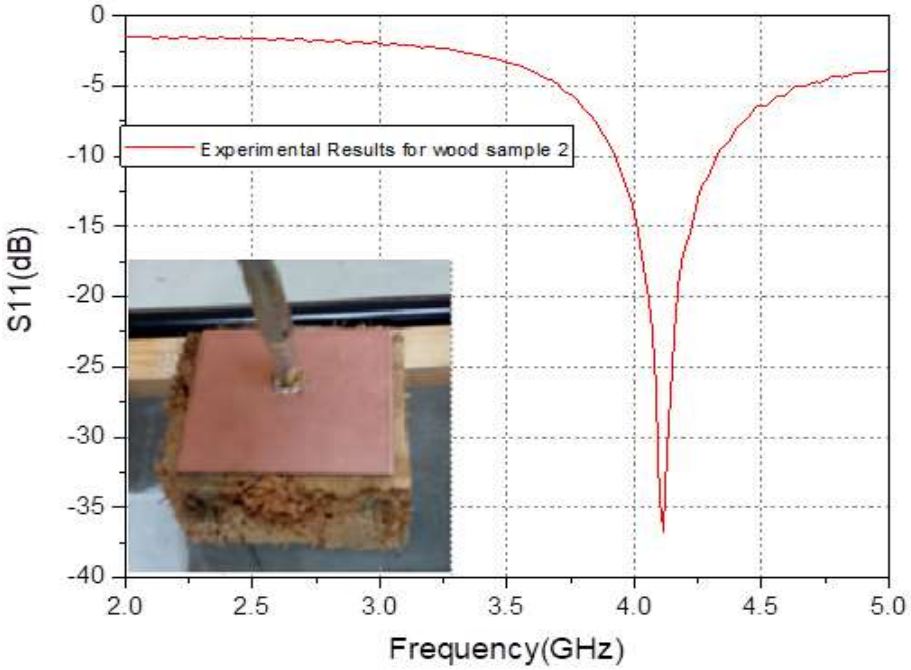

Figure 3.25: Experimental reflection response (S11) for a naturally dead palm tree-trunk (sample 2).

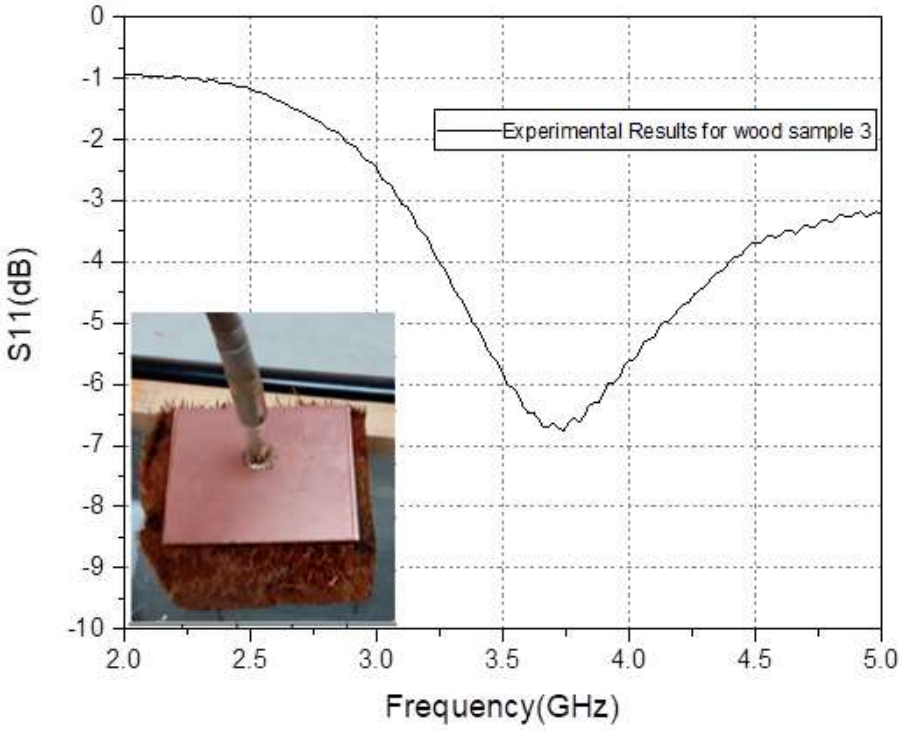

Figure 3.26: Experimental reflection response (S11) for a healthy palm tree-trunk (sample 3)

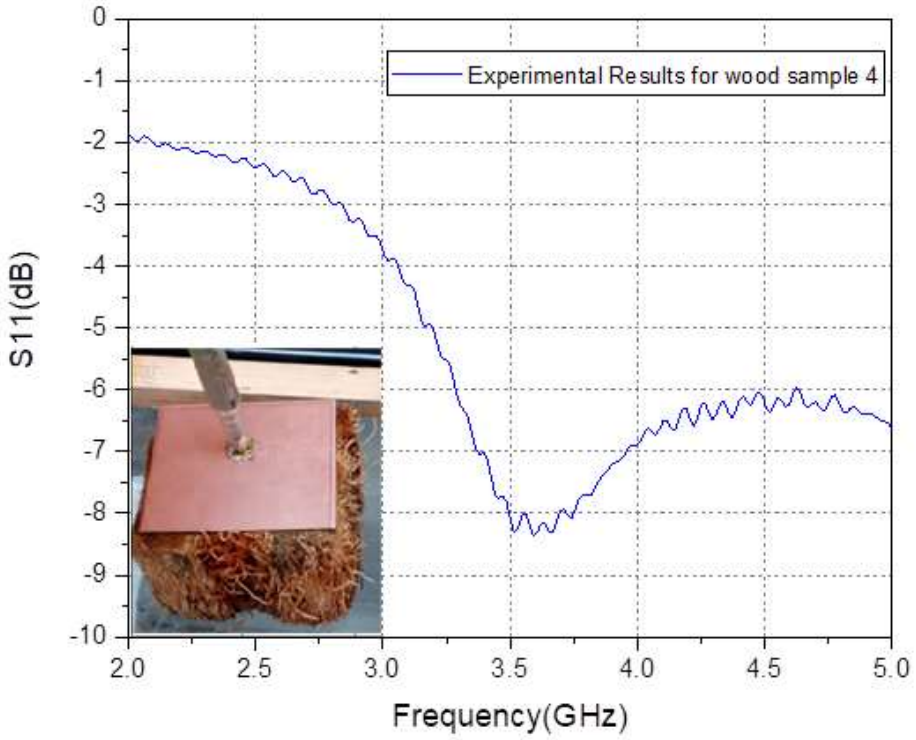

Figure 3.27: Experimental reflection response (S11) for a partially damaged palm tree-trunk (sample 4)

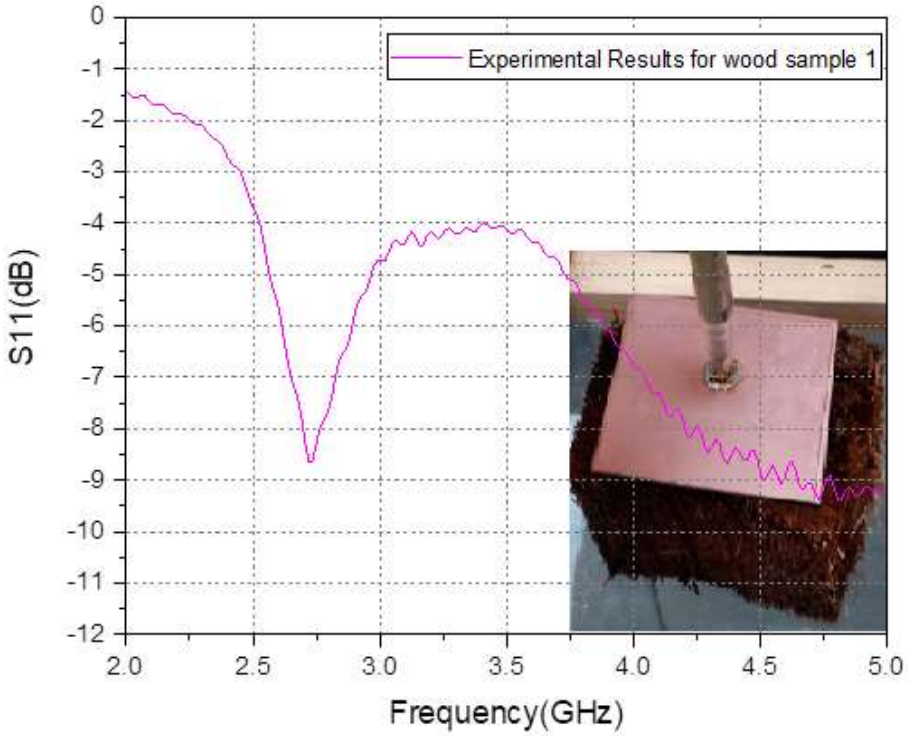

Figure 3.28: Experimental reflection response (S11) for a damaged palm tree-trunk (sample 4).

The experimentally observed reflection response of the tree trunk samples is tabulated in Table-3.3. Note that the change is resonance response due to RPW damage is nearly 28% of that of the healthy tree. To identify the different level of damage, further experimental studies are needed with a lot more tree samples. It is of note that the tree samples tend to dry up once they are cut/dissected to make experiment samples. So, methanol and water mixture is used to maintain the damaged status of the RPM infested palm tree-trunk sample.

Table 3:3: Performance of fabricated patch antenna with different wood superstrate.

Wood condition	Resonance Frequency (GHz)	% Change in resonance frequency	Return loss (dB)
Antenna only	4.22	0%	-13
Dry wood	4.20	0.5%	-37
Healthy	3.72	11.85%	-7
Partially damaged	3.5	17.06%	-8.5
Complete damaged	2.7	36.02%	-8.5

Figure 3.29 and 3.30 shows the E-plane and H-plane radiation pattern of the patch antenna with wood superstrate. It is of note that antenna radiation patterns seem to change with the health condition radiation palm tree-trunk. As the moisture increases the beam-width of the radiation pattern seems to become narrower.

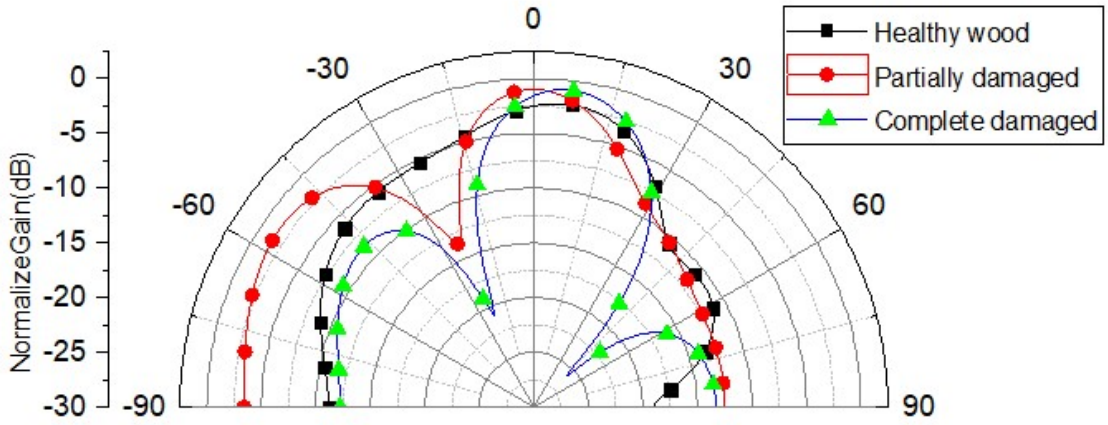

Figure 3.29: Experimental Radiation pattern at Phi=0 (E-plane)

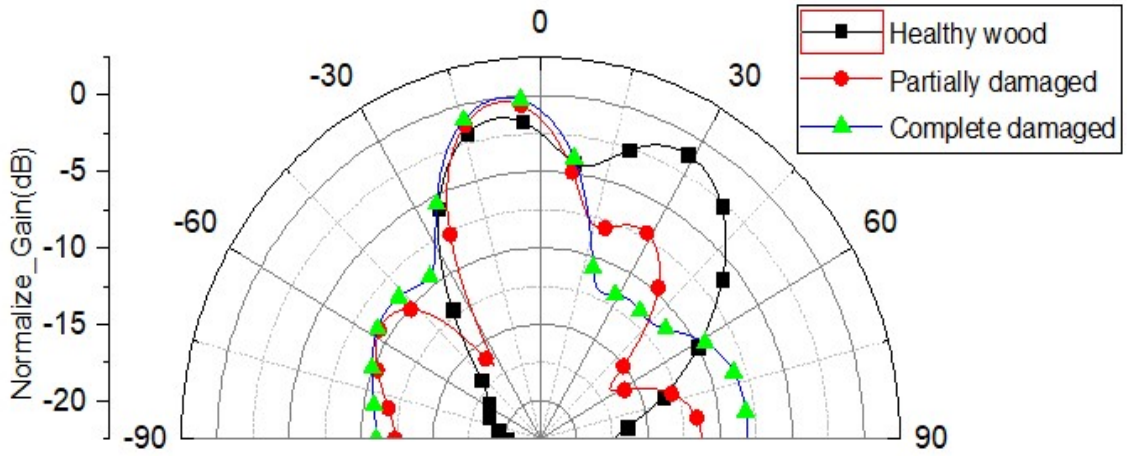

Figure 3.30: Experimental Radiation pattern at Phi=90 (H-plane)

3.13 DESIGN OF CIRCULAR MICROSTRIP RESONATOR

In the previous section we have designed and discussed about the rectangular structure microstrip resonator. One limitation of the previous design was the resonance frequency could be distinguishable up to 5cm of the wood superstrate. Since, the resonator was

designed to operate at S-band the resulting wavelength was very small as a result it had less penetration depth. Therefore, we decided to go down to lower frequency. In this section we will design and discussed a simple circular shaped microstrip resonator. The circular microstrip resonator is designed to resonate in air at lower frequency at 1GHz. This lower frequency design affix two advantages (i) it can scan larger area of the tree sample, (ii) improve the impedance matching for thick superstrate. The planer structure is designed on Rogers (TMM 6 (tm)") substrate with t=3.81mm shown in Figure 3.31.

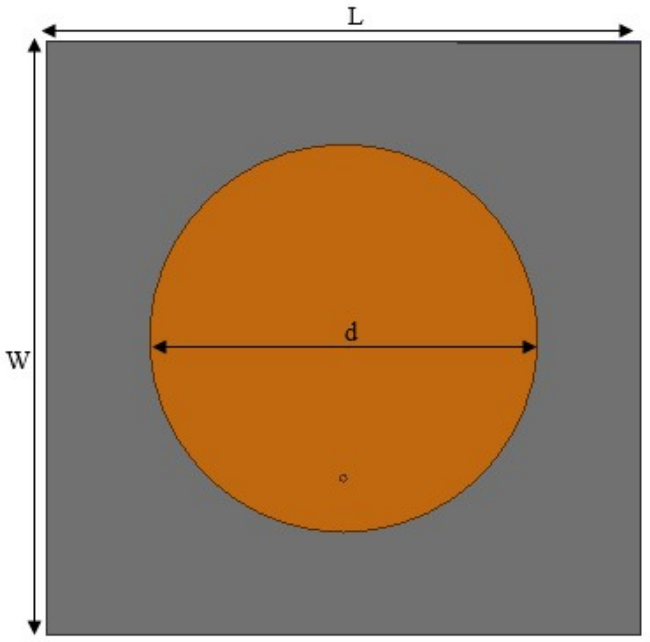

Figure 3.31: Geometry of the circular microstrip resonator.

Note that the model was simulated with different thickness of substrate, with increasing the substrate height the S_{11} has been improved. Thick substrate was chosen because it miniaturized the resonator dimension, more robust and the same time improved S_{11}. Unlike

previous design of rectangular patch where the resonator was matched for air superstrate. Here, in this case of circular resonator is matched for superstrate with permittivity value between of healthy and complete damage of date tissue. The length and width of the ground plane and substrate is 110mm and the radius of the patch was 38mm and thickness of the wood superstrate improved to 10cm. The fabricated porotype of the circular microstrip resonator shown in Figure 3.32. It also need to mention here that, during fabrication we used substrate with thickness 1.27mm which were stacked top of the other to form 3.81mm of thickness. The resonance characteristics of the fabricated porotype on air superstrate is plotted in Figure 3.33.

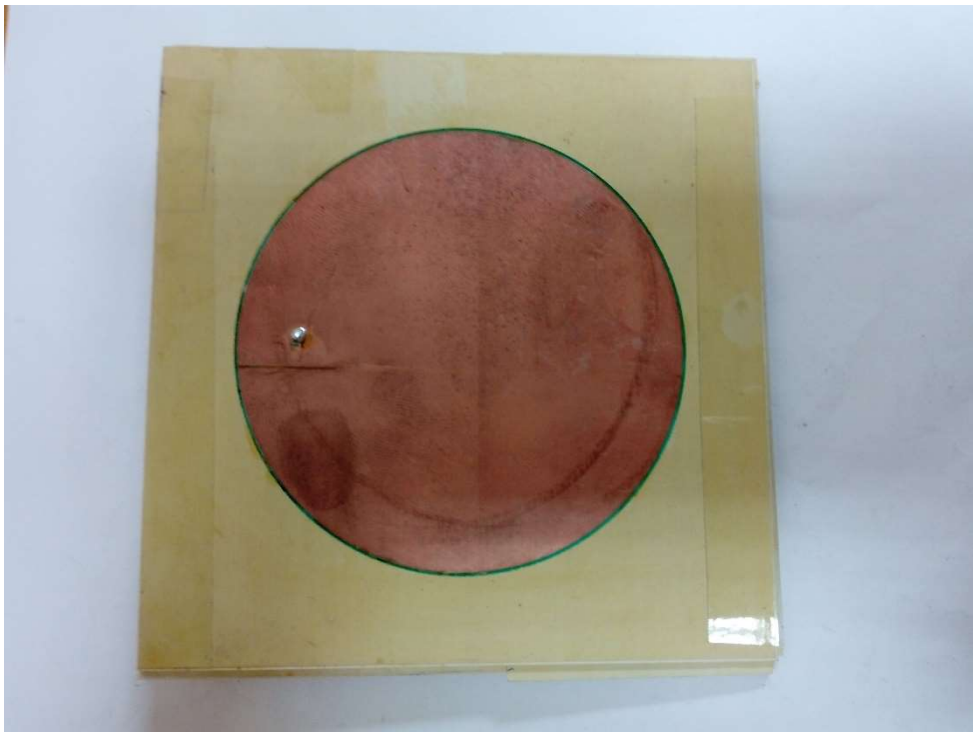

Figure 3.32: Fabricated circular microstrip resonator.

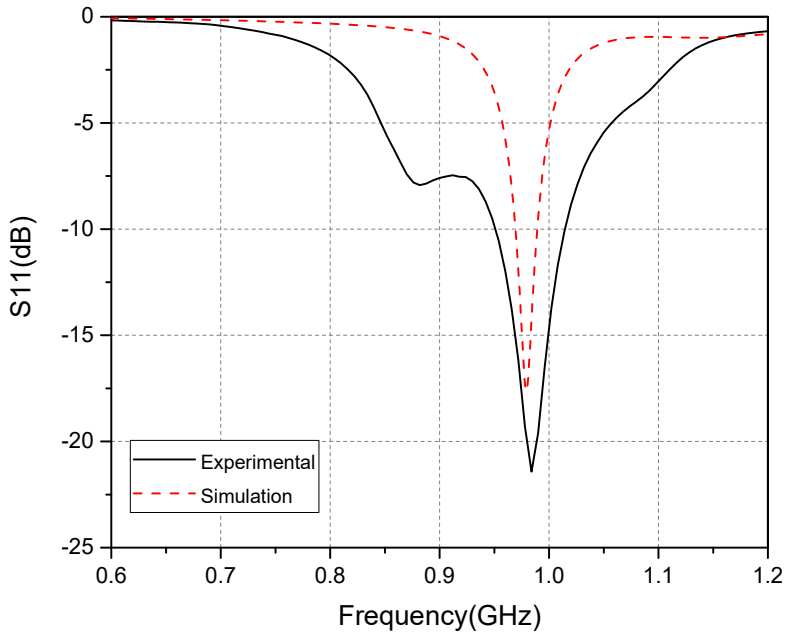

Figure 3.33: Simulated and Measured S_{11} for the circular resonator on air superstrate.

Now to check the sensitivity of the resonator due to the infestation in wood superstrate previous experimental setup shown in Figure 3.24 was used replacing only the rectangular microstrip resonator. The resonance frequency obtained from various fraction of infested wood samples is superimposed and compared in Figure 3.34. Note that the resonance frequency of the microstrip resonator went down with the increasing level of infestation. This is because with the increase of infestation the wood tissue become more wet as a result the effective dielectric constant increases. One drawback of this low frequency resonator is the level of resolution that can be measured are quite large and a maximum of 20% infestation can be detected.

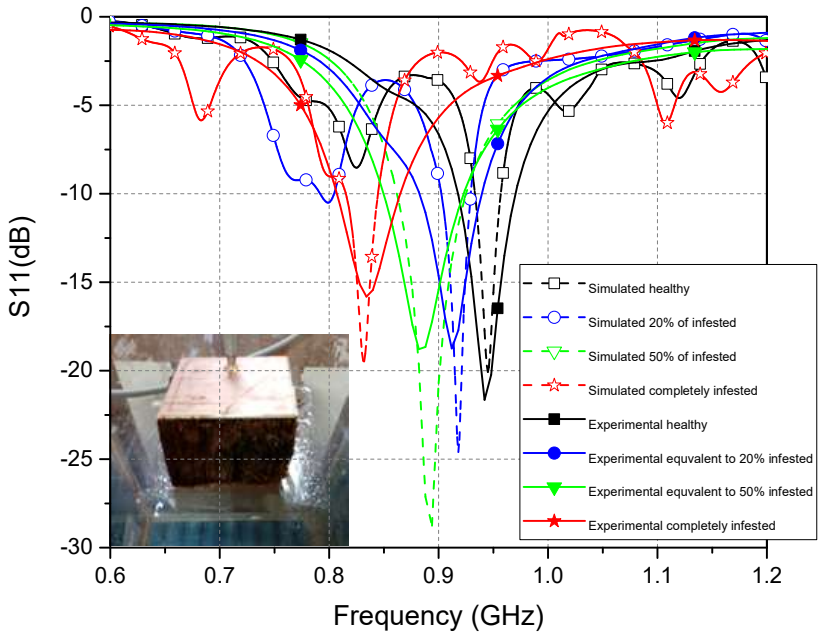

Figure 3.34: Comparison of Reflection Coefficient (S_{11}) for changed volume fraction of infestation.

3.14 DESIGN OF MICROSTRIP RING RESONATOR

In this section we will model a microstrip ring resonator for sensing changes in dielectric constant of dielectric overlay. Like the previous microstrip patch ring resonator is also highly sensitive to its effective permittivity due to dielectric superstrate causes change its resonance frequency. The resonance frequency of ring resonator is obtained, if the circumference of the ring is equal to the integral multiple of guided wavelength. The resonance frequency of a ring resonator is obtained as $f_0 = \frac{c}{2\pi r_m \sqrt{\varepsilon_{eff\,0}}}$; where, r_m is the mean radius $\varepsilon_{eff\,0}$ is effective dielectric constant. Using HFSS we design two port ring resonators for 1GHz resonance frequency. Low loss RT/Duriod 5580 with dielectric constant 2.2 and thickness 0.787mm is used as dielectric substrate. The dimension of

dielectric substrate is 141mm×87.5mmx0.787mm. The optimized thickness of ring strip is 2.4mm with outer ring radius 34.8mm and inner ring radius 32.4mm. The feed length is 35mm and coupling gap with the ring is 0.65mm.

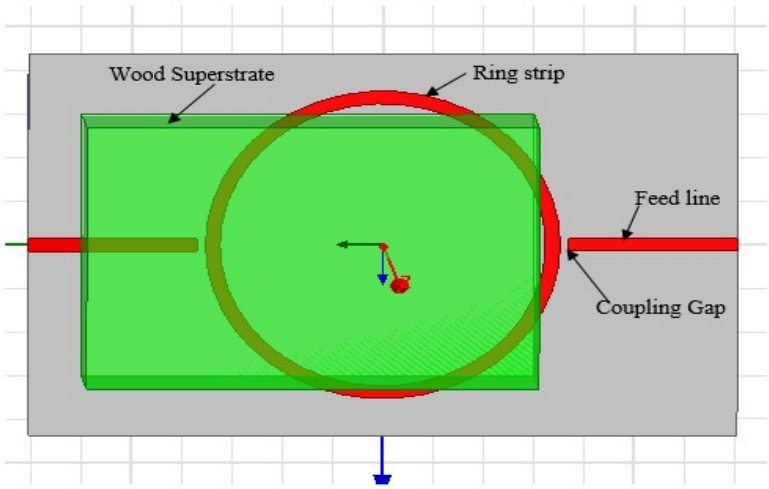

Figure 3.35: Microstrip ring resonator with optimized dimensions.

The optimized dimension of the ring resonator is shown in Figure 3.31. The insertion loss S_{21} for optimized design is shown in Figure 3.32. Note that the first resonance obtained at 1GHz also shows periodic resonance at one GHz interval.

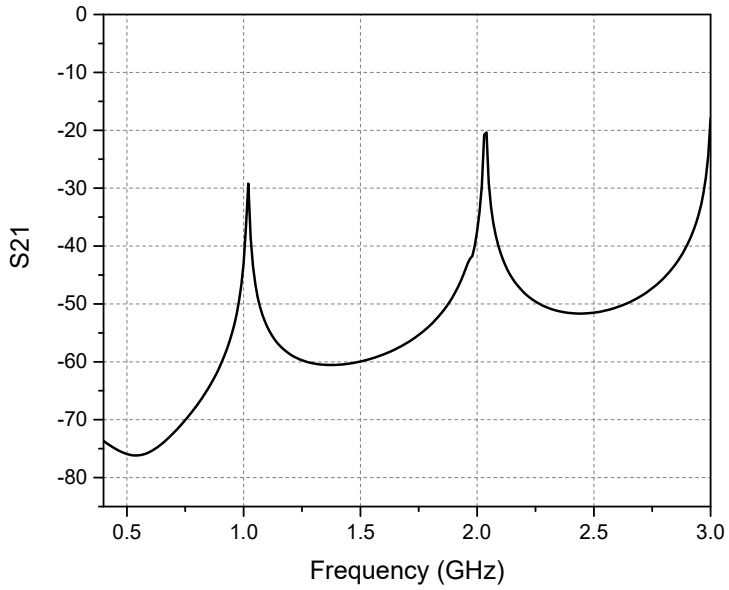

Figure 3.36: Resonance frequency of microstrip ring resonator.

In ring resonator the maximum electric field location is the coupling region between the feed and the ring, therefore, this coupling spacing region is more sensitive to superstrate sample variations. The wood sample with dimension 9x6x5cm is placed over the coupling gap to get maximum sensitivity. The simulation results with superstrate of the healthy and complete damage date tissue is shown in Figure 3.33. Note that for both healthy and damage tree superstrate the resonance frequency changes significantly. The shift of resonance frequency for healthy sample is around 13% and for damage tissue approximately 25%.

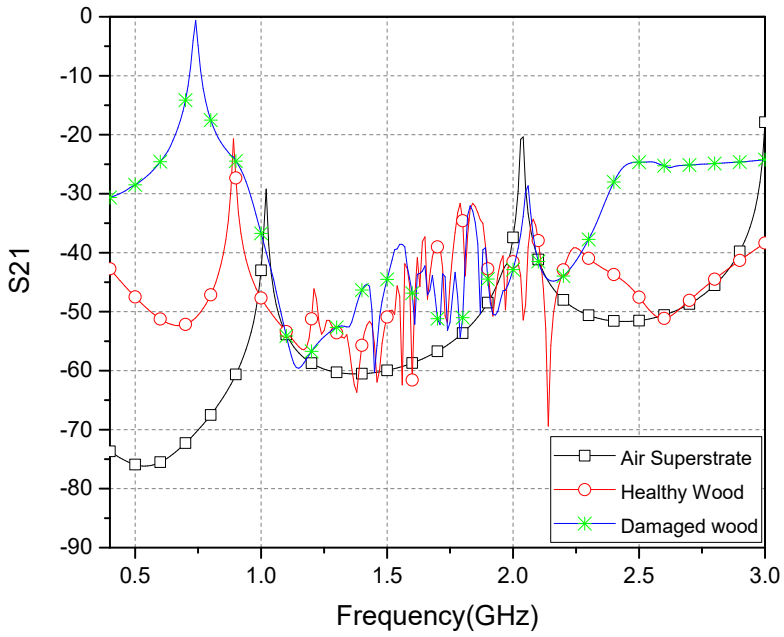

Figure 3.37: change of resonance frequency for dielectric wood superstrate.

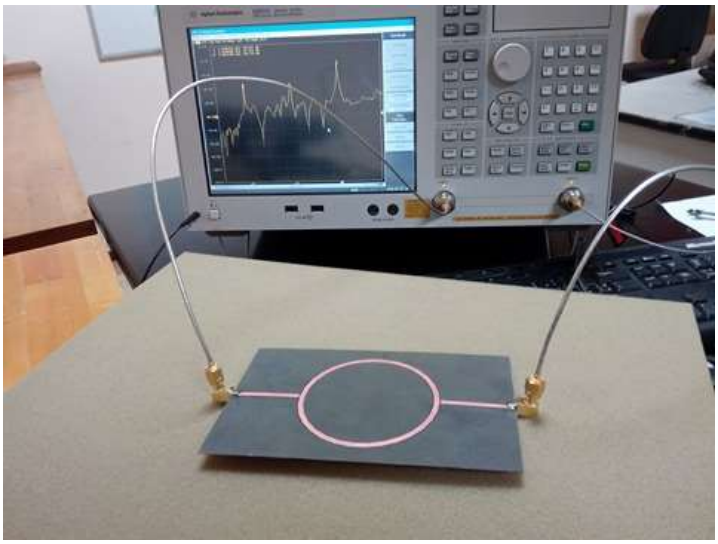

Figure 3.38: Fabricated microstrip ring resonator with measurement setup.

The fabricated ring resonator with measurement setup is shown in Figure 3.34. The measurement starts with the two-port calibration for reflection, transmission and isolation with the calibration kit of open, short and broadband load. The simulation and experimental results for insertion loss of the microstrip ring resonator both for healthy and damage wood superstrate is shown in Figure 3.35, 3.36, 3.37 respectively. The simulation and experimental results are in good agreement in terms sensing resonance frequency. However, there is some discrepancy in s21 magnitude this could be due the imperfect two port calibration, error in fabricating the structure and again samples are not exactly same size as simulation.

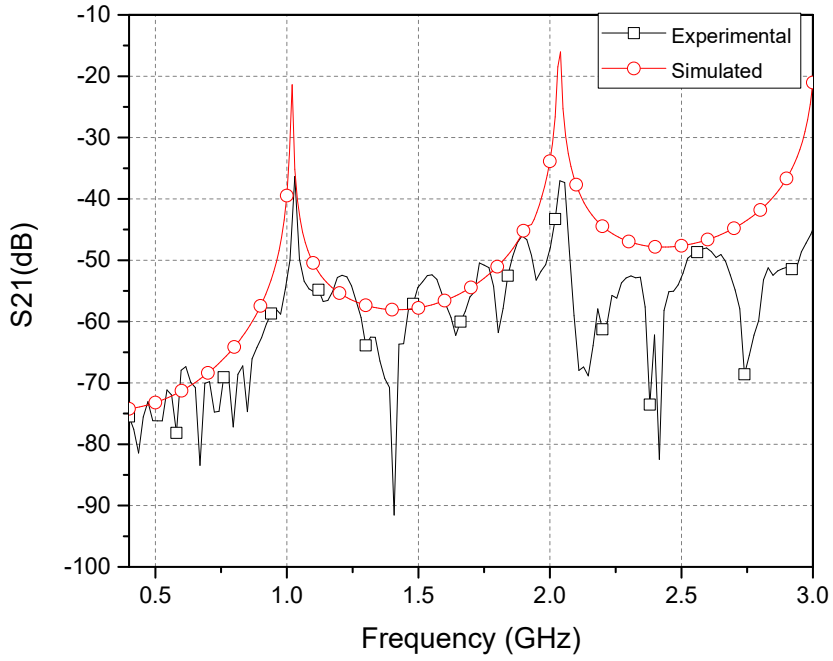

Figure 3.39: Simulated and measured S_{21} without superstrate.

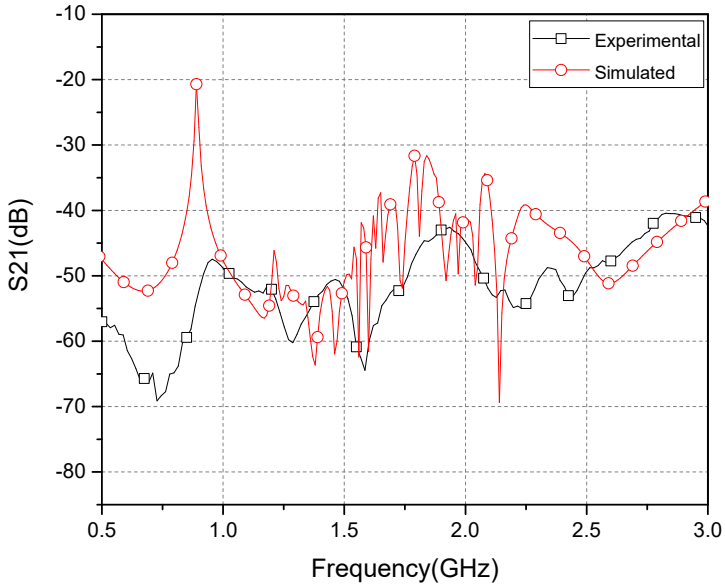

Figure 3.40: Simulated and measured S_{21} for healthy wood superstrate.

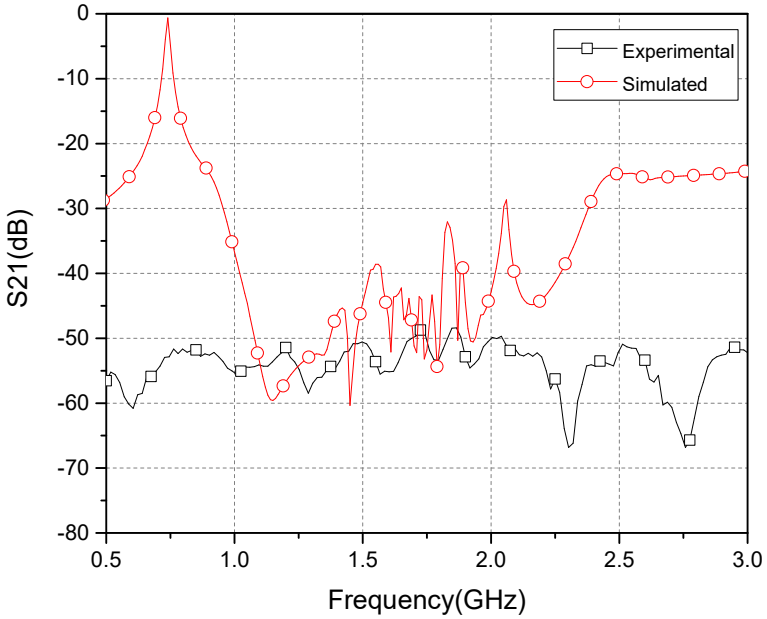

Figure 3.41: Simulated and measured S_{21} for damaged wood superstrate.

3.15 CONCLUSION

This chapter started with the theoretical analysis of superstrate based microstrip patch antenna. Then it continued with the design of a 4GHz microstrip antenna and analysis of its frequency response for different known dielectric materials as a superstrate. It is noticed that as the dielectric constant of the superstrate material increases the effective dielectric constant of the system increases and reduces the resonance frequency.

HFSS simulator software is used to model the proposed resonator excited by a 4-GHz microstrip patch antenna with date tree-trunk as a superstrate. A significant shift in the resonance frequency is observed with changing dielectric properties of the superstrate. However, the increase in superstrate height played an even significant role due to increased impedance match of the antenna.

The optimized resonator is fabricated and tested. The measured reflection coefficients (S_{11}) for healthy, partially-damaged and damaged tree samples are used to observe the different resonant response of the antenna. Note that resonance frequency shifted by 28% for healthy tree sample response to a completely damaged tree. These responses can be tabulated to prepare a look-up table that can be used in a date tree farm to identify an RPW damaged date palm tree.

CHAPTER 4

4 CAPACITANCES BASED DETECTION OF INFECTED PALM TREE

In this chapter, the palm tree capacitance-based detection technique is used to identify the infestation of red palm weevil (RPW). Initially, two semi-cylindrical electrodes are used to conduct laboratory-based capacitance measurements of healthy, partially-infected and infected palm trees to generate a look-up table. Since tree capacitances and the related dielectric properties are directly proportional, the idea is to detect infestation by comparing the values of the look-up table and the measured capacitances of a date palm tree located in a random date farm. Since varies soil type, surrounding environment and the tree parameters considerable affects the measured capacitance, a validated numerical method can be more suitable to generate region/farm-based look-up tables. They are capable of easily integrating the local variables in calculating the expected tree capacitance for healthy and infected palm trees. In this chapter, first I am going to review the background of electromagnetic materials, dielectrics parameters and basic discussion on capacitance. Then a numerical method is developed to calculate capacitance of palm tree. Measured capacitances are then used to validate the numerical model. A low-frequency electrostatic simulation software (Ansoft Maxwell®) is used to optimize the numerical results.

4.1 ELECTROMAGNETIC MATERIALS

In terms of electrical properties, materials are classified as conductors, semiconductors, dielectrics, and insulators. Again, in terms of magnetic properties materials can be classified as diamagnetic, paramagnetic and ferromagnetic materials. Characterization of material is crucial for selecting the correct material for a specific application. One common practice to differentiate between materials is to plot the related electron energies. In the atomic structure, the highest electronic energy band at 0°K is called valence band and there is conduction band above the valence band. Sometimes there is an energy band gap between the conduction and valence band called forbidden region. Depending on the size of this energy band gap materials are classified. Conductors have an overlap of the conduction band and valence band and example of good conductors are copper, aluminum, gold etc. In dielectric materials, electrons are very tightly bounded and held in place by atomic and molecular forces. There is a large band gap in dielectrics and supports conduction if sufficiently high external field is applied. Example of dielectric material includes: are Air, Glass, Water, wood etc. Semiconductors like Silicon, Germanium etc. have electrical properties in between conductors and dielectrics. They are neither good conductor nor good dielectrics. Science, the objective of this research work is to identify infected date palm trees through analyzing their dielectric behavior, detail discussion on dielectric properties of materials are presented below. Note that dielectric materials interact significantly with the incident electromagnetic waves and analyzing this interaction can be useful to characterize the material.

4.2 DIELECTRIC MATERIALS

4.2.1 POLARIZATION

Perfect dielectric materials do not hold free charges, where the dominant charges remain bounded and held in one place. Therefore, dielectric property generally introduces resistivity. If an external field is applied to the dielectric material, the bound charges do not move to the surface like a conductor. Rather the respective centroids of the charges shift slightly resulting numbers of dipoles pointing along the direction of the applied field. This is how dielectric material becomes polarized [61]. In practice, the behavior of these dipoles and bound charges are accounted by electronic polarization vector, ***P***. Dipole moment can be defined as the product of the magnitude of two opposite charge (q's) separated by a distance (d), which is a vector directed from the negative to the positive charge.

4.2.2 DIPOLE OR ORIENTATIONAL POLARIZATION

Dielectric materials possess a permanent dipole moment. However, these dipoles are randomly oriented in the absence of an external electric field. When applying an electric field, the dipoles tend to align with the applied field causing orientational polarization, such materials known as polar materials.

4.2.3 IONIC OR MOLECULAR POLARIZATION

In some materials like NaCl, there are positive and negative ions and the centers of this ions can be displaced by applying an electric field. The polarization or the displacement of positive and negative ions against each other is known as ionic polarization.

4.2.4 ELECTRONIC POLARIZATION

This polarization happens in molecule when electron clouds deviate from the equilibrium trajectory of the nucleus by an applied electric field. And Atomic polarization happens if adjacent positive and negative ions “stretch” due to an applied electric field. In many dry solids electronic and atomic polarizations are the dominant polarization, especially at radio frequencies.

4.3 DIELECTRIC CONSTANT

Relative permittivity or dielectric constant of a dielectric medium is defined as the ratio of the capability of a capacitor to store charge with that medium as a dielectric, to the charge stored when a vacuum is used as the dielectric medium. Michael Faraday first examines the consequence of filling the space between the plates of a capacitor with a dielectric material. He demonstrated that if a voltage from a DC source is applied across the parallel plate capacitor, more charge is stored if a dielectric material placed in between the plates than vacuumed. Therefore, capacitance depends on the dielectric constant of the materials.

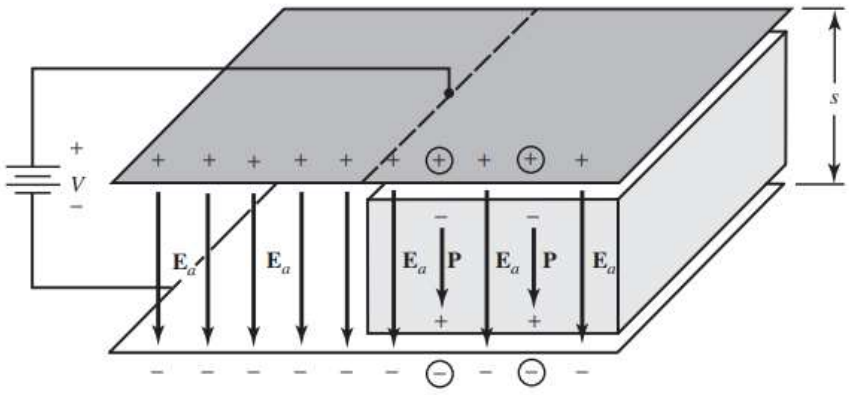

Figure 4.1: Dielectric slab subjected to DC voltage [61].

In Figure 4.1, when an external electric field E_a is applied, the electric flux density D_0 for free space part can be written as

$$D_0 = \varepsilon_0 E_a \tag{4.1}$$

Again, the electric flux density D for the dielectric portion is related to free space D_0

$$D = \varepsilon_0 E_a + P \tag{4.2}$$

The electric flux density D can also be related to electric field E_a and a parameter ε_s

$$D = \varepsilon_s E_a \tag{4.3}$$

From (2.2) and (2.3) the polarization vector P can be written as

$$P = \varepsilon_0 \chi_e E_a \tag{4.4}$$

$$\chi_e = \frac{1}{\varepsilon_0}\frac{P}{E_a} \tag{4.5}$$

where, χ_e is known as electric susceptibility, its value depends on the microscopic structure of the substance and external conditions such as temperature. The materials that follow equation (2.4) is called linear dielectric. Thus, for linear dielectric, we can write:

$$D = \varepsilon_s E_a + \varepsilon_0 \chi_e E_a = \varepsilon_0 (1 + \chi_e) E_a = \varepsilon E_a \tag{4.6}$$

where, $$\varepsilon = \varepsilon_0 (1 + \chi_e) \tag{4.7}$$

and ε is the permittivity of the material. The relative value of ε is given by:

$$\varepsilon_r = \frac{\varepsilon}{\varepsilon_0} = 1 + \chi_e \tag{4.8}$$

where, ε_r is commonly known as relative dielectric constant. The dielectric constant is the parameter that indicates the charge storage capabilities of a dielectric material; the larger its value the greater its ability to store charge. The permittivity is the complex quantity and depends on frequency and temperature. Typically, permittivity is referred to as ε^*

$$\varepsilon^* = \varepsilon_0 \varepsilon_r^* = \varepsilon_0 (\varepsilon_r' - j\varepsilon_r'') \tag{4.9}$$

where, ε_r^* is the complex relative permittivity. The imaginary part is zero for lossless materials and is used to define the material loss tangent ($\tan\delta_c$). It measures the amount of energy loss from the material due to an external electric field and is given by:

$$\tan\delta_c = \frac{\varepsilon_r''}{\varepsilon_r'} = \frac{\sigma}{\omega\varepsilon} = \frac{1}{Q} \tag{4.10}$$

where, Q is quality factor. The complex permittivity can be represented by a simple vector diagram shown in figure 4.2, where the real and imaginary components are 90^0 out of phase. Loss of a material is the ratio of the energy lost to the energy stored.

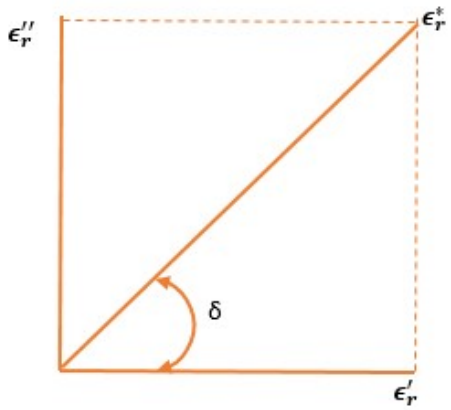

Figure 4.2: Phasor representation of loss tangent.

4.4 SENSING THEORY FOR SEMI CYLINDRICAL CAPACITOR

This capacitive sensor is made of two identical semi-cylindrical electrodes with radius 'r' and edge separation distance of 'd'. Figure 4.3 shows the designed semi-cylindrical capacitive sensors filled with an air dielectric. Although Maxwell's equations can be used to derive an exact expression, the analysis of the capacitive behavior can be difficult. But through simplifying the complexity of the electrostatic analysis, a very good approximation of the capacitance can be obtained. Note that in parallel plate capacitor the distance between the electrodes remains constant. But in a semi-cylindrical capacitor, this varies along the curved surfaces with a minimum gap at the edge and maximum separation at the center of the electrodes. To approximate the capacitance, electrode A is excited with positive charge +Q and electrode B with negative charge -Q.

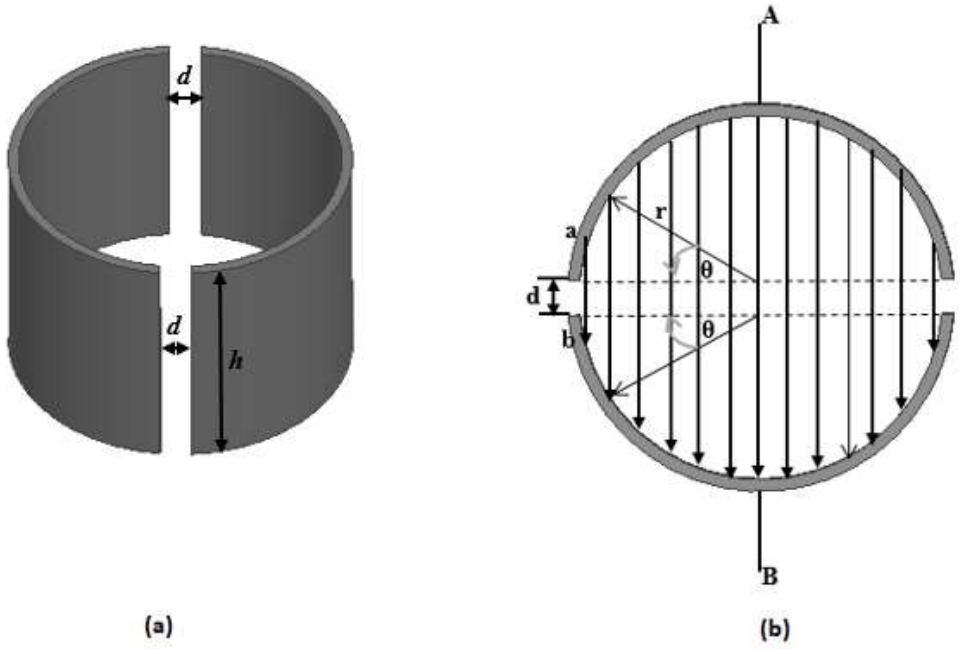

Figure 4.3: :(a) Schematic view of the semi-cylindrical capacitive sensor; (b) Top view with electric field distribution in the air and symbolic representation for numerical analysis method.

The electric field (E) between the two plates can be written as,

$$E = \frac{Q}{A\varepsilon_0} \tag{4.11}$$

where, $A = \pi rh$, is the surface area of the half cylindrical structure and 'h' is the height of the plate. Thus,

$$E = \frac{Q}{\pi rh\varepsilon_0} \tag{4.12}$$

To calculate the potential difference between the plates, following equation is used;

$$V = \int_a^b \vec{E}.d\vec{l} + \int_0^\pi \vec{E}.d\vec{l} \tag{4.13}$$

where the edge separation/gap of the electrode plates is fixed to 'd'. The variable separation between any two points on the curved surface of the electrode can be calculated by,

$L = 2r\sin\theta$, where θ is the angle between the radius and horizontal plane of the curved surface. The rate of change of the separation distance between the plates with respect to the angle θ is written as follows;

$$dL = 2r\cos\theta d\theta \tag{4.14}$$

Thus, the actual separation distance between two plates is given by;

$$dl = 2r\cos\theta d\theta + d \tag{4.15}$$

Now substituting 'dl' in equation (5.3), the expression for potential difference can be written as;

$$V = \frac{Qd}{\pi rh\varepsilon_0} + \int_0^{\pi} \frac{2Qr\cos\theta d\theta}{\pi rh\varepsilon_0} \tag{4.16}$$

$$V = \frac{Qd}{\pi rh\varepsilon_0} + \frac{2Qr\sin\theta}{\pi rh\varepsilon_0} \tag{4.17}$$

$$V = \frac{Q}{\pi rh\varepsilon_0}(2\,\mathrm{rsin}\,\theta + \mathrm{d}); 0 \le \theta \le \pi \tag{4.18}$$

Hence, the capacitance between the two semi-cylindrical plate can be written as;

$$C = \frac{Q}{V} \tag{4.19}$$

$$C = \frac{Q}{\frac{Q}{\pi rh\varepsilon_0}(2\,\mathrm{rsin}\,\theta + \mathrm{d})} \tag{4.20}$$

$$C = \frac{\pi r h \varepsilon_0}{(2\mathrm{r}\sin\theta + \mathrm{d})} \tag{4.21}$$

For our case, the metal plates are fixed over the outside wall of a tree trunk, and medium between the plates are air and the dielectric material of the tree-trunk with either healthy or damaged tissues (due to fermentation caused by RPW). Thus, the final equation for the capacitance measurement of the semi-cylindrical capacitance sensor is as follow;

$$C = \frac{\pi r h \varepsilon_0 \varepsilon_1 \varepsilon_2}{\left(2r\sin\theta + d\right)} \tag{4.22}$$

where, $\varepsilon_0 = 8.85 \times 10^{-12}$ and $\varepsilon_1, \varepsilon_2$, are a dielectric constant of air and the dielectric material of the tree-trunk, respectively. From above equation, it can be demonstrate that if the dielectric constant of the tree sample changes due to infestation by RPW, then the effective dielectric constant also changes. Therefore, measurement of dielectric constant of the damage tree is possible using the semi-cylindrical capacitive sensor.

4.5 DESIGN CONSIDERATION AND SIMULATION

This section presents the changes of the capacitive behavior of the structure due to three different electrode configurations of the semi-cylindrical capacitor. This analysis allowed the selection of the optimum structure, before embarking on the experimental verification process related to the calculated capacitance of the palm tree sections. For the application at hand, the designed semi-cylindrical electrode configurations of Figure 5.2 have been designed and simulated using professional software: Ansoft-Maxwell. Since our experimental tree sample has a diameter of 33cm, the electrodes are designed to cover this

diameter. An aluminum sheet of thickness t=0.1 cm is used to construct the semi-cylindrical electrode plates. In the first design, two semi-cylindrical electrodes of height 23-cm are wrapped around the dielectric sample with minimal 'd'. The simulation model created in Maxwell is shown in Figure 4.4. To observe the simulated response of the capacitive sensor, the solution type is set to electrostatic and one plate is excited with a positive voltage and another plate is excited with a negative voltage. In addition, equation (4.22) is also used to predict the effect on the capacitance due to changing edge separation/gap 'd'. It is observed that the capacitance of the structure decreases with increasing value of 'd'. In Figure 4.5, the calculated and simulated results are superimposed for an air-filled semi-cylindrical capacitor with changing values of edge separation/gap of 'd'.

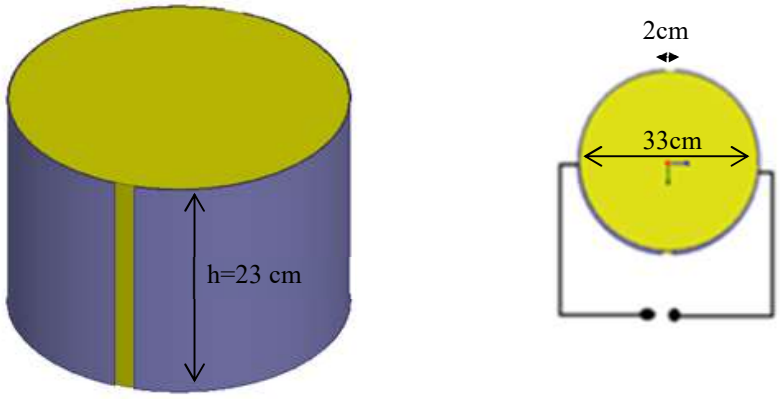

Figure 4.4: A simulation model of capacitive sensor, made of two semi-cylindrical electrode plates.

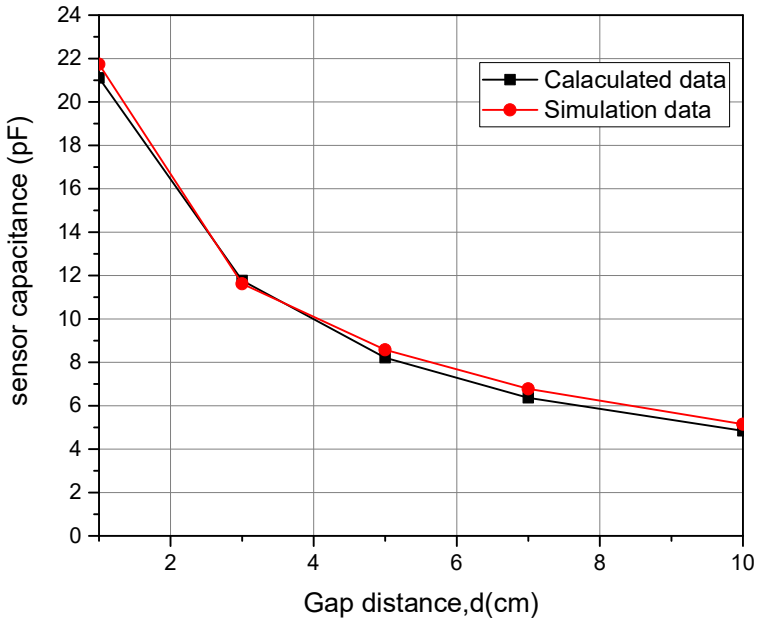

Figure 4.5: Capacitance of the semi-cylindrical air-filled electrodes with changing edge gap 'd'.

To study the sensitivity of this semi-cylindrical electrode configuration, the cavity inside the electrodes is filled with a dielectric material with ε_r. Keeping a fixed separation/gap of d=2cm, the simulator is used to monitor the changes in capacitance with changing dielectric properties of the material. Figure 4.6 shows the capacitance versus the dielectric constant (ε_r) plot of the structure. Note that changing capacitance of the structure is linearly related to changing the dielectric constant of the semi-cylindrical capacitor. The range of dielectric constant values is selected to include ε_r values for air and salty water, as the trunk carries water contents from soil to the leaves of the tree.

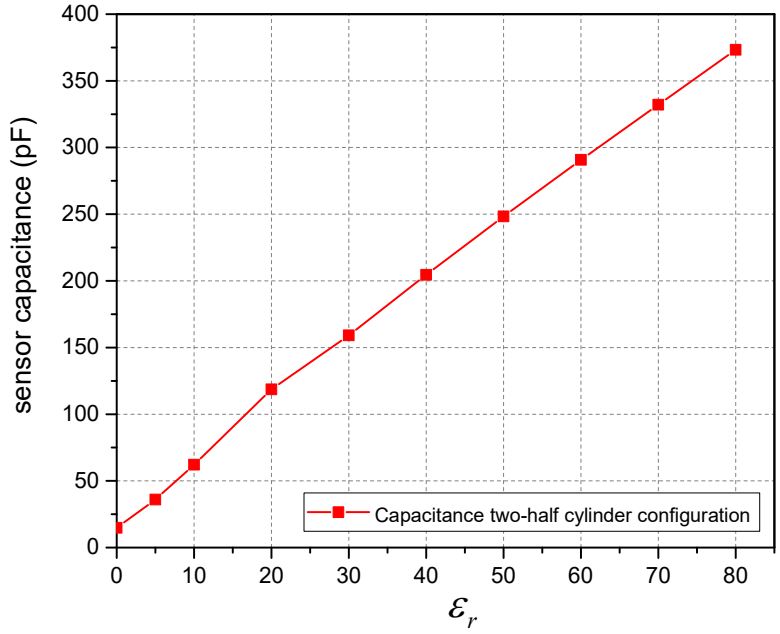

Figure 4.6: Capacitance versus dielectric constant plot of a dielectric-filled semi-cylindrical capacitor.

In the second model, shown in Figure 4.7, four electrodes with heights of 23cm are used to construct the cylindrical capacitor with diameter 33cm. In this electrode configuration, two opposite side plates is shorted and excited with positive polarity of the voltage and other two with negative polarity of the voltage. The gap between two consecutive plates is fixed at 1cm and simulation is performed with varying dielectric constant. Figure 4.8 plots the capacitance of the sensor configuration against ε_r, which shows the linear relationship between these parameters.

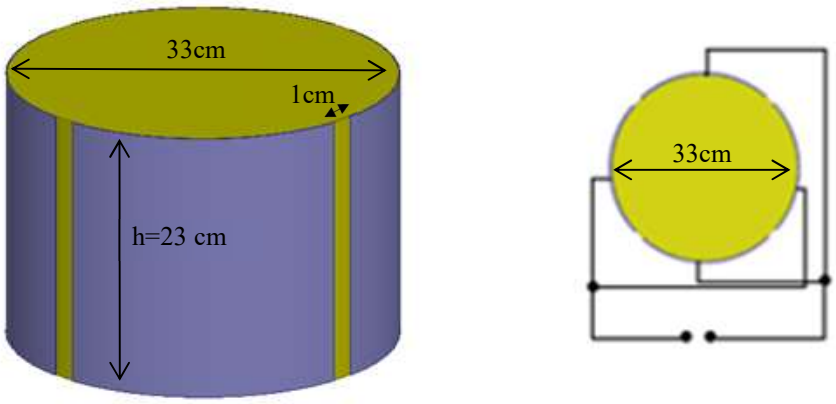

Figure 4.7: Electrode configurations of two pairs cylindrical strip.

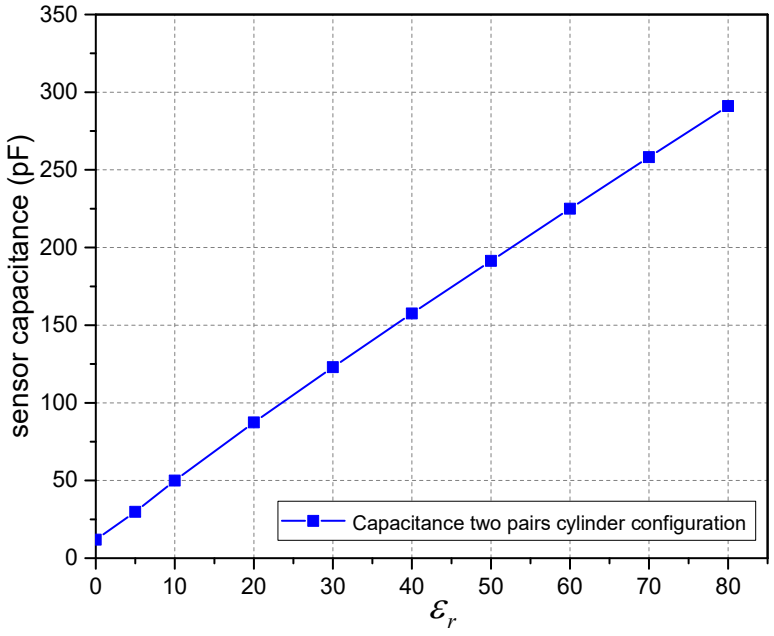

Figure 4.8: Capacitance of the four electrode plates around the cylindrical dielectric sample with ε_r.

In the third model, shown in figure 4.9, two electrode rings have been used to wrap around the cylindrical tree sample. Each ring has a diameter of 33cm and a height 10 cm. The gap

between the ring electrodes is set to be 3cm to cover the sample height of 23 cm. The two rings are excited with positive and negative voltages, respectively. Simulated capacitance versus dielectric constant (ε_r) plot is shown in figure 4.10.

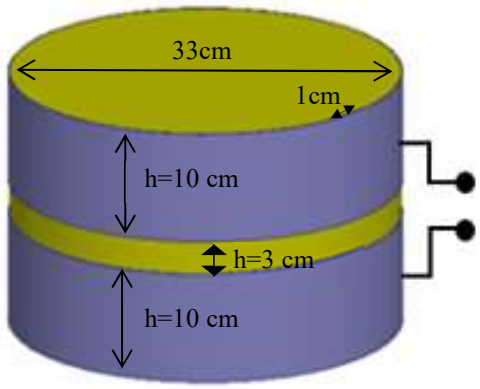

Figure 4.9: Electrode configurations of two ring structure

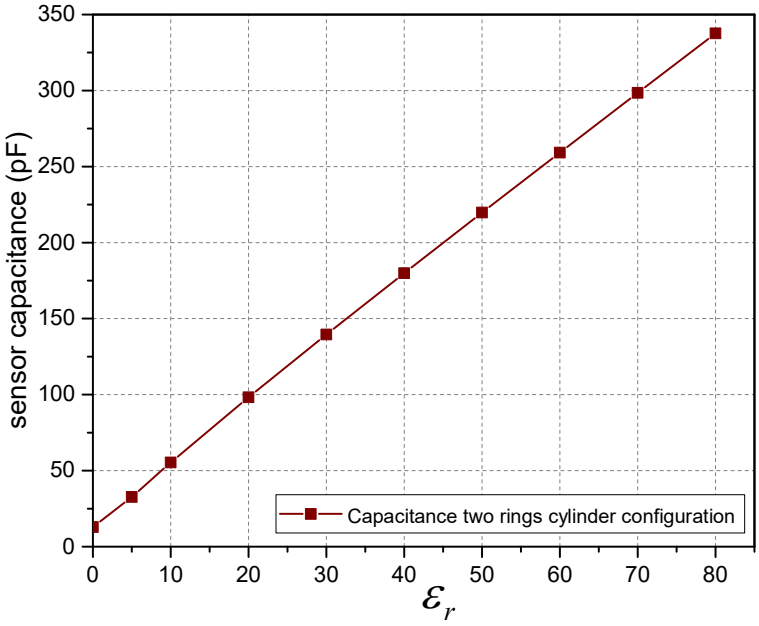

Figure 4.10: Capacitance of the two-ring electrode capacitor with dielectric (ε_r) filling.

The capacitance responses of these three models are compared to select the optimum design for this study. The results are shown in Figure 4.11 and tabulated in Table 4.1. From these calculations, it can be concluded that the best-suited sensor configuration for this work is the one with two half-cylindrical electrodes. This configuration provided the best sensitivity from a relatively easy prototype. But the challenge is to keep the gap edges constantly during the experimental measurement process.

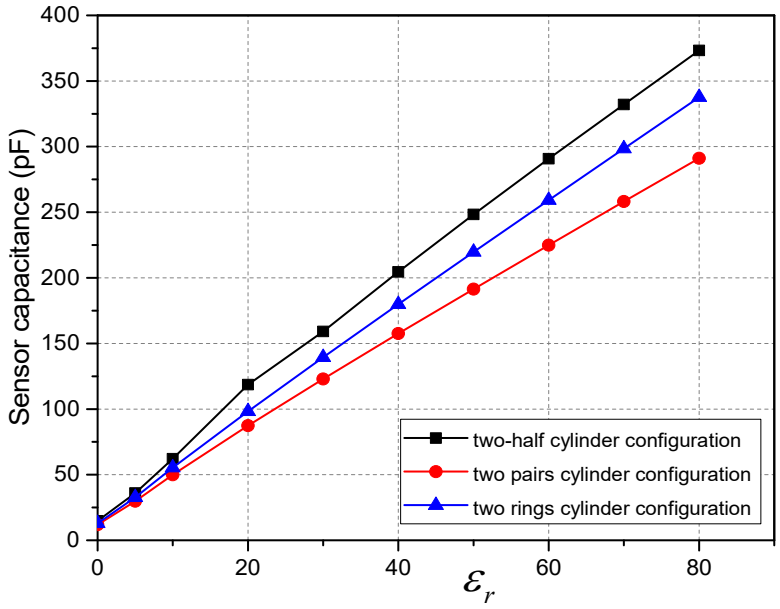

Figure 4.11: Capacitance for three types of electrodes configurations.

Table 4:1: Capacitance sensitivity for different types of electrodes configurations

Parameters	Sensor Configurations		
	Two half-cylinders	Two pairs of cylinders	Two rings
Capacitance in Air, C_0 (pF)	13.29	11.93	12.89
Capacitance for ε_r =80, C (pF)	383.34	281.06	327.64
Sensitivity: $\frac{C - C_0}{C} \times 100$	96.5%	95.7%	96%

4.6 FABRICATION PROCESS

The electrodes are designed and constructed from two Aluminum plates of length 54cm and height of 23 cm. Each plate has been bent to a semi-cylindrical shape, shown in Figure 4.12. First, the capacitance of the air-filled capacitor is measured to validate simulated and calculated data. A Keysight E4980A precision LCR meter with operating range of 10 Hz to 2 MHz is used to measure the capacitance. Calibration of the device is performed to avoid stray capacitances from connector leads. The calculated, simulated and measured capacitance values for different edge separation/gap are plotted in Figure 4.13. Note that curves are almost identical, which re-validates the predicted capacitances from the simulation model.

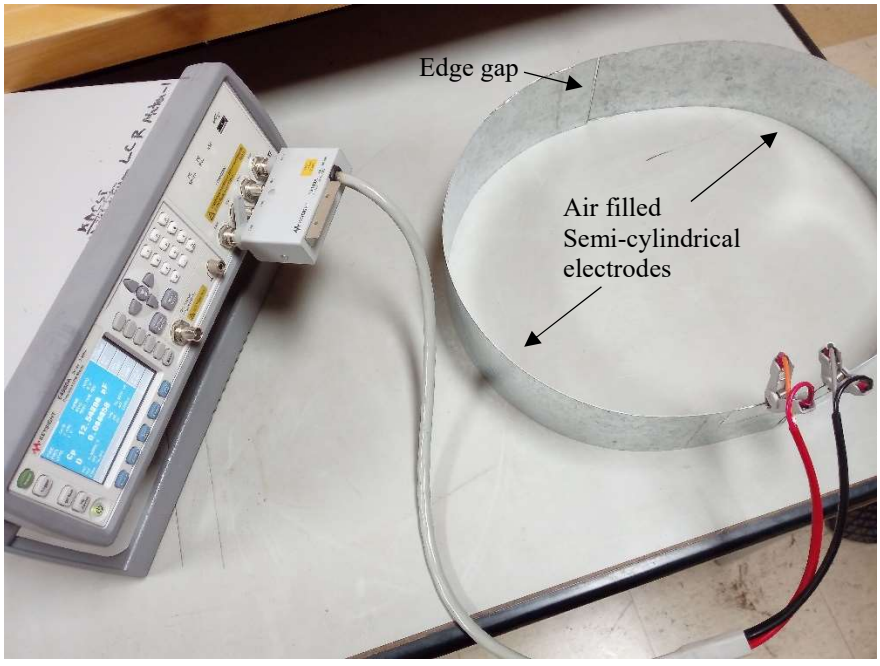

Figure 4.12: Capacitances measurement of an Air filled Semi cylindrical electrodes with LCR meter.

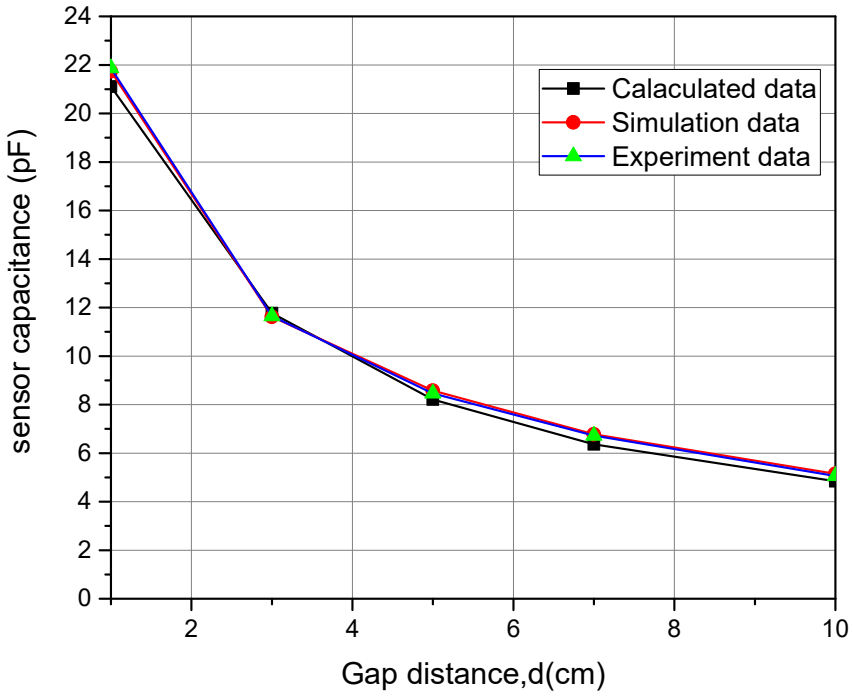

Figure 4.13: Capacitance of the semi-cylindrical capacitive sensor with varying edge gap (d).

4.7 CAPACITANCE MEASUREMENT OF DATE TREE SAMPLE

In the literature review chapter, traditionally used dielectric constants of healthy/damaged date palm tree and the red palm weevil (RPW) are identified. In the previous section, a numerical simulator is used to relate tree capacitances with dielectric properties, which can include the environment and tree related variables within the calculation. These predicted values are validated here using simple experiment. Although we are interested to measure the variation of tree capacitance due to damage caused by RPW infestation, other forms of natural and inflected tree damage also exist. Hence, this work mainly focuses on finding damages caused by RPW infestation, where the presence of bacteria in the infected zone causes fermentation. This results in the tree trunk to become more moisturized and fibrous,

leading to an increase in trunk permittivity with a dielectric constant ranging from 49 to 51. Another interesting fact is that most of the RPW infestation starts from the bottom of the tree trunk and ends when they reach the top. On the other hand, natural damage to the tree trunk causes is to become drier. This leads to a reduced trunk permittivity with a dielectric constant ranging from 2 to 10.

4.7.1 PREPARATION OF THE TREE SAMPLE

During the experimental process, samples of a healthy and RPW infested date tree is collected. Note that it was a very difficult process, as it needed coordination with KFUPM authorities responsible for trees maintenances, trash removal, and the security services. Since the tree samples were very heavy, it took a lot of effort to carry them to the lab. The 2nd step in the experimental process was to cut the tree samples in required shapes to fill the semi-circular electrodes. Electric saw machine is used for this purpose and a picture related to this process is shown in figure 4.14(a). Next step is to install the semi-cylindrical electrode places around the tree sample and measure the capacitances using the Precession LCR meters. The only challenge in this installation process is to maintain the required edge gap between the electrodes. Figure 4.14(b) shows a healthy and a slightly damaged tree-trunk sample. During the experimental process, water and methanol (with a similar dielectric constant of larva state of RPW) mixture is introduced in a controlled manner to deteriorate tree damage.

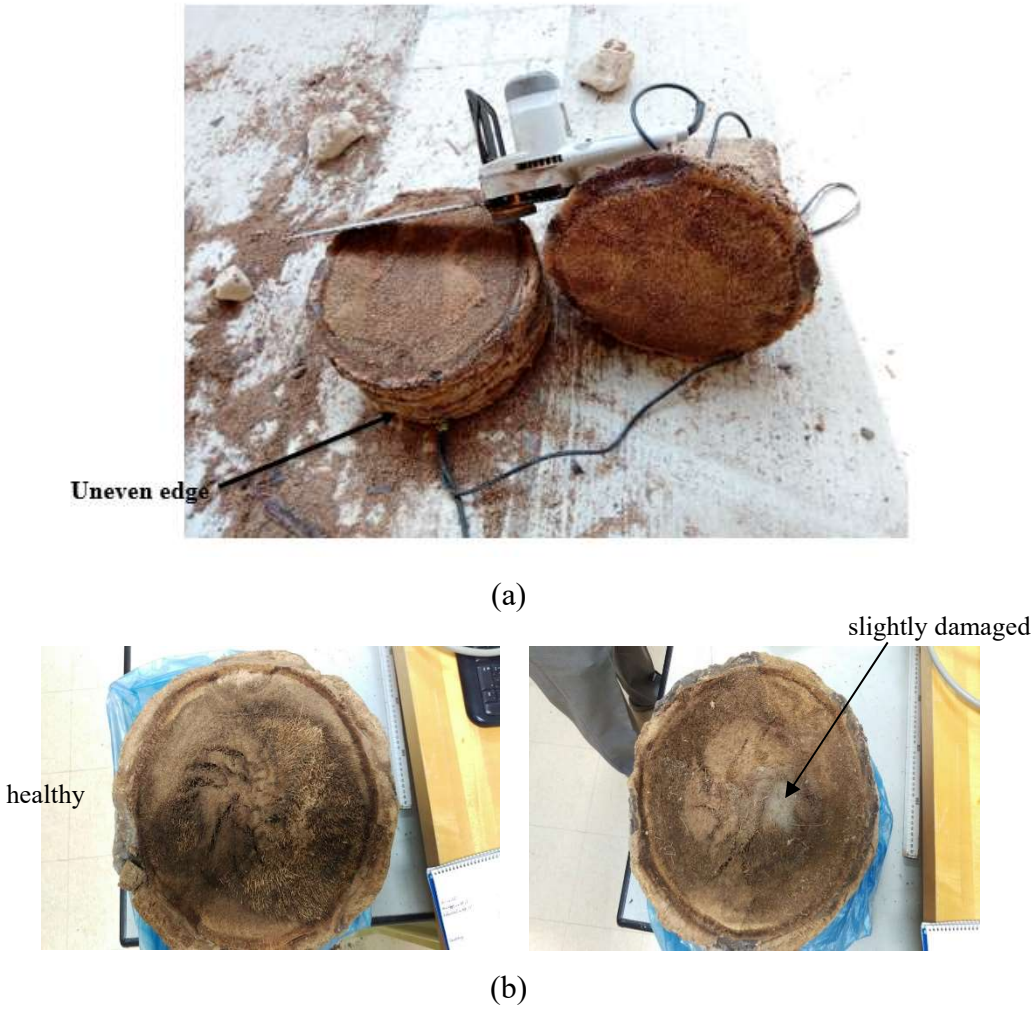

Figure 4.14: (a) Preparing tree trunk samples for experiment. (b) Healthy and slightly-damaged samples

4.7.2 CAPACITANCE MEASUREMENT FOR VOLUME FRACTION OF INFESTATION

Before beginning the measurement process, two tree trunk samples are selected which can visually identify as healthy and damaged. Since it was difficult to accumulate multiple tree samples with different stages of infestation/damage, controlled tree damage is inflected by introducing methanol and water mixture contents within the slightly damaged tree-trunk. The designed semi-cylindrical electrode plates were filled with the tree-trunk sample with

diameter 33cm and height 23cm and the gap between the plate 2cm on both sides. These values are selected so that experimental data can verify the simulated results and once verified; simulation model can be used to create the look-up table for farm-based experiment. The experimental setup is shown in figure 4.15. The tree sample shown represents a healthy trunk with uniform trunk-fiber distribution and no visible damage. In the following measurement case, the healthy tree sample is replaced with a slightly damaged tree trunk sample. Once the capacitance values are recorded, methanol and water mixture with known dielectric properties are introduced within the slightly damaged tree to increase the trunk damage in a controlled manner.

Figure 4.16 shows the superimposed curves representing the simulated and experimental results. Although the curves of this figure follow the same path, measured capacitances were considerably lower than the simulated values. These discrepancies are mainly due to the uneven edges of the tree-trunk, used in the experimental setup. The resulted difference in the dielectric filling is mainly due to the air pockets between the uneven

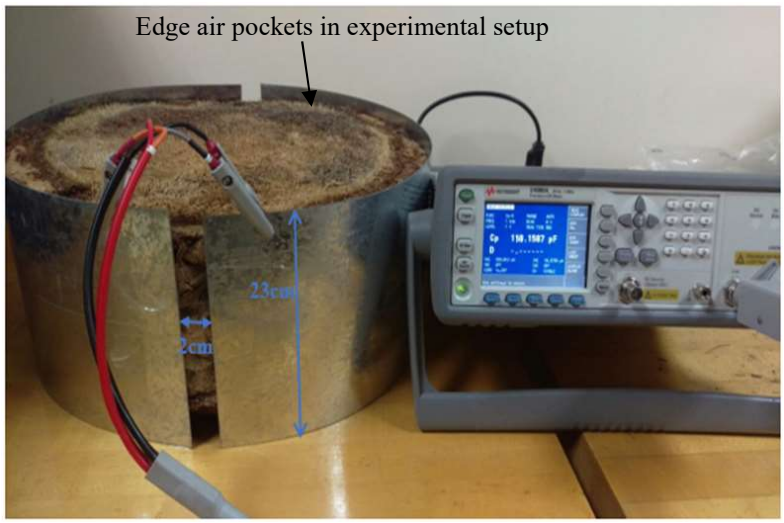

Figure 4.15: Experimental setup for capacitance measurement.

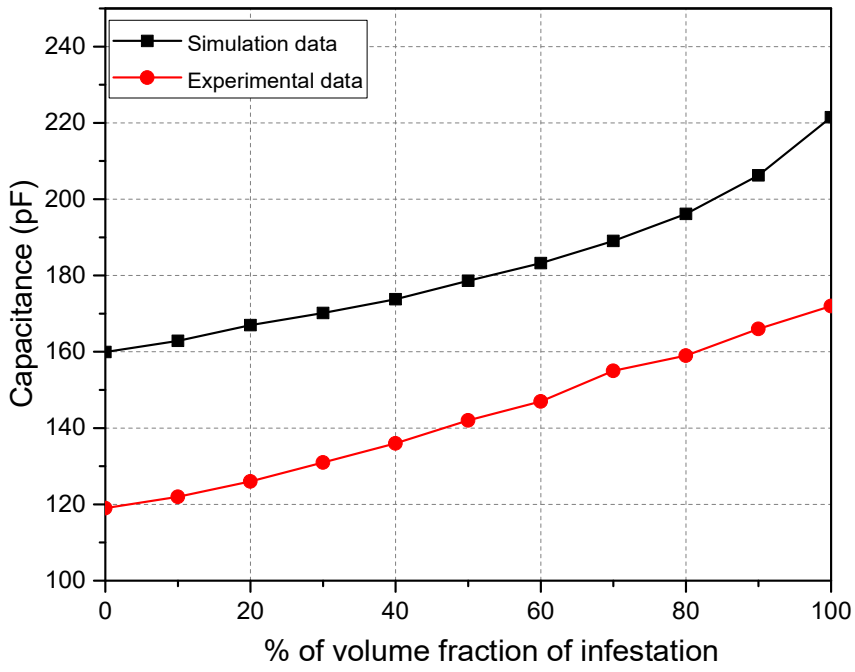

Figure 4.16: Variation of capacitance due to the changes of the volume fraction of the damage.

edge of the tree-trunk and the semi-cylindrical electrodes. To remedy this situation, the simulation model of the tree-trunk is modified. Instead of using infinite segments to create the edge of the cylinder, a polyhedral with 20 edge segments is selected to represent the simulated trunk edge. The 3D and top view of the modified simulation model are shown in Figure 5.17 (a) and (b), respectively. Figure 4.18 plots the updated simulated capacitance values. Note that the simple correction in the simulation model considerably reduced the differences between the experimental and simulated results. Thus, simulation results can be considerably improved by including a more realistic model of tree-trunk.

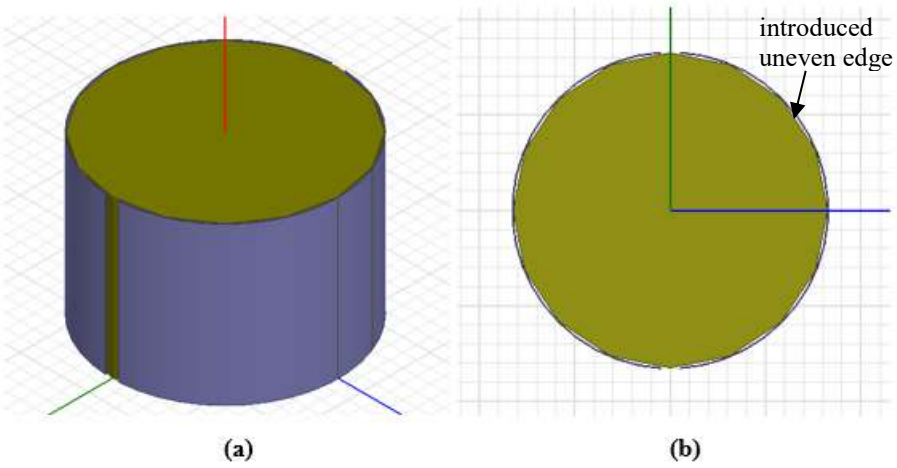

Figure 4.17: Updated simulation model with air-pockets between tree trunk edge and electrodes: (a) 3D view, (b) top view.

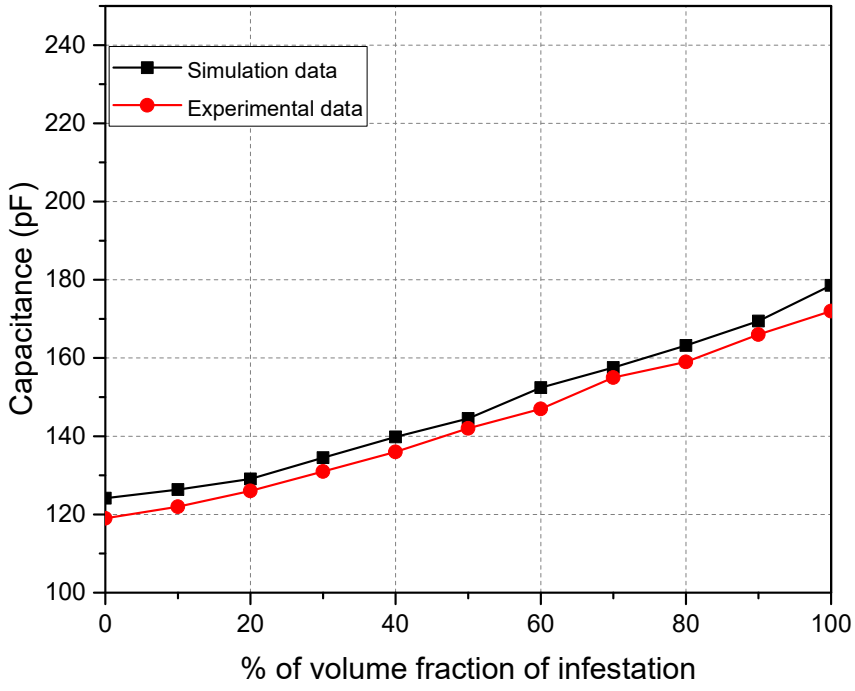

Figure 4.18: Capacitance due to the modified simulated model with un-even edges of the tree trunk.

Table 4:2: Simulated Look-up table for a semi-cylindrical capacitor.

Healthy Date Palm Tree			Damaged Date Palm Tree		
Diameter of tree(cm)	Capacitance Calculated (pF)	Capacitance simulation (pF)	Diameter of tree(cm)	Capacitance Calculated (pF)	Capacitance simulation (pF)
30	122	157.38	30	178	218
33	126	160	33	182	222
36	130	161	36	190	222.5
39	134	162	39	195	224
41	136	165	41	199	228
44	140	166	44	204	230
47	143	166	47	207	230
50	146	167	50	212	231

4.8 CONCLUSION

This chapter presents the design of a semi-cylindrical capacitive sensor to measure tree capacitances. A professional simulator is used to extract dielectric constant from the measured capacitances for three different sensor configurations. The simulated results showed that the capacitance decreases linearly with increasing edge-gap (d) of the electrodes or decreasing dielectric constant (ε_r). The configuration with two semi-cylindrical-electrodes is selected for this study due to easier implementation and improved sensitivity.

For a simple air filled semi-cylindrical capacitor, calculated, simulated and measured capacitances are compared to validate the measurement process. Measured capacitances for healthy, partially-damaged and damaged tree trunks are recorded using calibrated LCR meter. The discrepancy between the simulated and measured capacitances is reduced by updating the simulation model with polyhedral structure with 20 edge segments.

A simulated look-up table, prepared for similar experimental setup and tree-sample, is used to determine the dielectric constant of the measured cylindrical tree-trunk. This process allowed us to categorize the experimented tree-trunk as a healthy or damaged sample. To a certain extent, the level of damage can also be determined. The sensitivity error for 0.1 volume fraction of damage is around 34% and for the complete damage 28%. However, for the updated simulation model, the respective error is only around 5%.

CHAPTER 5

5 CONCLUSION AND FUTURE WORK

5.1 CONCLUSION

Early detection of RPW infected palm trees is crucial to avoid the safety hazards related to unexpected collapse of the palm tree. This also helps to limit the infestation by removing infected tree before the grown PRW starts to exit the tree trunk. Typically, the larvae of the RPW penetrate the lower part of the tree trunk and create cavities and tunnels by chewing the trunk tissue. The presence of bacteria in the infected zone causes fermentation. This causes the tree trunk to become more moisturized and fibrous, leading to an increase in trunk permittivity. So accurate measurement of the dielectric properties related to tree-trunk can result in the identification of RPW infested defected palm trees. In this research, dielectric properties of the tree trunk are measured using two novel approaches to determine the health condition of a date palm tree.

In the 1st approach, microwave resonance technique is used to determine the dielectric properties of a certain segment of the tree-trunk. In this method, the tree is excited with microwave signals and the reflection (S_{11}) and transmission (S_{21}) properties are observed. A 4-GHz patch antenna is initially used for this purpose. Tree samples are collected and used for a controlled experiment in the lab, where dielectric properties of healthy to totally damaged trees are determined by monitoring the shift of the resonance frequencies

associated with the tree-trunk. A major obstacle in this method is to facilitate measurement just after the tree is dissected/cut to collect experimental trunk-samples. Delaying this process leads the trunk to dry out which changes the dielectric properties.

In the 2nd approach, a semi-cylindrical capacitive sensor is designed to measure the tree capacitances and a simulator is used to extract dielectric properties from the measured values. Three sensor configurations are discussed before selecting the one with two semi-cylindrical-electrodes due to easier implementation and improved sensitivity. The simulated results showed that the capacitance decreases linearly with increasing edge-gap (d) of the electrodes or decreasing dielectric constant (ε_r). This process is initially validated by comparing the calculated, simulated and measured capacitances of a simple air filled semi-cylindrical capacitor. Measured capacitances for healthy, partially-damaged and damaged tree trunks are then recorded using calibrated LCR meter. The discrepancy between the simulated and measured capacitances is reduced by updating the simulation model with polyhedral structure with 20 edge segments. Simulated look-up table of capacitances versus dielectric constants is then used to categorize the experimented tree-trunk as a healthy, damaged or partially damaged the sample. The sensitivity error for the updated simulation model is observed to be as low as 5%.

Comparing the two methods, it can be concluded that the capacitive sensor (2nd method) is more suitable to field test as it does not require complicated power source and analyzers, as required in the microwave resonator (1st method) case.

5.2 FUTURE WORK

The microwave sensor proposed in this thesis work can be further studied for improving its sensitivity. Some recommendations for future work as follows:

- For method 1:
    - Transmission coefficients can be analyzed in terms of the deviation of magnitude and phase due to RPW infestation after attaching multiple patch elements to the tree surface. This might give information about the approximate location of the damaged tissue.
    - A field experiment can be performed using microwave senor to detect the damaged tree-trunk due to RPW infestation.
- For method 2:
    - Similar to the microwave field experiment, a capacitive sensor based experiment can also be done. Since it does not require microwave source and analyzer, this should be easier and cost effective than the microwave sensing.
    - Develop a capacitive model that can predict tree-capacitances which is independent of the tree dimensions (radius).

REFERENCES

[1] A. M. Al-Ajlan, "Red palm weevil, Rhynchophorus ferrugineus (Olivier) (Coleoptera: Curculionidae)," *Encycl. Entomol. Springer Netherlands, 2008. 3127-3130.*, pp. 3127–3131, 2001.

[2] N. AlDosary, S. AlDobai, and J. Faleiro, "Review on the Management of Red Palm Weevil Rhynchophorus ferrugineus Olivier in Date Palm Phoenix dactylifera L," *Emirates J. Food Agric.*, vol. 28, no. 1, p. 34, 2016.

[3] J. D. (eds) Jain SM, Al- Khayri JM, "Date Palm Biotechnology," *Springer, Dordr. Johnson DV Worldw. dispersal date palm from its homeland. Acta Hort 882369–375*, vol. 3, no. January, 2011.

[4] V. A. Abraham, M. A. A. I. Shuaibi, J. R. Faleiro, R. A. Abozuhairah, and P. S. P. V Vidyasagar, "An integrated management approach for red palm weevil Rhynchophorus ferrugineus Oliv. a key pest of date palm in the Middle East," *J. Agric. Mar. Sci. [JAMS]*, vol. 3, no. 1, pp. 77–83, 1998.

[5] A. I. Mahmud, J. Farminhao, and E. R. A. Viez, "Red palm weevil (Rhynchophorus ferrugineus olivier, 1790): Threat of palms," *J. Biol. Sci.*, vol. 15, no. 2, pp. 56–67, 2015.

[6] V. SOROKER *et al.*, "Early Detection and Monitoring of Red Palm Weevil: Approaches and Challenges," *Afpp – Palm Pest Mediterr. Conf. Nice – 16, 17 18 January 2013*, no. January, 2013.

[7] M. E.-F. Mozib and H. A. El-Shafie, "Effect of red palm weevil, Rhynchophorus ferrugineus (Olivier) infestation on temperature profiles of date palm tree," *J. Entomol. Nematol.*, vol. 5, no. 6, pp. 77–83, 2013.

[8] T. A. M. Editors, *Sustainable Pest Management in Date Palm : Current Status and Emerging Challenges Sustainability in Plant and Crop Protection*. .

[9] I. A. Ali, "FDTD Analysis of Differential Electromagnetic Energy Absorption by a Biological Body embedded in a Host Material inside a Shorted Waveguide Section," *Int. J. Eng. Technol. IJET-IJENS Vol13 No03*, vol. 13, no. 3, 2013.

[10] C. Yamen Khatib, A. Isotton, C. Pasqualotto, and L. Bernabei, "Ecopalm ring machine: The microwaves technology for the total disinfestations of the palm trees affected by the red palm weevil," in *IV International Date Palm Conference 882*, 2010, pp. 1027–1032.

[11] R. Massa *et al.*, "Microwave treatment for pest control: the case of Rhynchophorus ferrugineus in Phoenix canariensis," *EPPO Bull.*, vol. 41, no. 2, pp. 128–135, 2011.

[12] M. Suliman, A. Shwear, and H. Remili, "Three-Dimensional Simulation of

Microwave Treatment of the Red Palm Weevil Insect," *Int. J. Emerg. Technol. Adv. Eng.*, vol. 6, no. 2, pp. 115–122, 2016.

[13] R. Massa *et al.*, "Experimental and numerical evaluations on palm microwave heating for Red Palm Weevil pest control," *Nat. Publ. Gr.*, no. March, pp. 1–8, 2017.

[14] M. D. Janezic and D. F. Williams, "Permittivity characterization from transmission-line measurement," in *Microwave Symposium Digest, 1997., IEEE MTT-S International*, 1997, vol. 3, pp. 1343–1346.

[15] S. Roberts and A. Von Hippel, "A new method for measuring dielectric constant and loss in the range of centimeter waves," *J. Appl. Phys.*, vol. 17, no. 7, pp. 610–616, 1946.

[16] W. E. Courtney, "Analysis and evaluation of a method of measuring the complex permittivity and permeability microwave insulators," *IEEE Trans. Microw. Theory Tech.*, vol. 18, no. 8, pp. 476–485, 1970.

[17] O. V Tereshchenko, F. J. K. Buesink, and F. B. J. Leferink, "An overview of the techniques for measuring the dielectric properties of materials," *Gen. Assem. Sci. Symp.*, pp. 1–4, 2011.

[18] P. Juan-Garc'\ia and J. M. Torrents, "Measurement of mortar permittivity during setting using a coplanar waveguide," *Meas. Sci. Technol.*, vol. 21, no. 4, p. 45702, 2010.

[19] A. Cataldo, E. De Benedetto, and G. Cannazza, *Broadband reflectometry for enhanced diagnostics and monitoring applications*, vol. 93. Springer Science & Business Media, 2011.

[20] H. A. Bethe and J. Schwinger, *Perturbation theory for cavities*. Massachusetts Institute of Technology, Radiation Laboratory, 1943.

[21] M. Giordano, F. Momo, and A. Sotgiu, "On the design of a re-entrant square cavity as resonator for low-frequency ESR spectroscopy," *J. Phys. E.*, vol. 16, no. 8, p. 774, 1983.

[22] M. D. Janezic and J. Baker-Jarvis, "Full-wave analysis of a split-cylinder resonator for nondestructive permittivity measurements," *IEEE Trans. Microw. Theory Tech.*, vol. 47, no. 10, pp. 2014–2020, 1999.

[23] S. Gabriel, R. W. Lau, and C. Gabriel, "The dielectric properties of biological tissues: II. Measurements in the frequency range 10 Hz to 20 GHz," *Phys. Med. Biol.*, vol. 41, no. 11, p. 2251, 1996.

[24] M. A. Stuchly and S. S. Stuchly, "Dielectric properties of biological substances—Tabulated," *J. Microw. Power*, vol. 15, no. 1, pp. 19–25, 1980.

[25] W. Scott and G. Smith, "Dielectric spectroscopy using monopole antennas of general electrical length," *IEEE Trans. Antennas Propag.*, vol. 34, no. 7, pp. 919–

929, 1986.

[26] P. A. Bernard and J. M. Gautray, “Measurement of dielectric constant using a microstrip ring resonator,” *IEEE Trans. Microw. Theory Tech.*, vol. 39, no. 3, pp. 592–595, 1991.

[27] D. Shimin, “A new method for measuring dielectric constant using the resonant frequency of a patch antenna,” *IEEE Trans. Microw. Theory Tech.*, vol. 34, no. 9, pp. 923–931, 1986.

[28] I. J. Bahl and S. S. Stuchly, “Analysis of a microstrip covered with a lossy dielectric,” *IEEE Trans. Microw. Theory Tech.*, vol. 28, no. 2, pp. 104–109, 1980.

[29] N. Alexopoulos and D. Jackson, “Fundamental superstrate (cover) effects on printed circuit antennas,” *IEEE Trans. Antennas Propag.*, vol. 32, no. 8, pp. 807–816, 1984.

[30] H. Yang and N. Alexopoulos, “Gain enhancement methods for printed circuit antennas through multiple superstrates,” *IEEE Trans. Antennas Propag.*, vol. 35, no. 7, pp. 860–863, 1987.

[31] A. Bhattacharyya, “Effects of dielectric superstrate on patch antennas,” *Electron. Lett.*, vol. 24, no. 6, pp. 356–358, 1988.

[32] R. Q. Lee, A. J. Zaman, and K. F. Lee, “Effects of dielectric superstrates on a two-layer electromagnetically coupled patch antenna,” in *Antennas and Propagation Society International Symposium, 1989. AP-S. Digest*, 1989, pp. 620–623.

[33] A. K. Verma and others, “Resonant frequency of uncovered and covered rectangular microstrip patch using modified Wolff model,” *IEEE Trans. Microw. Theory Tech.*, vol. 41, no. 1, pp. 109–116, 1993.

[34] A. K. Verma, A. S. Omar, and others, “Microstrip resonator sensors for determination of complex permittivity of materials in sheet, liquid and paste forms,” *IEE Proceedings-Microwaves, Antennas Propag.*, vol. 152, no. 1, pp. 47–54, 2005.

[35] Y. K. Verma and A. K. Verma, “Accurate determination of dielectric constant of substrate materials using modified Wolff model,” in *Microwave Symposium Digest. 2000 IEEE MTT-S International*, 2000, vol. 3, pp. 1843–1846.

[36] A. K. Verma, “Determination of dielectric constant and loss-tangent of substrate sheet using microstrip patch resonator,” *Microw. Opt. Technol. Lett.*, vol. 35, no. 3, pp. 175–179, 2002.

[37] R. Kumar and P. Malathi, “Effects of superstrates on the resonant frequency of rectangular microstrip antennas,” *Microw. Opt. Technol. Lett.*, vol. 49, no. 12, pp. 2946–2950, 2007.

[38] Y. Li, S. Member, N. Bowler, S. Member, and D. B. Johnson, “A Resonant Microwave Patch Sensor for Detection of Layer Thickness or Permittivity Variations in Multilayered Dielectric Structures,” vol. 11, no. 1, pp. 5–15, 2011.

[39] Y. Li, S. Member, N. Bowler, and S. Member, “Resonant Frequency of a Rectangular Patch Sensor Covered With Multilayered Dielectric Structures,” vol. 58, no. 6, pp. 1883–1889, 2010.

[40] N. Chattoraj and G. S. Roy, “Application of Genetic Algorithm to the Optimization of Microstrip Antennas with and without Superstrate,” *Mikrotalasna Rev.*, pp. 32–35, 2006.

[41] S. Chakraborty, S. Mandal, and B. Gupta, “Neural network modeling for the fast estimation of superstrate loading effect on rectangular microstrip patch antennas,” in *Applied Electromagnetics Conference, 2007. AEMC 2007. IEEE*, 2007, pp. 1–3.

[42] H. A. Hammas, “Radiation Performance Evaluation of Microstrip Antenna Covered With a Dielectric Layer,” *Eng. Tech. J.*, pp. 1280–1286, 2009.

[43] M. S. Boybay and O. M. Ramahi, “Material Characterization Using Complementary Split-Ring Resonators,” *IEEE Trans. Instrum. Meas.*, vol. 61, no. 11, pp. 3039–3046, 2012.

[44] C. Yang, C. Lee, A. Member, K. Chen, S. Member, and K. Chen, “Noncontact Measurement of Complex Permittivity and Thickness by Using Planar Resonators,” *IEEE Trans. Microw. Theory Tech.*, vol. 64, no. 1, pp. 247–257, 2016.

[45] C. Lee, A. Member, and C. Yang, “Single-Compound Complementary Split-Ring Resonator for Simultaneously Measuring the Permittivity and Thickness of,” *IEEE Trans. Microw. Theory Tech.*, vol. 63, no. 6, pp. 2010–2023, 2015.

[46] M. Daneshmand, “Non-Contact Liquid Sensing Using High Resolution Microwave Microstrip Resonator,” *Microw. Symp. (IMS), 2015 IEEE MTT-S Int. IEEE*, pp. 1–4, 2015.

[47] S. Alahnomi, Rammah A And Zakaria, Z And Ruslan, E And Bahar, Mohd And Azuan, Amyrul And Ab Rashid, “High Sensitive Microwave Sensor Based On Symmetrical Split Ring Resonator For Material,” *Microw. Opt. Technol. Lett.*, Vol. 58, No. 9, Pp. 2106–2110, 2016.

[48] M. Taha, W. Peng, M. Zaka, and U. Rehman, “Microwave sensor for non-destructive dielectric characterization of biological systems,” *Int. J. Appl. Electromagn. Mech.*, vol. 50, pp. 353–363, 2016.

[49] R. Yadav, Rk And Yadava, “S Uperstrate L Oaded R Ectangular M Icrostrip P Atch A Ntennas - A N Overview,” *J. Information, Intell. Knowl.*, Vol. 3, No. 2, 2011.

[50] A. Azuan *Et Al.*, “Dielectric Analysis Of Liquid Solvents Using Microwave Resonator Sensor For High,” *Microw. Opt. Technol. Lett.*, Vol. 59, No. 2, Pp. 367–371, 2017.

[51] W. Technologies and J. Rammal, “Near-field microwave microscopy for the characterization of dielectric materials,” *Int. J. Microw. Wirel. Technol.*, vol. 6, no. 6, pp. 549–554, 2018.

[52] J. Dong *et al.*, “Noncontact Measurement of Complex Permittivity of Electrically Small Samples at,” *IEEE Trans. Microw. Theory Tech.*, vol. 64, no. 9, pp. 2883–2893, 2016.

[53] K. T. M. Shafi and A. K. Jha, “Improved Planar Resonant RF Sensor for Retrieval of Permittivity and Permeability of Materials,” *IEEE Sens. J.*, vol. 17, no. 17, pp. 5479–5486, 2017.

[54] S. Hardinata, F. Deshours, G. Alquié, H. Kokabi, and F. Koskas, “Miniaturization of Microwave Biosensor for Non-invasive Measurements of Materials and Biological Tissues,” *IPTEK J. Proc. Ser.*, pp. 90–93, 2017.

[55] A. Azuan, M. Bahar, Z. Zakaria, S. Rosmaniza, A. Rashid, and A. A. Isa, “Microstrip Planar Resonator Sensors for Accurate Dielectric Measurement of microfluidic solutions,” *Electron. Des. (ICED), 2016 3rd Int. Conf. on. IEEE*, pp. 416–421, 2016.

[56] C. Hsu, K. Chen, C. Lee, S. Member, and C. Yang, “Improved Approach Using Multiple Planar Complementary Split- Ring Resonators for Accurate Measurement of Permittivity .,” *Wirel. Symp. (IWS), 2016 IEEE MTT-S Int. IEEE*.

[57] C.-T. Chiang and Y.-C. Huang, “A semicylindrical capacitive sensor with interface circuit used for flow rate measurement,” *IEEE Sens. J.*, vol. 6, no. 6, pp. 1564–1570, 2006.

[58] A. Jaworek and A. Krupa, “Gas/liquid ratio measurements by rf resonance capacitance sensor,” *Sensors Actuators A Phys.*, vol. 113, no. 2, pp. 133–139, 2004.

[59] S. Das, T. S. Sarkar, and B. Chakraborty, “A semi-cylindrical capacitive sensor used for soil moisture measurement,” *Int. J. Electr. Robot. Electron. Comm. Engg.*, vol. 8, no. 1, 2014.

[60] C. Balanis, “Antenna theory : analysis and design / Constantine A. Balanis,” *SERBIULA (sistema Libr. 2.0)*, 1982.

[61] C. A. Balanis, *Advanced engineering electromagnetics*. John Wiley & Sons, 1999.

[62] E. Newman and P. Tulyathan, “Analysis of microstrip antennas using moment methods,” *IEEE Trans. Antennas Propag.*, vol. 29, no. 1, pp. 47–53, 1981.

[63] E. Yamashita and R. Mittra, “Variational method for the analysis of microstrip lines,” *IEEE Trans. Microw. Theory Tech.*, vol. 16, no. 4, pp. 251–256, 1968.

[64] J. Svacina, “Analysis of multilayer microstrip lines by a conformal mapping method,” *IEEE Trans. Microw. Theory Tech.*, vol. 40, no. 4, pp. 769–772, 1992.

Vitae

Name	:FORHAD HOSSAIN
Nationality	:BANGLADESHI
Date of Birth	:12/25/1990
Email	:forhad.eee09@gmail.com
Address	:C\O: Lutfor Rahman, Village: Chaknarayanpur, P.S,Bagha P.O: Bagha, Rajshahi 6280,Bangladesh
Academic Background	: MS in Electrical Engineering (Major: Electromagnetics) KFUPM, Dhahran 2018
	BSc. in Electrical and Electronic Engineering
	American Intl. University Bangladesh 2013